December 2021

Mass Spectrometry Directed Pre-Clinical Studies of Asthma Candidate MIDD0301 and Its Analogs

Md Shadiqur Rashid Roni
University of Wisconsin-Milwaukee

MASS SPECTROMETRY DIRECTED PRE-CLINICAL STUDIES OF ASTHMA CANDIDATE MIDD0301 AND ITS ANALOGS

by

Md Shadiqur Rashid Roni

A Dissertation Submitted in

Partial Fulfillment of the

Requirements for the Degree of

Doctor of Philosophy

in Chemistry

at

The University of Wisconsin-Milwaukee

December 2021

ABSTRACT

MASS SPECTROMETRY DIRECTED PRE-CLINICAL STUDIES OF ASTHMA CANDIDATE MIDD0301 AND ITS ANALOGS

by

Md Shadiqur Rashid Roni

The University of Wisconsin-Milwaukee, 2021
Under the Supervision of Professor Alexander (Leggy) Arnold

Asthma is one of the most prevalent global health problems. More than 25 million Americans are suffering from asthma and their symptoms especially in children are not well controlled with current medications. The current therapeutic options to control symptoms are limited and are commonly based on inhaled corticosteroids. There are several reasons for uncontrolled asthma symptoms that includes steroid resistance, improper use of inhalers and very few orally available medications. Thus, there is an unmet medical need for a novel non-steroidal oral asthma medication. To address this issue, our research group is targeting the amino butyric acid type A receptors ($GABA_AR$) in the lung using two strategies. First of all, subtypes selective compounds, exploiting the fact that the expression of $GABA_ARs$ subtypes differ between the central nervous system (CNS) and peripheral tissue. Secondly, $GABA_AR$ ligands with the inability to cross the blood brain barrier (BBB) to reduce CNS exposure. The objective of our current studies was to characterize our asthma lead compound MIDD0301 in respect to physicochemical properties, pharmacokinetics, and metabolism.

Many *in vitro* and *in vivo* assays were designed and successfully implemented to better understand the pharmacokinetics and pharmacodynamics of MIDD0301. Most investigations included the use of liquid chromatography tandem mass spectrometry to analyze complex biological samples such as blood, tissue, urine and feces. Several preparation, extraction, purification, and clean-up procedures were developed and optimized to achieve our objective. Additionally, we were able to determine aqueous solubility, permeability, lipophilicity and pKa to understand the *in vivo* behavior of MIDD0301. The two major findings were: a) a suitable aqueous formulation that provided the best oral bioavailability and b) by studying the kinetics of a seven-membered ring-opening reaction in acidic conditions, it was found that the *in vivo* interconversion neither affects the original stereochemistry of MIDD0301 nor its bioavailability.

Favorable physicochemical properties encouraged us to develop a scalable synthesis for MIDD0301. The manufacturing processes of a lead compounds become especially important when the NCE (new chemical entity) is part of an IND (investigational new drug) application. To support the analysis of such a process, two reverse phase and three normal phase chromatographic methods were optimized to determine purity and optical purity.

Next, we evaluated drug metabolism and pharmacokinetics study (DMPK), which included metabolite identification and characterization of the metabolic excretion profile. We were able to measure absorption, distribution, metabolism, and excretion and found that MIDD0301 is absorbed quickly and did not undergo phase I biotransformation. MIDD0301 was found in urine and feces and underwent phase II conjugation by forming glucuronide, glucoside, and taurine conjugates. MIDD0301 glucuronide was identified as the main metabolite. A

comparative study of MIDD0301 enantiomers showed similar binding affinities and PKPD properties that differed in the ability of form the glucoside conjugate.

At the same time, we continued to explore new asthma candidates that unlike MIDD0301 formed a neutral species at physiological pH but were still unable to cross the BBB. Substituted analogs of MIDD0301 bearing long hydrophobic chains are now being evaluated with the goal to achieve long-acting property and limited phase II conjugation.

To

my parents,

my wife,

and my children Nammam and Rasifah

TABLE OF CONTENTS

LIST OF FIGURES

LIST OF TABLES

LIST OF SCHEMES

LIST OF ABBREVIATIONS

ADME	absorption, distribution, metabolism, and excretion
AHR	airway hyperresponsiveness
APCI	atmospheric pressure chemical ionization
APPI	atmospheric pressure photo ionization
ASM	airway smooth muscle
AUC	area under the curve
BBB	blood-brain barrier
BZD	benzodiazepine
C_{MAX}	maximum concentration
CNS	central nervous system
CRO	contracted research organization
CYP_{450}	cytochrome P450
DAD	diode array detector
DART	direct analysis in real time
DESI	desorption electrospray ionization
DMF	dimethyl formamide
DMPK	drug metabolism and pharmacokinetics
DMSO	dimethyl sulfoxide
EI	electron ionization
ESI	electrospray ionization

FAB	fast atom bombard
FDA	Food and Drug Administration
GABA	γ-aminobutyric acid
$GABA_AR$	γ-aminobutyric acid type A receptor
HEK	human embryonic kidney cells
HPMC	hydroxy propyl methyl cellulose
HRMS	high-resolution mass spectrometry
HPLC	high-performance liquid chromatography
IACUC	Institutional Animal Care and Use Committee
IC_{50}	half maximal inhibitory concentration
ICS	inhaled corticosteroids
IND	investigational new drug
IP	intraperitoneal
IS	internal standard
ISTD	internal standard
IV	intravenous
LABA	long-acting β_2 agonist
LC	liquid chromatography
LCMS	liquid chromatography-mass spectrometry
LCMS-IT-TOF	liquid chromatography-mass spectrometry ion trap time-of flight
LIT	linear ion trap
LOD	limit of detection

LOQ	limit of quantification
MALDI	matrix assisted laser desorption/ionization
MAM	microsomal assay mixture
MRM	multiple reaction monitoring
NDA	new drug application
Ova s/c	ovalbumin sensitized challenged
PAMPA	parallel artificial membrane permeability assay
PBS	phosphate buffered saline
PDA	photodiode array
PD	pharmacodynamics
PDSP	Psychoactive Drug Screening Program
PEG	polyethylene glycol
ppm	parts per million
PK	pharmacokinetics
QIT	quadrupole ion trap
SPE	solid phase extraction
TEA	triethyl amine
TFA	trifluoroacetic acid
$t_{1/2}$	time taken for the plasma concentration of a drug to reduce to half its original value
T_{max}	time when maximum concentration is observed
TOF	time of flight

UDP	uridine diphosphate
UDPGA	urindine diphosphate glucuronic acid
UDP Glc	uridine diphosphate glucose
UGT	UDP-Glucuronosyltrasferase

ACKNOWLEDGEMENTS

First and foremost, I would like to express my deepest appreciation to my research advisor Professor Alexander (Leggy) Arnold. Without his constant guidance and continuous support, my PhD journey could have been a very rough one. Without any exception, in last five years regardless of whether he was in the vacation outside the country or busy at the end of a semester, he had always time for me to discuss my research. I am also genuinely indebted to Dr. Arnold as he had given me the freedom of maintaining my own research time according to my convenience to fulfill responsibilities. As a grad student and being parents of two kids, this flexibility made the balance between my work and family life less stressful, and I felt more committed toward my research.

I would like to extend my sincere gratitude to my doctoral committee members, Dr. Cook, Dr. Dietz, Dr. Aldstadt, Dr. Mirza and Dr. Stafford for their time-to-time constructive criticism, sharing their extensive knowledge and advice throughout the graduate years. I also like to mention here the well-designed AQEs for analytical section along with mass spectrometry and separations courses that were offered, really helped me to become ready for this long journey in the field of analytical chemistry.

I am grateful to all past and present members of Arnold group whom I interacted with. It was a privilege to work with such well organized, intelligent, and generous people. I also worked closely with some members of the Cook's group. I especially like to thank Dr. Daniel Knutson and Md Yeunus Mian for their collaboration and co-operation.

Special thanks to Professor M Mahmun Hossain. He is like a local guardian to me, and I think most of the Bangladeshi students at UW Milwaukee feel similar way because of his personal interaction and willingness to help each of us.

I am immensely grateful to my parents and my elder brother Rana for their unparallel support throughout my whole life. They valued the higher education for me over everything and provided me best resources they could afford so that I could get the chance to pursue my dream.

Kids are the blessing, infinite source of happiness and inspiration behind moving forward. As parents, we would do anything in our capacity to make them feel happy. But in last two years, due to COVID-19 situation, our kids could not go to school, no social gathering, not much indoor or outdoor activities, in addition to that I had to close my room although I was at home to keep my research going. This was the most frustrating time for them which my loving wife Tabinda managed single handedly with her utmost patience and skill. So, in this special occasion, I would like to thank her from the bottom of my heart for her endless assistance and sacrifice that helped me to triumph over the struggles that I went through these graduate years.

Chapter 1: Introduction

1.1 Preclinical study

Discovery and development of a drug candidate and the approval for human consumption is a very long and extremely expensive process. It usually takes more than 13 years for a drug to advance from discovery stage to market and 95% of the drugs that reach clinical trials fail.[35] Evaluation of physical and chemical properties help researchers to identify appropriate candidates from hundreds of drug-like molecules. For the initial screening, Lipinski's rule of 5 is widely used. According to this rule, a molecule fails to demonstrate drug-like properties when its hydrogen bond donors are more than 5, hydrogen bond acceptors are more than 10, log P is over

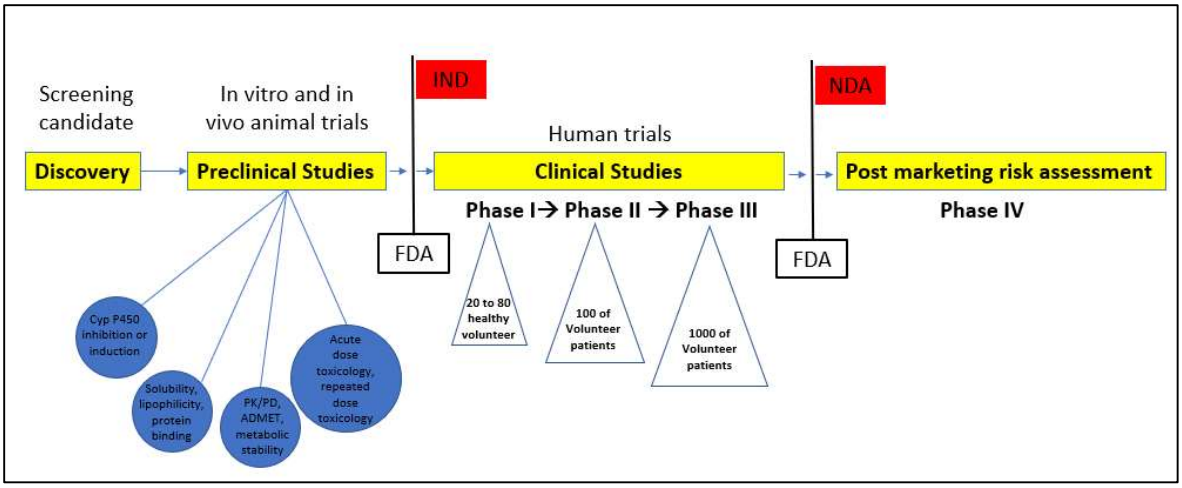

Figure 1. General steps involved in drug discovery

5 and molecular weight is above 500.[34] Though fundamental steps of development are common (Figure 1), duration, complexity, and route to reach FDA approval are unique for each drug. Attractive are projects that identified a target inside body that is responsible to manifest certain pharmacological effect directly or indirectly upon ligand binding. Next, new molecules are designed that bind to the target and once synthesized, molecules are evaluated with well-

designed *in vitro* assays followed by pharmacodynamic studies. Preclinical studies include *in vitro* and *in vivo* toxicity evaluation to determine a safe dose for first-in-human studies. For an oral drug, insufficient intestinal absorption and extensive enzymatic biotransformation in the liver can lead to a small therapeutic window. Solubility, lipophilicity, and permeability assay can predict the intestinal absorption of a novel compound. *In vitro* biotransformation can be evaluated with microsomal stability assays. *In vivo* pharmacokinetics studies are used to determine absorbance and clearance. Unspecific protein binding of drug-like molecules or their metabolites can influence dosage and drug-drug interaction and might lead to toxicity and consequently failure in clinical trial. It is paramount to identify all possible *in vivo* metabolites produced in rodents as they are usually relevant to human metabolic pathways. However, if a substrate is rapidly cleared in rodents due to fast metabolism, it can still induce toxicity in human if the metabolism is significantly slower. Furthermore, the specific metabolism in rodents can be slow, which might lead to a higher concentration of the parent drug and therefor toxicity in human.[36] The identification of metabolites provides us valuable information about biotransformation, reactive centers of the parent drug, enzymes that are responsible for a metabolic reaction, and insights into possible drug-drug interaction for co-administration. One concern is the translation of pre-clinical studies to human trials, which has led to inconsistencies and irreproducible results.[35] Therefore, pre-clinical study should be well designed to evaluate possible toxicities and carried out with high precision.

1.2 Asthma, current medications and our novel approach to use $GABA_A$ receptors as pharmacological targets

Asthma is one of the most prevalent global health problems. More than 25 million Americans are suffering from asthma. It is also the most common chronic disease among children. Seven percent of children have asthma.[1] Common asthma symptoms include wheezing, coughing, shortness of breath, and chest tightness or inflammation.[3] During asthma attacks chronic airway

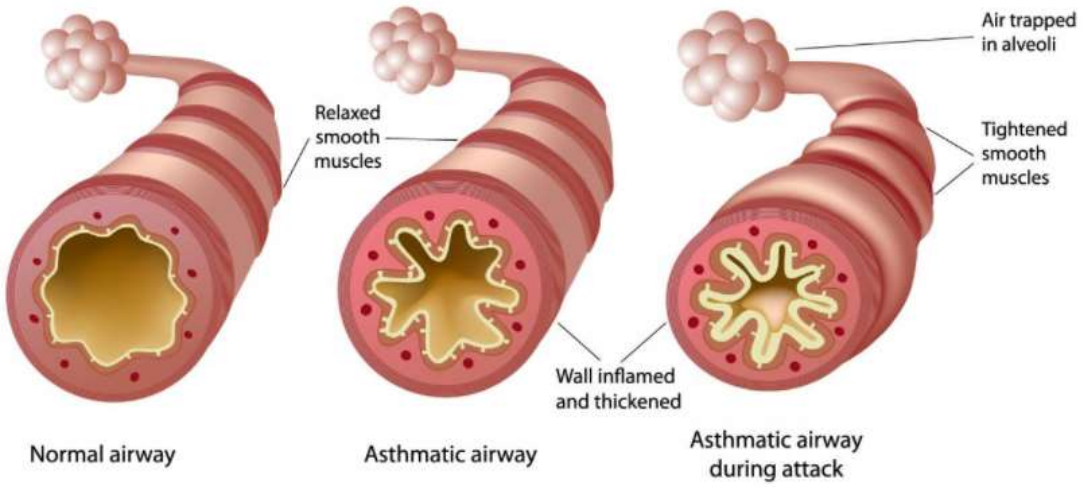

Figure 2. Comparative illustration of normal and asthmatic airway[50]

inflammation leads to airway remodeling, hyperactivity to external stimuli, and results in airway obstruction.[2] Current therapeutic options to control symptoms are limited and the most common ones are inhaled corticosteroids (ICS). For more severe asthma conditions, they are accompanied with long-acting β2 adrenergic receptor agonists, oral corticosteroids, or other immune modulating agents.[4] One of the few oral substitutes for asthma patients that are resistant to inhaled steroids are leukotriene receptor antagonists, such as montelukast.[5] However, montelukast has limited efficacy due to variations in leukotriene signaling genes rendering it ineffective for many patients.[6,7,8] Injectable IL-5 monoclonal antibodies are the latest alternatives

but due to high costs are limited to severe condition.[9, 10] Taken together, the heterogeneity of the asthma patient population, limited safe and effective treatment options, and high costs for biologics represent an unmet medical need for a large number of asthma patients. To address this issue, our group is targeting the amino butyric acid type A receptors ($GABA_AR$). $GABA_ARs$ are ligand-gated chloride ion channels which are well-known for their role in CNS inhibitory neurotransmission. $GABA_ARs$ are membrane receptors mainly consisting of combinations of 19

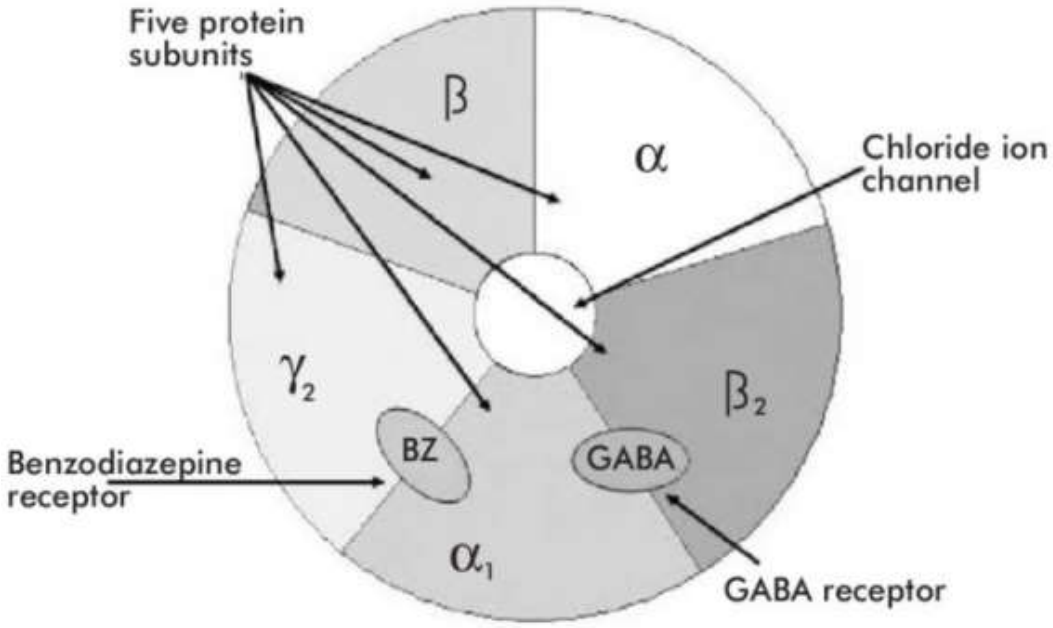

Figure 3. $GABA_AR$ and typical subunit distribution

different subunits (α1−6, β1−3, γ1−3, δ, ε, π, θ, ρ1−3). Classical heteropentameric $GABA_ARs$ consist of 2 alpha, 2 beta, and one "tertiary" subunit (γ, δ, ε, θ, or π).[15,16] Even though $GABA_ARs$ are prevalent in the CNS, they were also identified in peripheral tissue such as airway smooth muscle, airway epithelium and immune cells. Interestingly, $GABA_AR$ subtypes in these peripheral tissues are expressed differently than in the brain,[12,13,17–21] which allows the development of ligands that selectively bind and modulate the $GABA_ARs$ in the lung without adverse CNS

effects.[12-14] The subtype selectivity of ligands depends on the combination of subunits that form a high affinity $GABA_AR$. $GABA_ARs$ in the brain contain among others α1, α2 or α3 subunits in which α1 targeted ligands are responsible for sedation whereas α2 or α3 targeted ligand can diminish anxiety.[25-27] On the other hand, $GABA_ARs$ containing the α4 and α5 subunit are found in mammalian airways[28] and immune cells[31-33] can be targeted with ligands to relax pre-contracted airway smooth muscle[29-30] and reduce the recruitment of immune cells.[22]

1.3 $GABA_AR$ modulator ligands and our lead compound

To modulate α4 and α5 subunit containing peripheral $GABA_ARs$, many ligands have been synthesized and evaluated by our group. Benzodiazepines are well known for their affinity toward

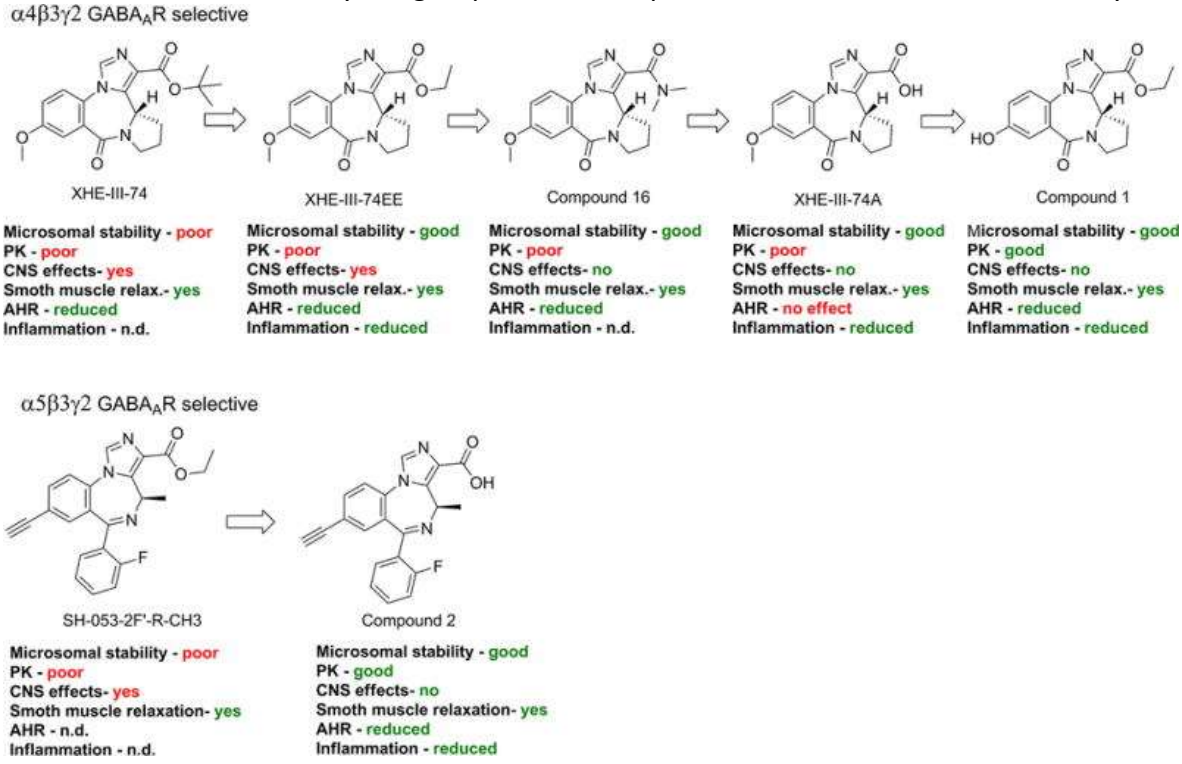

Figure 4. Some of $GABA_AR$ modulators with PKPD properties[13]

$GABA_ARs$, can cross the blood brain barrier, and are responsible for various CNS effects such as sedation.

However, selective activation of peripheral $GABA_AR$s and absence of CNS effects have just recently been introduced. Figure 4 summarizes our subtype selective $GABA_AR$ modulators. Compound 2 is an α5 selective imidazobenzodiazepine. MIDD0301 (aka GL-II-93) is our current lead compound, which in contrast to compound 2, reduced inflammation by direct interaction

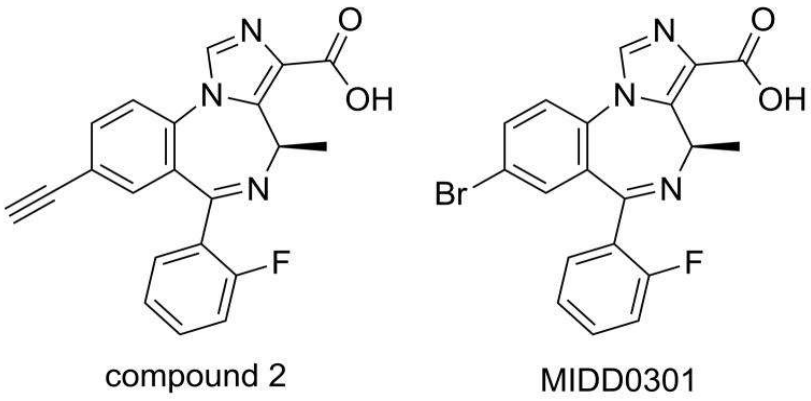

Figure 5. Structure of compound 2 (previous hit) and MIDD0301 (lead compound)

with CD4+ T cells.[22] The different pharmacological effect between the two compounds is mediated by the aryl substitution (acetylene vs bromine). Both compounds have a carboxylic acid function that increases polarity and reduces the ability to cross the BBB. Both compounds can relax constricted airway smooth muscle, attenuate airway hyper-responsiveness (AHR), decrease the numbers of eosinophils and macrophages and lower the number of CD4+ T cells in the lung without causing systemic immune suppression when given orally.[22-24] Recently, efficacy of MIDD0301 was also evaluated using nebulized administration which achieved rapid onset of action.[11]

1.4 Mass spectrometry in drug discovery and development

Mass spectrometers can detect m/z (mass to charge ratio) but require analytes to be converted into a gaseous ion. There are three major components of a mass spectrometer which are i) ion

source, ii) mass analyzer and iii) detector. In this section, a brief description of those components of a mass spectrometer and various available options for each component will be discussed.

1.4.1 Ion source

After more than 100 years of development, mass spectrometry has been advanced with many ionization techniques such as electron ionization (EI), fast atom bombardment (FAB), atmospheric pressure chemical ionization (APCI), atmospheric pressure photo ionization (APPI),

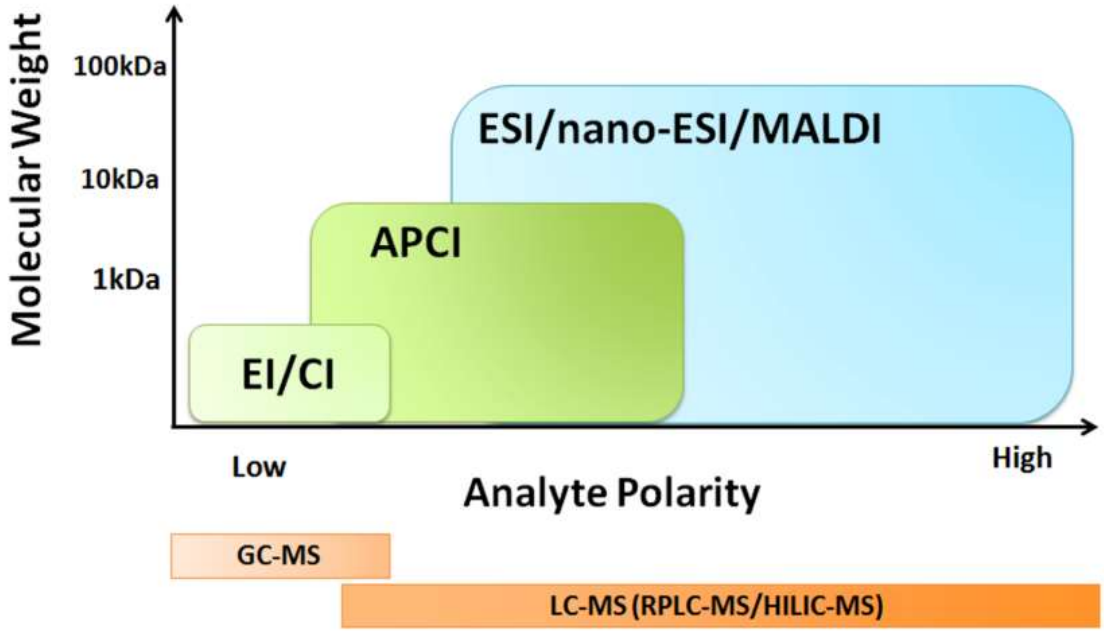

Figure 6. Molecular weight coverage comparison among various ionization technique [51]

electrospray ionization (ESI), matrix assisted laser desorption ionization (MALDI), desorption electrospray ionization (DESI) and direct analysis in real time (DART).[37] EI was the earliest ionization technique, limited to molecules that are volatile, thermally stable and have a molecular weight less than 600 Da.[38] For this technique, gaseous molecules are bombard with high energy electrons (70eV) which convert molecules into positive fragment ions. The ion signals can be used

as a fingerprint for each individual molecule.[39] A revolution of bioanalysis occurred after the

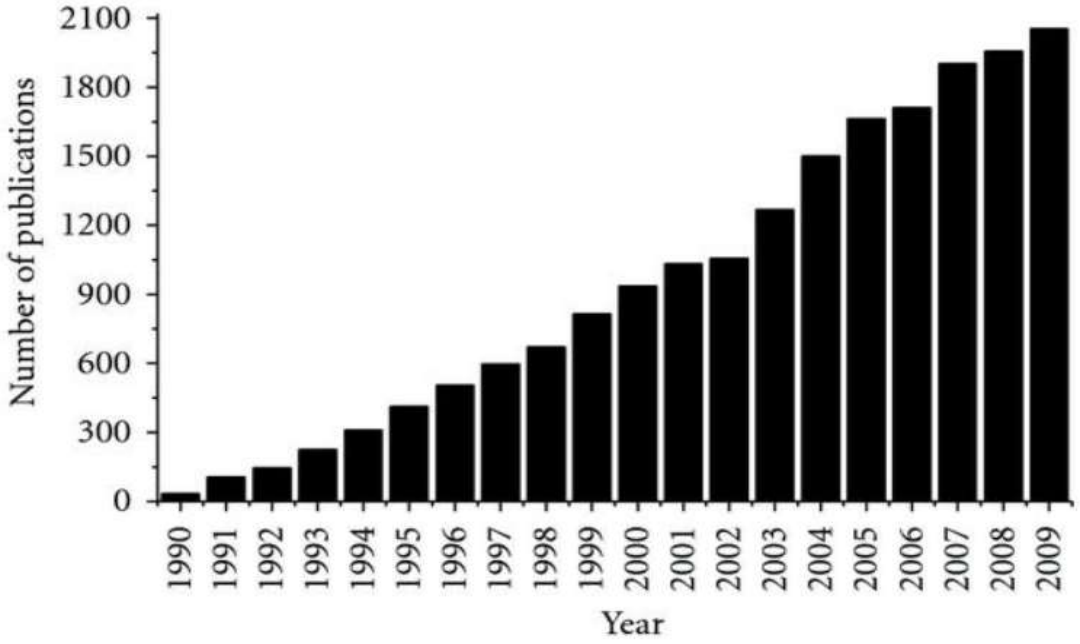

Figure 7. Number of annual publications for ESI-MS after its introduction[42]

invention of ESI and MALDI in 1988. Both are soft ionization techniques.[40] For soft ionization, ionization occurs by protonated or deprotonated. John Fenn and Koichi Tanaka shared Nobel Prize in 2002 for the development of soft ionization techniques (ESI and MALDI) for the analysis of biological macromolecules using mass spectrometry. The use of ESI-MS has increased

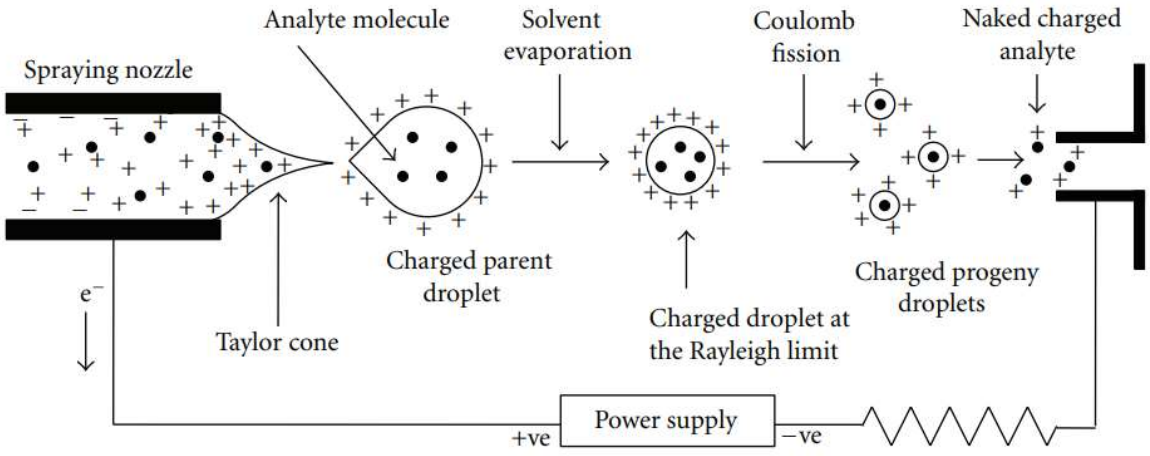

Figure 8. Schematics of electrospray ionization (working principle). [42]

exponentially since its invention[42] (Figure 7). One reason is the compatibility with liquid

chromatography and analysis of polar molecules.[41] In this technique, samples with proper dilution in volatile solvent are sprayed through a stainless steel needle or capillary with a low flowrate. The tip of the capillary has a very high voltage which results in charged droplets. With the aid of a nebulized gas and drying gas during spraying, density of charged analytes increase in the droplet through solvent evaporation and finally, due to coulombic repulsion charge droplets are blasted into individual charged analytes before entering the mass analyzer.[42] A schematic diagram in Figure 8 demonstrates the transformation of nebulized droplets into gaseous ions.

For a MALDI experiment, the analyte is surrounded by a large excess of matrix molecules and irradiated with a laser pulse. The matrix molecules absorb laser energy, ablate from the target plate with the analyte into the gaseous phase and are protonated by matrix molecules. Matrix molecules are small molecules with a conjugated π-system and can be easily irradiated with a UV

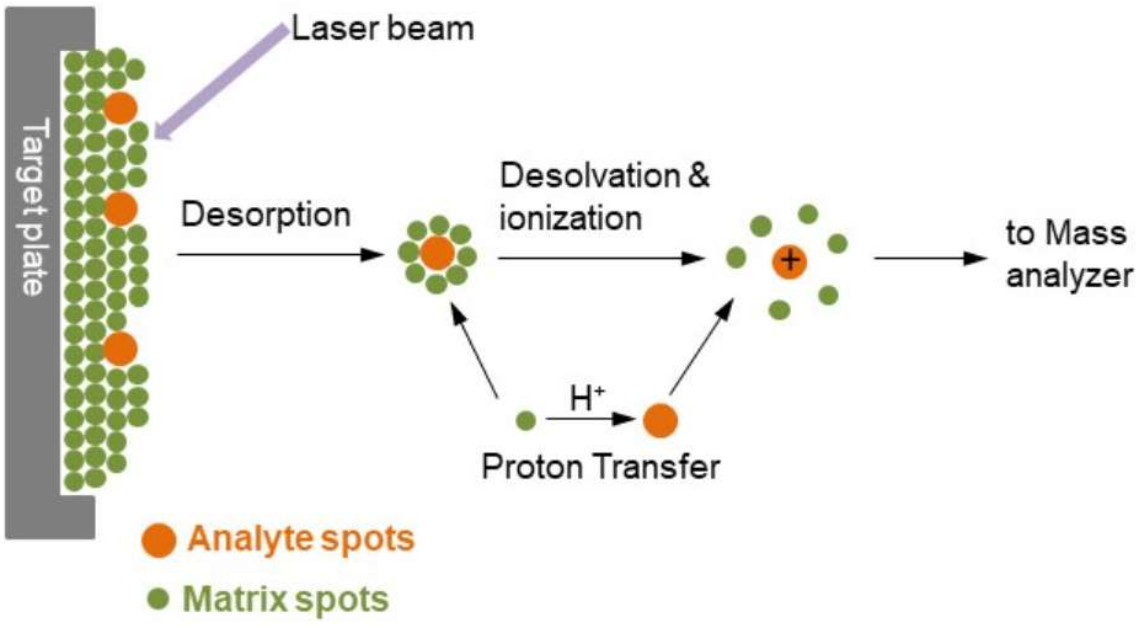

Figure 9. Schematics of matrix assisted laser desorption ionization (MALDI) working principle [48]

laser pulse. Common matrix molecules are sinapinic acid, α-cyano-4-hydroxycinnamic acid and

2,5-dihydroxybenzoic acid. Sometimes, 0.1% trifluoroacetic acid is added to the matrix solution to enhance protonation.[43]

1.4.2 Mass analyzer

The next part of a mass spectrometer is the mass analyzer. Many types of analyzers are now available such as magnetic sector, quadrupole, ion trap, and time of flight (TOF). The quadrupole

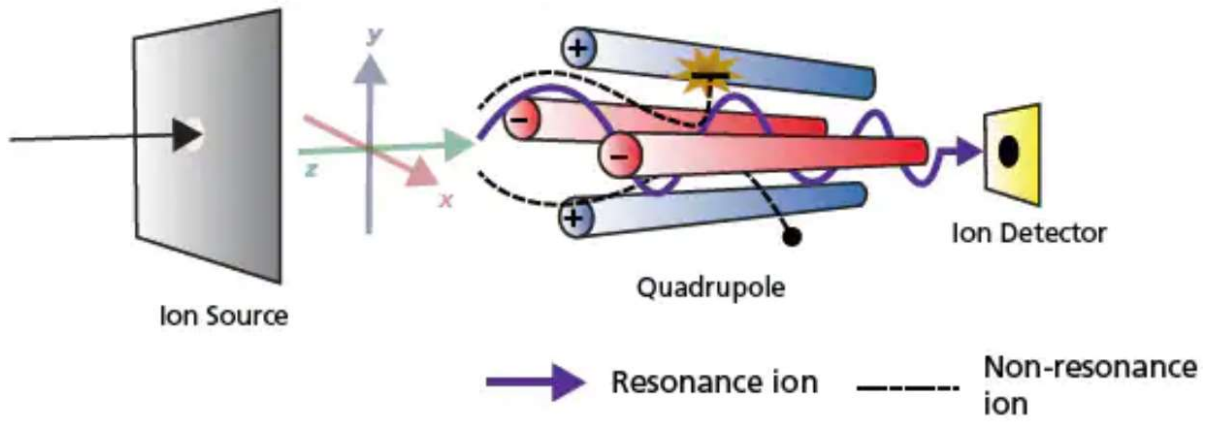

Figure 10. Schematics of a quadrupole mass analyzer. [52]

type mass analyzer (Figure 10) is the most common and less expensive among all. Though its mass resolution is not as good as other analyzers, it can work at low vacuum, which is desired when interfaced with liquid chromatography system. A quadrupole mass analyzer is comprised of four perfectly parallel cylindrical rods connected to RF and DC voltage. DC and RF voltages are applied in way that allows only a selected range of ions to have stable trajectory enabling them to reach the detector.

For a magnetic sector type mass analyzer, path and velocity of charged molecules are deflected with a magnetic field. Lighter ions are more deflected than the heavier ions. This type of mass analyzer has high resolution and good mass accuracy.

Another high-resolution type of analyzer is the TOF mass analyzer. Instead of using an electric

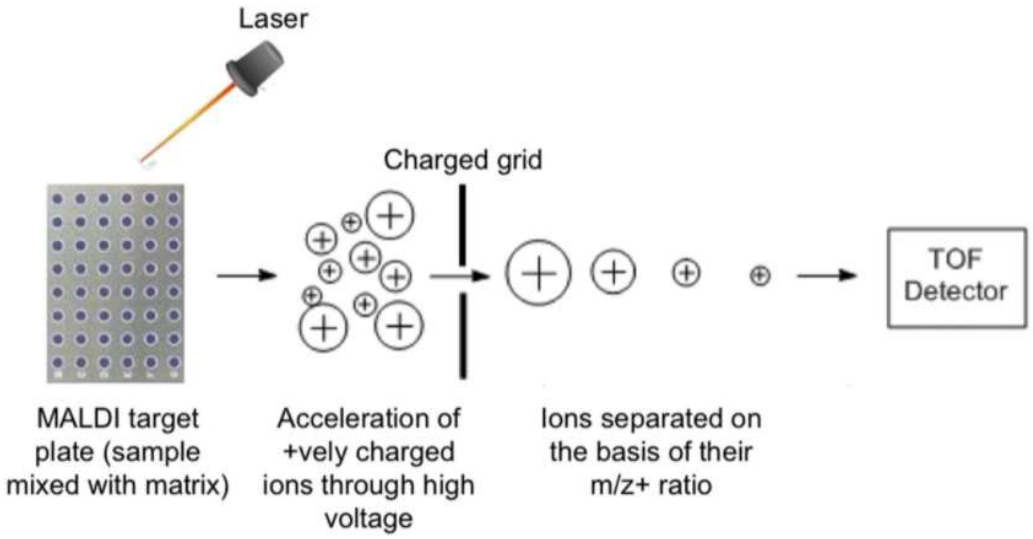

Figure 11. Schematics of a TOF analyzer [53]

field or magnetic field, TOF analyzers separate ions by time that is required to travel the same distance by each ion based on their kinetic energy and velocity. Ions enters the drift tube with the same kinetics energy but their velocities differ according to mass. Lighter ions reach the detector faster than heavier ones enabling separation (Figure 11).

The ion trap analyzer applies an oscillating electric field in such a way that enables the storage of ions by creating a stable trajectory. There are mainly two types of ion traps, a 3D and 2D ion trap.

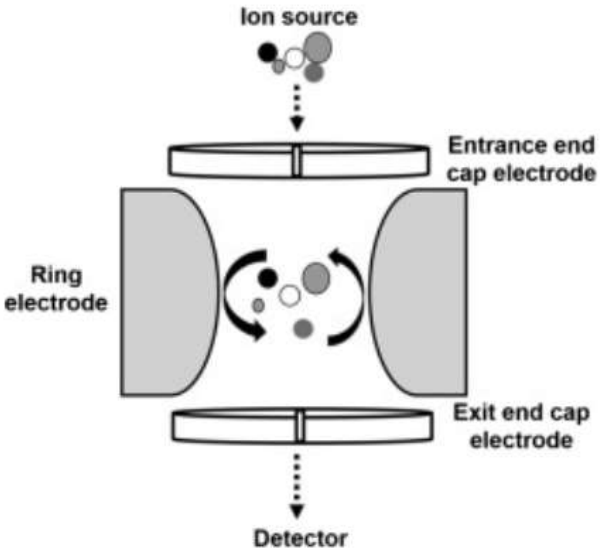

Figure 12. Schematic of Ion trap analyzer[54]

A 3D ion trap has two endcap electrodes and one ring electrode known as quadrupole ion trap (QIT) whereas 2D ion trap is called a linear ion trap (LIT).[44] An ion trap can work in multiple stages, where in the first stage selects the ions and next stage fragments these ions by collision with an inert gas. This process can be repeated to enable MS^n steps. Therefore, ion traps can produce a lot of structural information. Most recently a different type of ion trap has evolved which is called an orbitrap. This device uses electrostatic trapping, which enables high-resolution MS.

1.4.3 Ion detector

The final part of a mass spectrometer is the ion detector. Electron multipliers have been commonly used for mass detectors for a long time. When an ion hits an atom of the surface, it ejects secondary electrons. Copper-beryllium (CuBe) dynode multipliers are the oldest and can

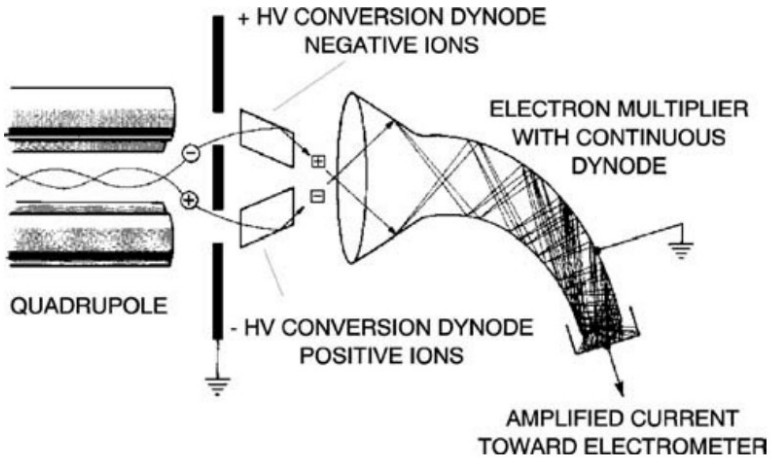

Figure 13. Continuous dynode electron multiplier[44]

produce high output currents but are relatively unstable. Aluminum-based dynodes are more stable, bulky, and relatively expensive. To increase the secondary electron emission for higher mass ions, conversion dynodes can be used. Also, there are many other detectors for tandem mass spectrometer.[45]

1.4.4 Tandem mass spectrometry

To increase the selectivity and sensitivity, mass analyzers are used in tandem mode. This mode includes multiple mass analyzers in linear configuration.[44] Tandem mass spectrometry has improved the accuracy of bioanalytical research and drug discovery and development. Many

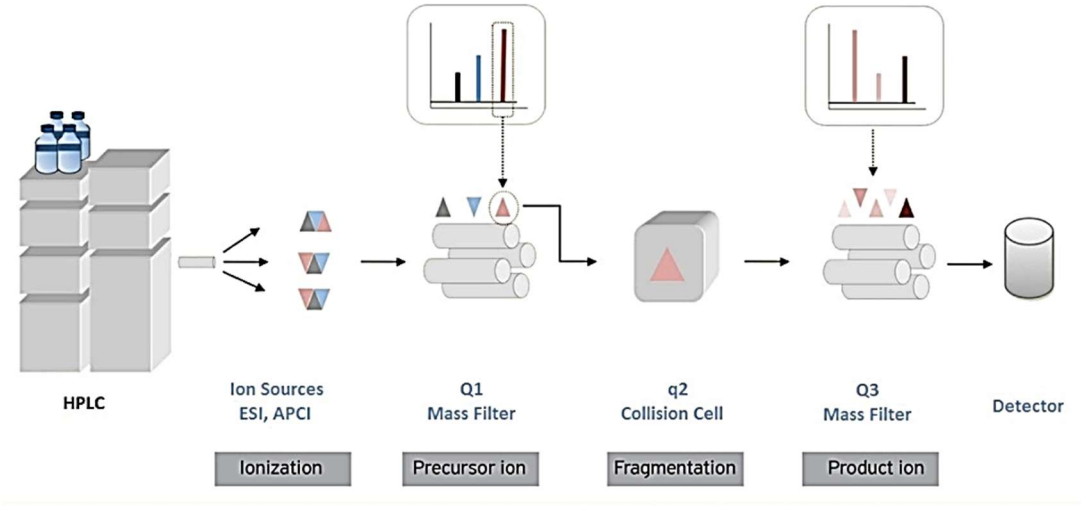

Figure 14. Schematic diagram of triple quadrupole tandem MS coupled with a LC system.

combinations of mass analyzer can be used for tandem mass spectrometry. The most widely used tandem mass spectrometer, which is well suited with liquid chromatography, is the triple quadrupole type. We already discussed the working principle of quadrupole type mass analyzer in the previous section. This type of tandem mass spectrometer has three quadrupole mass analyzers arranged in series. The first and third quadrupole act as mass filter whereas the second quadrupole acts as a collision chamber. Molecules that pass through the first quadrupole undergo fragmentation after colliding with an inert gas. ESI and/or APCI are ion sources for a triple quadrupole mass analyzer. We already know that ESI and APCI are both soft ionization techniques. Protonated or deprotonated molecules enter the first quadrupole. After ion filtration of the desired mass, fragmentation occurs in the second quadrupole entering the third quadrupole for quantification. So, even if we have multiple compounds with the same molar

mass, after fragmentation they will produce different ions. This enables the quantification of compounds in a complex matrix making the triple quadrupole a very powerful tool for clinical research.

1.5 Mass spectrometry in our pre-clinical study

Even though mass spectrometry is one of best tools for bioanalytical analysis, it demands suitable instrumentation and a skilled person for method optimization and data interpretation. Overcoming interference that can be associated with analytes in biological matrixes can be very challenging. Established analysis under GLP guidelines and exploratory analysis during the drug discovery and development stage are not same. The established analysis of a particular analyte in a specific matrix must be fully validated, which requires reference standards, a calibration curve, a quality control sample, accuracy, precision, selectivity, specificity, linearity, range, LOD and LOQ.[46] During the discovery phase, validation is not always feasible. Sometimes, synthesized standards of analytes or metabolites are not available, or stability and potency may be not known. Small changes to existing protocols are very common during the development steps but

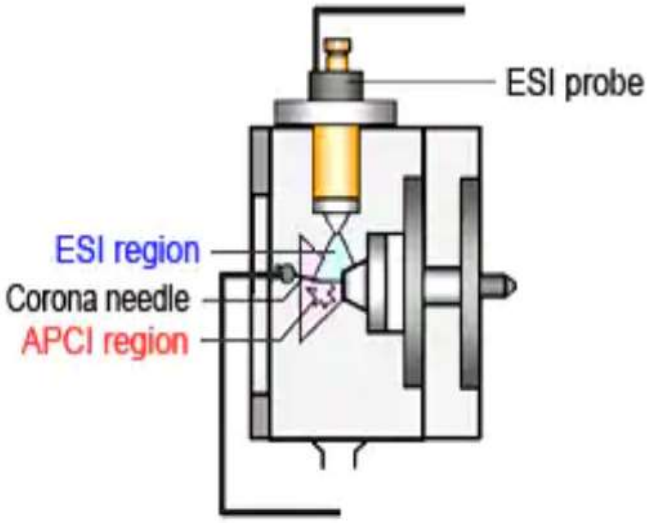

Figure 15. Schematics of Shimadzu DUIS ESI probe used in LCMS 2020 and LCMS 8040. [52]

require full validation at a later stage.[46] However, avoiding matrix effects is difficult without complete validation. So, each method should be examined for matrix effects. Calibration curves should be generated in same biological matrix if possible and internal standards should not interfere with any native signal from the matrix.

In our investigation, we used a Shimadzu LCMS 2020 (single quadrupole), a LCMS 8040 (triple quadrupole), a LC-IT-TOF and a MALDI-TOF-TOF mass spectrometer. Both single quadrupole and triple quadrupole mass spectrometer have a DUIS probe that enables both ESI and APCI ionization simultaneously (Figure 15). The LCMS 2020 is equipped with a photodiode array detector (PDA) in addition to a mass detector to enable purity determination. Area normalization of PDA signals were used for purity calculation and mass spectra were used to confirm peak purity and identification of impurities. Samples derived from urine and feces that contained very high concentrations were analyzed with the LCMS 2020-PDA. However, there were several advantages of exploring unknown metabolites with a triple quadrupole mass analyzer due to its higher sensitivity and reduced background.

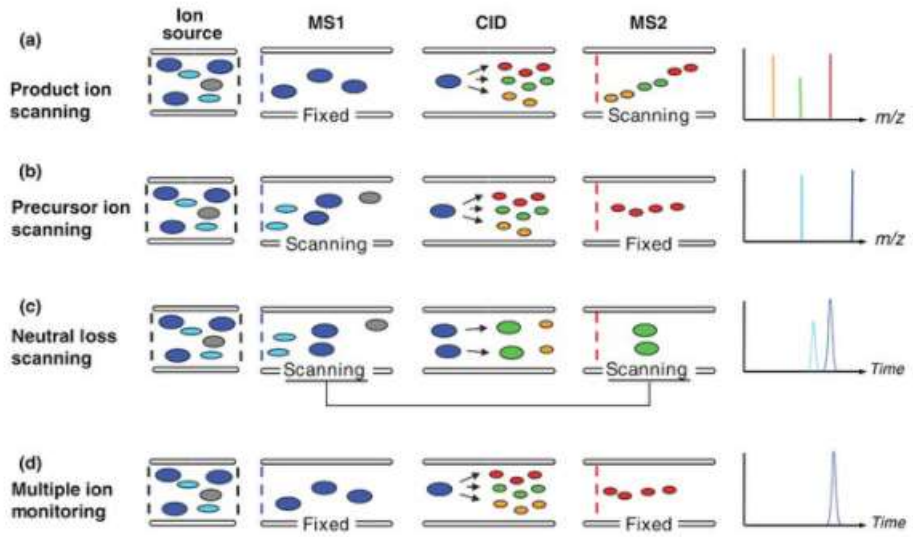

Figure 16. Different types of scanning in triple quadrupole[49]

There are four different scanning options for a triple quadrupole in addition to the full mass scanning, which include product ion scan, precursor ion scan, neutral loss scan and multiple reaction monitoring. These scanning modes that include mass isolation, mass fragmentation and mass scanning are widely used as metabolite identification strategies for small molecules in drug discovery.[47] Precursor ion scanning involves scanning in the 1st quadrupole based on specific or fixed product ion selected in the 3rd quadrupole after fragmentation in the 2nd quadrupole. This enables the identification of m/z precursor masses of a pre-selected fixed product ion. In neutral loss scanning, both the 1st quadrupole and 3rd quadrupole scanning are performed along with collision in the second quadrupole. The results depict the m/z of those precursor masses that lost a pre-selected neutral molecule during collision. These two scanning modes are very useful for detecting *in vivo* conjugation of small molecules with carbohydrates such as glucuronic acid or glucose or with amino acid such as glycine and taurine.

Most of my work was focused on quantitation that involved the LCMS 8040 in multiple reaction monitoring (MRM) mode where multiple pairs of fixed precursor ion to fixed product ion

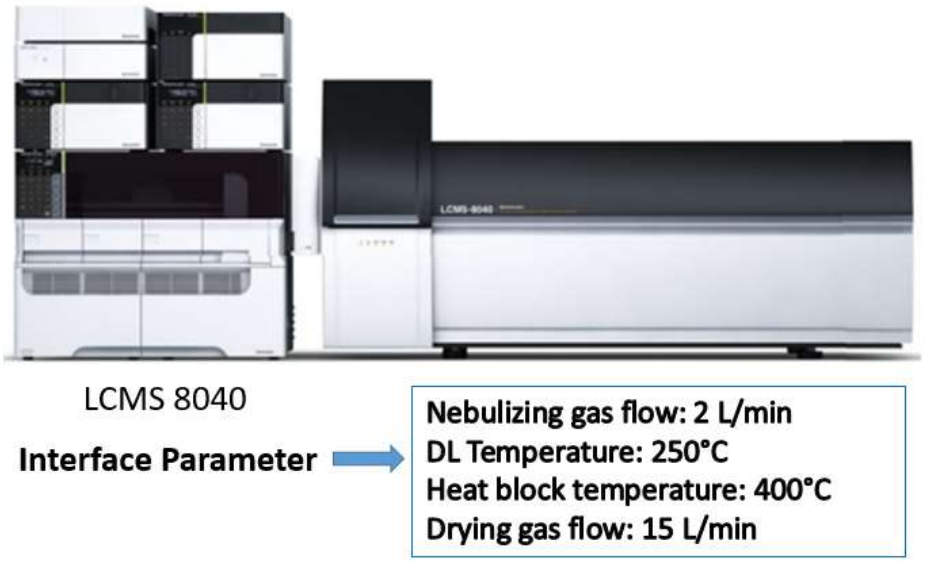

Figure 17. LCMS 8040 and its interface parameters.

transitions are used. Several precursor ions can have the same m/z but they should not have

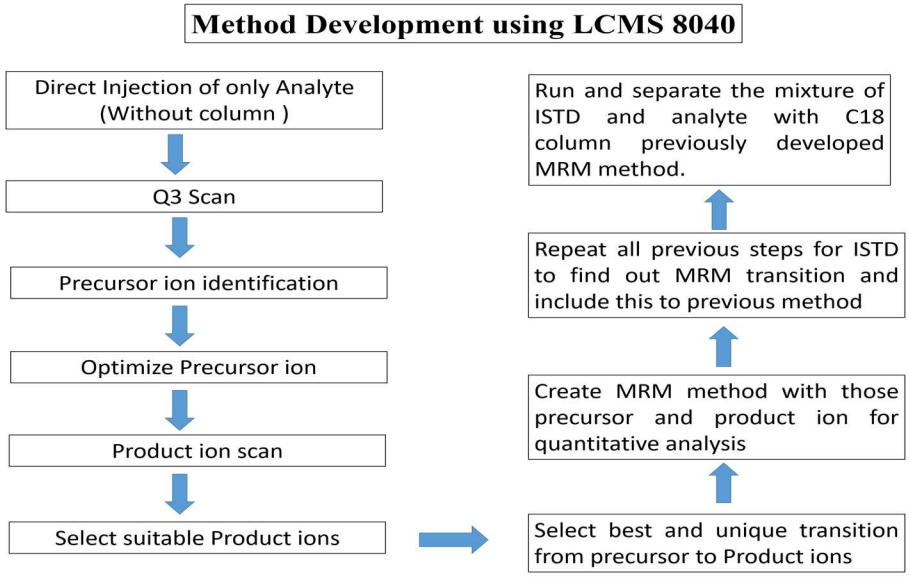

Figure 18. Schematics of method optimization in LCMS 8040

same product ions, which makes this MRM mode very selective to an analyte of interest. A schematic for general method optimization in the MRM mode is shown in Figure 18. Also, interface parameters between LC and MS units are given in Figure 17 along with the instrument. For the MRM mode, one product ion is used for quantification and at least one product ion is used for identification. More MRMs for the same analyte increase selectivity but decreases the total number of data points and can lead to non-ideal peak shape and injection to injection variation of signal. For our study, we included seven analytes and each analyte had three more MRMs except the glucoside metabolite which had two MRMs (details are in Chapter IV). To

Type	Event#	+/-	Compound Name m/z	Time (0.000 min - 10.000 min)
MRM	1	+	XHE-Acid 314.1000>268.1000, 314.1000>278.1000, 314.1000	
MRM	2	+	MIDD0301 415.9500>304.9000, 415.9500>397.9500, 413.950	
MRM	3	+	Glucoside 578.1000>416.0500, 576.1000>414.0500	
MRM	4	+	SH Acid 360.2000>249.1000, 360.1000>273.1000, 360.2000>	
MRM	5	+	Glucuronide 592.1000>305.0000, 592.1000>416.0500, 590.10	
MRM	6	+	Taurine conjugate 523.1000>356.9500, 523.1000>398.0500,	
MRM	7	+	Methyl ester midd0301 429.9000>397.9000	

Figure 19. Example of a segmented event MRM method used in our study

reduce the number of MRMs at a given time, events are segmented according to their relevant

retention time of the analytes (Figure 19). This approach is only possible if good chromatographic separation is achieved among all analytes. Alternatively, reduction of the number the MRMs to two for each analyte can be used.

Chapter 2: Physicochemical properties of asthma drug candidate MIDD0301

Physical and chemical properties of a molecule or material affect its therapeutic behavior. Some general physicochemical properties have been postulated for small molecule drugs. Lipinski's rule of five is most widely accepted for prediction of a drug-like molecule. The rule includes molecular weight, number of hydrogen bond donors and acceptors, and lipophilicity. However, there are FDA-approved drugs that do not fall within the rule of five. In this study, we determined the physicochemical properties of MIDD0301 to better understand its pharmacokinetic profile.

2.1 Plasma protein binding

An orally administered drug or xenobiotic is absorbed in the gut and undergoes first pass metabolism in the liver where biotransformation and/or elimination can occur before reaching systemic circulation. The percentage of drug that reaches systemic circulation is a measure of its bioavailability. A significant amount of drug will non-specifically bind blood plasma proteins and form an equilibrium with unbound drug. Plasma protein binding acts as a drug reservoir and can release drug gradually into the blood when "free" drug is metabolized or excreted. For this reason, the *in vivo* half-life is usually long for compounds with high protein binding. Although serum albumin and α-1-acid glycoproteins are primarily responsible for binding of acidic and basic drug, globulins and lipoproteins can also bind xenobiotics. There are several methods to determine plasma protein binding such as ultracentrifugation, ultrafiltration and equilibrium dialysis. All three methods have advantages and disadvantages; however, equilibrium dialysis is

still considered the best method for determining plasma protein binding because some of the drawbacks such as non-specific binding and protein leakage across the membrane can be minimized or avoided.[55]

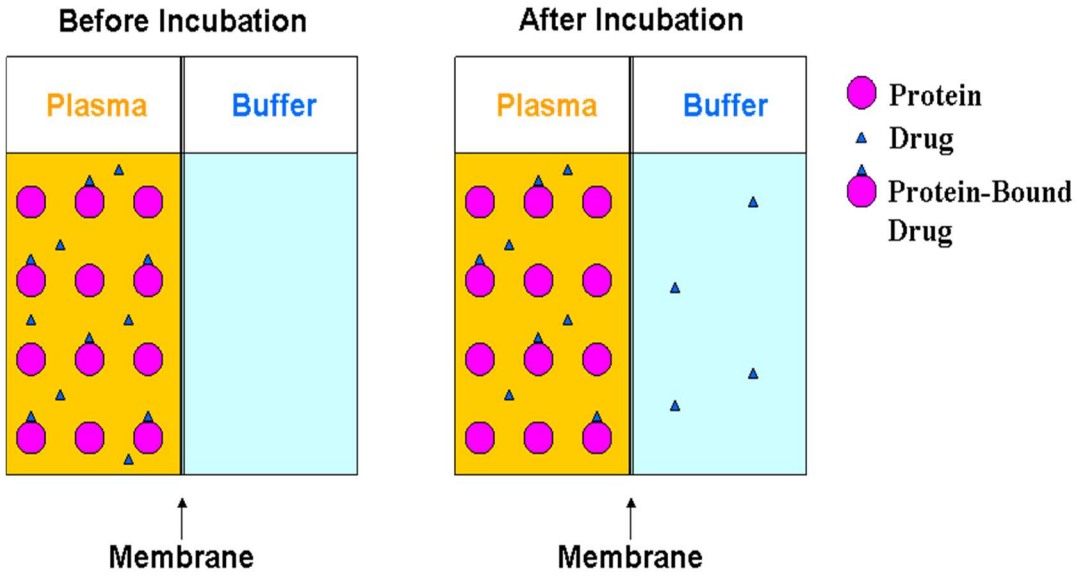

Figure 20. Illustration of equilibrium dialysis

2.1.1 Equilibrium dialysis

To conduct an equilibrium dialysis assay, a special device called rapid equilibrium dialysis (RED) plate manufactured by Thermo Scientific was used. The plate consists of 48 pairs of adjacent wells for plasma and buffer solutions. Each plasma and buffer well of a pair is separated with a membrane through which plasma protein or protein bound molecule cannot pass. Unbound drug can pass through diffusion to reach each buffer chamber. According to the manufacturer's instructions, the equilibrium dialysis plate was incubated in 37°C for 4 h while agitated at 250 rpm rotation. After incubation, the drug concentration in plasma and buffer chambers were

determined by LCMS/MS and the unbound drug concentration was determined using following equation:

% Free = (Concentration buffer chamber/Concentration plasma chamber) × 100%

% Bound = 100% - % Free

2.1.2 Method optimization using a triple quadrupole LCMS for quantitative analysis

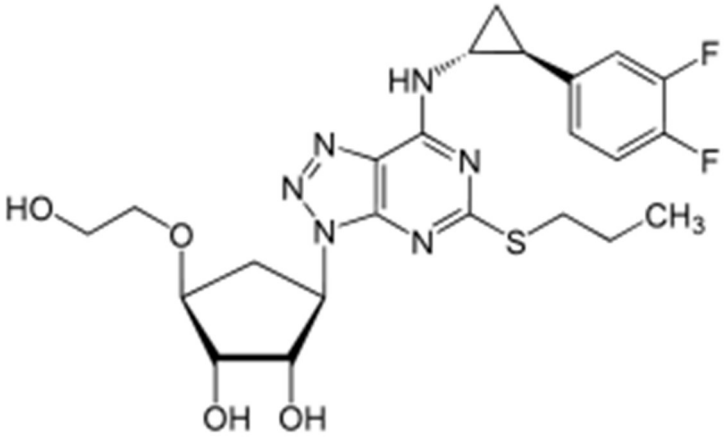

Figure 21. Structure of Ticagrelor

To optimize an assay for equilibrium dialysis, we chose ticagrelor as positive control. Its reported protein binding is 99.8%.[56] We optimized a LCMS/MS method using positive ionization and 4,5-

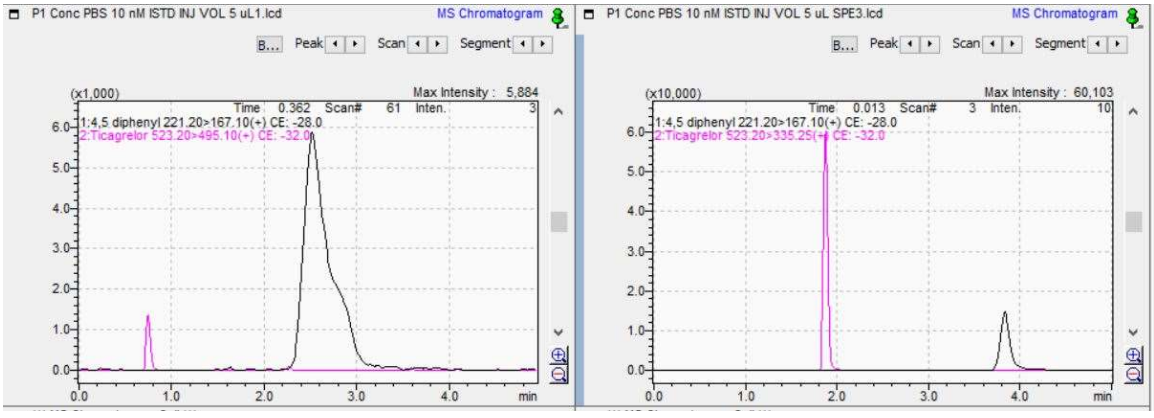

Figure 22. Mass chromatogram of ticagrelor in plasma sample after equilibrium dialysis without SPE (left) and with SPE.

diphenylimidazole as internal standard. At this point, the triple quadrupole mass spectrometer

present in Shimadzu Laboratory at Kenwood Interdisciplinary Research Complex (KIRC) was equipped with an online solid phase extraction unit. We experienced significant signal suppression near the 1 min region without online SPE (Figure 22).

At a later stage, it was found that employing a drying and reconstitution step during the sample preparation will avoids the ionization suppression. However, at that time we optimized the

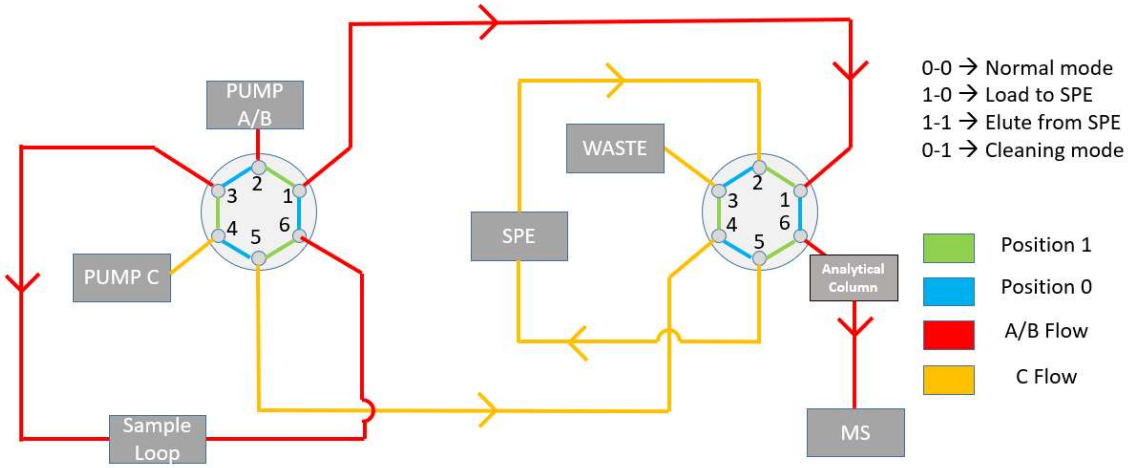

Figure 23. Diagram of online SPE unit to Shimadzu 8040

method using SPE. A schematic diagram of online SPE depicted in Figure 23. After achieving a successfully analysis with ticagrelor, we applied this protocol to analyze MIDD0301 to determine the plasma protein binding for human and mouse plasma. The optimized method is described in section 2.1.3

2.1.3 Experimental

Solutions of 1 mM MIDD0301 and 500 nM of 4,5 diphenyl imidazole were prepared in methanol. Mouse plasma was thawed on ice and 495 µl was dispensed into an Eppendorf tube together with 5 µl of 1 mM MIDD0301. 400 µl of this solution was transferred into the red marked retainer well of a rapid equilibrium dialysis device (Thermo Scientific). 600 µl PBS buffer was added to the

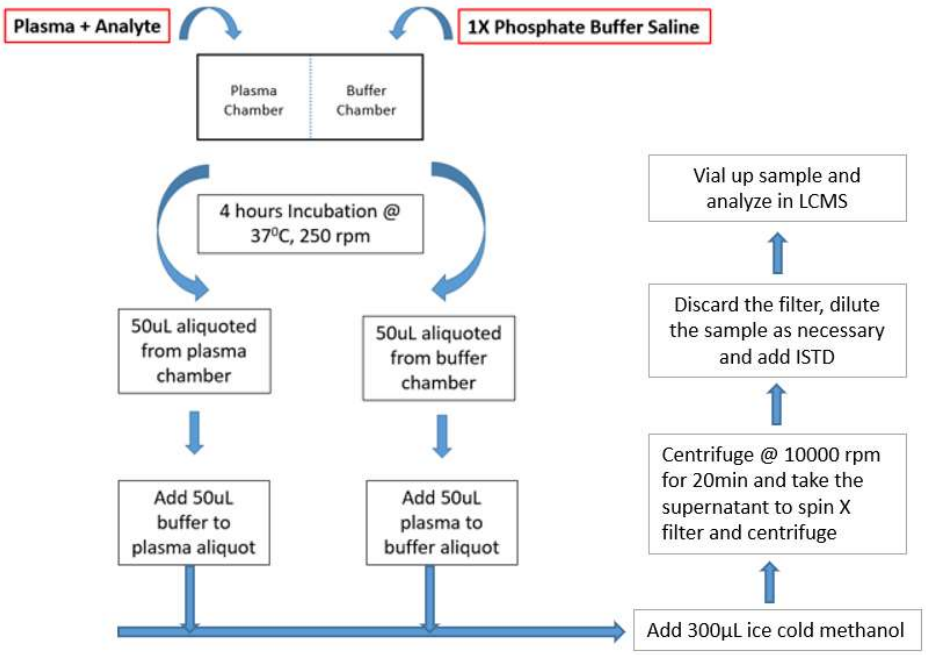

Figure 24. Schematics of equilibrium dialysis assay

adjacent buffer chamber. This was repeated three times at different locations in the plate. The plate was sealed with tape and placed into a shaker for 4 h using an orbital shaking rate of 250 rpm. A 50 µl sample from the red well was transferred to an Eppendorf tube and combined with

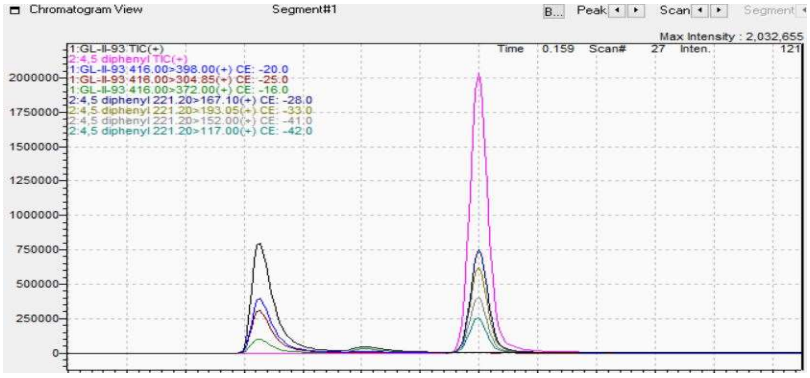

Figure 25. An exemplary mass chromatogram of optimized MIDD0301 and ISTD

50 µl PBS. Similar, a 50 µl sample from the buffer well was transferred to an Eppendorf tube and combined with 50 µl mouse plasma. 300 µl of ice-cold methanol was added to each of the tubes to precipitate proteins. The tubes were vortexed and incubated 30 min on ice followed by

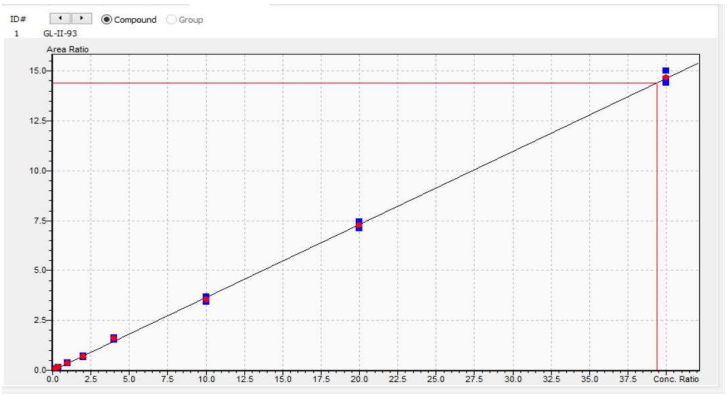

Figure 26. An exemplary calibration curve of MIDD0301 and ISTD

centrifugation for 10 min at 11,000 x g. 50 µl of supernatant was added to a new Eppendorf tube and combined with 25 µl of a 500 nM 4,5-diphenylimidazole solution as ISTD followed by the addition of 425 µl of methanol. The samples were analyzed by LCMS/MS using a Shimadzu 8040 instrument. Quantifications was achieved by using a calibration curve. The assay was repeated three times.

2.1.4 Results and discussion

It was found that MIDD0301 is highly bound to mouse and human plasma proteins. The average free drug found in mouse plasma was 11.3 % whereas for human plasma it was 4.3 %. MIDD0301

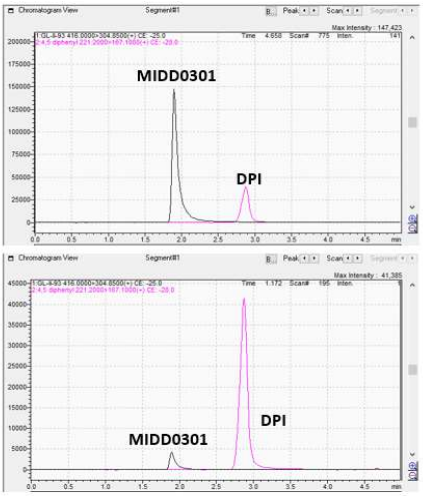

Conditions (Reverse phase)
System: Shimadzu LCMS 8040
Mobile phase A: 0.1% formic acid in water
Mobile phase B: 01% formic acid in Methanol
Flow rate: 0.6 mL/min
Column: Pinnacle II C18 5um
Dimension: 50X4.6mm

For online SPE
Cartridge: Ultra II BiPh
Mobile phase C:80/20 : 0.1formic acid in water/Methanol
Pump C flow: 0.2mL/min
Loading time: 1min

Gradient time program
(Pump A &B)

	Time	Module	Command	Value
1	0.01	Pumps	B.Conc	75
2	1.00	Column Oven	CTO.RVR	1
3	1.00	Pumps	B.Conc	75
4	3.50	Pumps	B.Conc	85
5	3.75	Pumps	B.Conc	99
6	4.00	Column Oven	CTO.RVL	0
7	4.15	Pumps	B.Conc	99
8	4.50	Column Oven	CTO.RVL	1
9	4.50	Column Oven	CTO.RVR	0
10	4.50	Pumps	B.Conc	75
11	5.00	Controller	Stop	

Figure 27. Chromatograms of MIDD0301 from plasma (top) and buffer chamber of an equilibrium dialysis plate using mouse plasma.

has a carboxylic acid group, thus most of the protein binding can be attributed to serum albumin. The average concentration of serum albumin found in human plasma is 35-50 mg/mL, whereas less than 35 mg/mL are found in mouse plasma.[57,58] Thus, it can be concluded that the lower free concentration of MIDD0301 in human plasma is due to the higher concentration of serum albumin.

Table 1 Unbound MIDD0301 in mouse plasma

ID	MIDD0301 concentration in Plasma (nM)	MIDD0301 concentration in Buffer (nM)	Free Drug %
Assay 1	1551.25	172.08	11.09
Assay 2	1503.45	178.90	11.90
Assay 3	1687.80	185.73	11.00

Table 2 Unbound MIDD0301 in human plasma

ID	MIDD0301 concentration in Plasma (nM)	MIDD0301 concentration in Buffer (nM)	Free Drug %
Assay 1	1676.04	73.50	4.39
Assay 2	1769.75	76.07	4.30
Assay 3	1644.98	69.21	4.21

2.2 pKa, pH dependent aqueous solubility, interconversion kinetics of closed and open MIDD0301 and effect of pH on bioavailability

MIDD0301 has a carboxylic acid function and a basic imine. These features result in a pH-dependent compound solubility and conversion of the seven-membered ring to an open-ring benzophenone structure under acidic conditions. The equilibrium has been evaluated for 1,4-benzodiazepin-2-ones using NMR (diazepam,[60] fludiazepam,[60] and flurazepam[61]) and UV absorption (diazepam,[62] triazolobenzodiazepine estazolam[63] and imidazobenzodiazepine midazolam).[64] Sternbach et al. reported the formation of 1,4-benzodiazepin-2-ones under basic conditions and speculated that similar but less pronounced pharmacological properties of acyclic aminoacetoamido compounds were due to cyclization in vivo.[65] A later report from Hoffmann-LaRoche confirmed the ring opening reaction for imidazobenzodiazepines under acidic conditions in addition to the isolation of a dihydrochloride salt.[66] MIDD0301 is an oral medication and will therefore be first exposed to acidic environment in the stomach and more basic conditions in the intestine. So, it is very important to determine the ring opening and ring closing kinetics of MIDD0301 and how these interconversions affect the bioavailability. In this project, a detailed evaluation of pH-dependent solubility and lipophilicity (log D) of MIDD0301 is described. Kinetics of the ring opening and closing reactions at gastric and intestinal pH were determined by NMR and spectrophotometry. Finally, different formulations were examined to determine if gastrointestinal pH differences influence the *in vivo* absorption of MIDD0301.

2.2.1 Experimental – Determination of pKa value of MIDD0301

To determine the acid−base behavior of MIDD0301, two different methods were employed, which included a titration of a basic MIDD0301 solution with 1 N HCl while recording the pH values and a spectrophotometric method using MIDD0301 solutions with different pH.

2.2.1.1 Titration method

A 50 µM solution of MIDD0301 was prepared in 0.1 M aqueous NaOH with 30% DMSO. The solution was stirred continuously at 25°C with an emerged pH electrode. To this solution a 1M HCl solution was added in small intervals and pH values were continuously recorded. The solution was clear throughout the experiment. pH vs amount of acid added was plotted and the pH of the transition was determined by nonlinear regression. Several attempts were made to use less DMSO for this experiment but between pH 2 and 4 the solution became cloudy if the percentage of DMSO was less than 30%.

2.2.1.2 Spectrophotometric method

Two microliters of a 5 mM solution of MIDD0301 was added into a 96 well polypropylene plate (Nunc, 249944) followed by the addition of 198 µL of buffered water at different pH values. The following buffers were used and adjusted with KCl to an ionic strength of 0.1 M: pH 9, 12.5 mM borate buffer; pH 8, 7, and 6, 50 mM phosphate buffer; pH 5, 4, and 3, 50 mM acetate buffer; and pH 2 and 1, 50 mM phosphoric acid buffer. The solutions were mixed four times by aspiration and dispensing. Two 40 µL of aliquots from the same well were transferred into a 384 well plate (Coring UV star, 781801). The plate was incubated at room temperature for 24 h followed by absorbance detection over a range of 230−400 nm with 2 nm increments (Tecan M1000).

Buffered water (198 µL) with 2 µL of DMSO was used for background subtraction. The absorbance average of two independent measurements in duplicate were plotted versus the wavelength.

2.2.2 Experimental – Determination of pH dependent solubility

Two milligrams of closed MIDD0301 were added to 200 µL of buffered water at different pH values and agitated with a horizontal shaker in a closed vial for 24 h. The mixtures were transferred to an Eppendorf tube and centrifuged for 5 min at 16,000 x g followed by pH determination of the supernatant. Three independent aliquots of 10 µL were added to 190 µL of 50:50 methanol/buffer water (25 mM phosphate buffer, pH 10), and after mixing, 40 µL was transferred into a 384 well plate (Coring UV star, 781801) for UV detection at 270 nm (Tecan M1000). The assay was carried out with three independent measurements for each pH. The concentration of each solution was determined with a calibration curve in 50:50 methanol/buffer water (25 mM phosphate, pH 10).

2.2.3 Experimental – Determination of pH dependent equilibria of close and open ring MIDD0301

Ten milliliters of 50 µM aqueous solution of closed MIDD0301 was adjusted to pH 1 using 0.1 M HCl. Before adjusting the pH value to 2 using a 10% ammonium hydroxide solution, a 400 µL of aliquot was taken and labeled as pH 1. This procedure was repeated until pH 9 was reached. Aliquots were kept at room temperature for 24 h followed by final pH determination. The

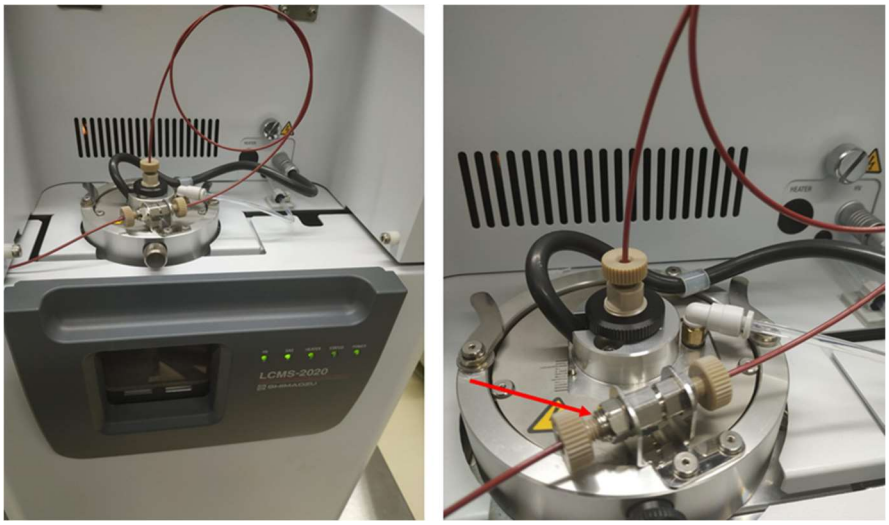

Figure 28. (A) Mass detector of LCMS 2020 (single quadrupole). (B) MIDD0301 solutions injected directly (arrow indicated) to the interface with a help a syringe and adapter without mobile phase.

solutions were injected directly into a mass detector with a syringe, needle adapter, and connector without any additional solvent (Shimadzu 2020). The peak heights of 414 and 432 m/z were measured to determine the ratio between the open and closed form of MIDD0301.

2.2.4 Experimental – In vitro interconversion kinetics between close and open ring MIDD0301

Four aliquots of 5 µL of a 1 mM solution of closed or open form of MIDD0301 were added to a 384 well plate (Coring UV Star) followed by the addition of 75 µL of buffered water at pH 2 or 8.

The solutions were mixed, and absorbance at 246 nm were recorded every 30 seconds over a period of 260 min. Buffered water with 5 µL of DMSO was used for background subtraction. The average absorbance was plotted versus time and analyzed using first-order kinetics to determine k and half-life.

2.2.5 Experimental – Pharmacokinetic studies of different formulations of MIDD0301 to evaluate their effect on bioavailability

Six-week-old female Swiss Webster mice (Charles River Laboratory, WIL, MA) were housed under specific pathogen-free conditions, under standard conditions of humidity, temperature, and a controlled 12 h light and dark cycle, and had *ad libitum* access to food and water. All animal experiments were in compliance with the University of Wisconsin-Milwaukee Institutional Animal Care and Use Committee (IACUC). Animals received an intragastric gavage of the closed or open form of MIDD0301 formulated in different vehicles at a dose of 25 mg/kg. At 60 min, blood was collected via cardiac puncture and placed into heparinized tubes. Lungs and brains were harvested and stored in liquid nitrogen until analysis (n = 4).

Blood samples were thawed on ice and vortexed for 10 sec and a 100 µL aliquot was combined with 400 µL of cold methanol containing 300 nM XHE-III-74A as the internal standard (I.S.). Samples were vortexed for 30 s and centrifuged at 16,000 x g for 10 min at 4 °C. The supernatant layer was then transferred into clean tubes and evaporated using a Speedvac concentrator. The residue was reconstituted with 400 µL of methanol and spin-filtered through 0.22 µm nylon centrifugal filter units (Costar). After reconstitution, the samples were diluted if needed and 4,5-diphenylimidazole was added as instrument standard. The injection volume was 5 µL (LCMS/MS,

Shimadzu 8040). Brain and lung tissue samples were thawed, weighed, and homogenized directly into 400 or 600 µL of methanol, respectively, containing 300 nM XHE-III74A[67] (I.S.) using a Cole-Palmer LabGen 7B Homogenizer. Samples were centrifuged for 10 min at 16,000 x g at 4 °C. The supernatant was then spin-filtered through 0.22 µm nylon centrifugal filter units (Costar) and evaporated using a Speedvac concentrator. After reconstitution with 200 or 400 µL of methanol for the brain and lung, respectively, 4,5-diphenylimidazole was added after spin-filtration through 0.22 µm nylon centrifugal filter units. The injection volume was 5 µL (LCMS/MS, Shimadzu 8040). High-performance liquid chromatography was performed with Shimadzu Nexera X2 LC30AD series pumps (Shimadzu, Kyoto, Japan). Analytes were separated with an Agilent RRHD Extend-C18 (2.1 mm × 50 mm, 1.8 µm particle size) column with gradient elution at a flow rate of 0.5 mL/min. The mobile phase was methanol and water (both containing 0.1% formic acid). Time program: 20% B (0 min) → 45% B (2 min) → 99% B (4 min), hold at 99% B (4.75 min), return to 20% B (5 min), hold at 20% B (1.5 min); column temperature: ambient. Analytes were monitored under positive mode using a Shimadzu 8040 triple quadrupole mass analyzer (Shimadzu, Kyoto, Japan) electrospray and atmospheric pressure ionization run in dual (DUIS) mode. The following transitions were monitored in multiple reaction monitoring (MRM) mode. Ion pairs were as follows: closed MIDD0301: m/z 415.95 > 305.00, m/z 415.95 > 398.00, m/z 415.90 > 357.0, and m/z 415.90 > 329.00; open MIDD0301: m/z 433.90 > 276.95, m/z 433.90 > 398.95, and m/z 433.90 > 347.00; and XHE-III74A: m/z 314.10 > 368.10, m/z 314.10 > 278.10, and m/z 314.10 > 296.15. Transition pairs for 4,5-diphenylimidazole were m/z 220.80 > 193.10, m/z 220.80 > 166.90, m/z 220.80 > 151.95, and m/z 220.80 > 116.10. Collision energy was optimized for each transition to obtain optimal sensitivity. The mass spectrometer was operated with a heat

block temperature of 400 °C, drying gas flow of 15 L/min, desolvation line temperature of 250 °C, nebulizing gas flow of 1.5 L/min, and both needle and interface voltages of 4.5 kV. The response acquisition was performed using LabSolutions software. Standard curves were fitted by a linear regression, and the validation samples were calculated back by the calibration curve of that day. The mean and the standard deviation were calculated accordingly.

2.2.6 Results and discussion

The acid titration of a basic solution of MIDD0301 resulted in a sharp decrease in pH after

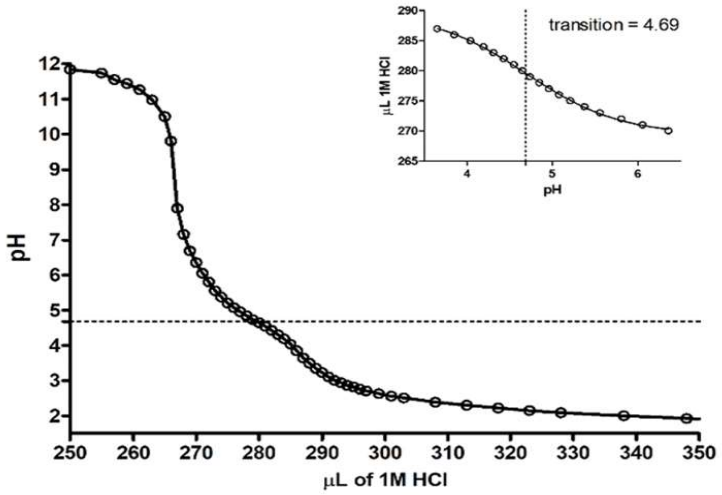

Figure 29. Acid titration of MIDD0301 dissolved 0.1 M NaOH in water with 30% DMSO.

neutralization of the initial NaOH solution (Figure 29). At pH between 7 and 6, a very small change in the curve was observed but it was less pronounced than the change between pH 5 and 4. Using nonlinear regression, the inflection was calculated to occur at pH 4.69. Additionally, we used the pH-dependent absorbance plots depicted in Figure 30A and plotted the change of each plot for the absorbance at 252 and 292 nm versus pH to determine the pH value of the transition (Figure 30B).[68] The pH value of 4.34 was similar to the value calculated by the titration experiment.

Investigations with imidazobenzodiazepine midazolam reported pKa values for imidazole

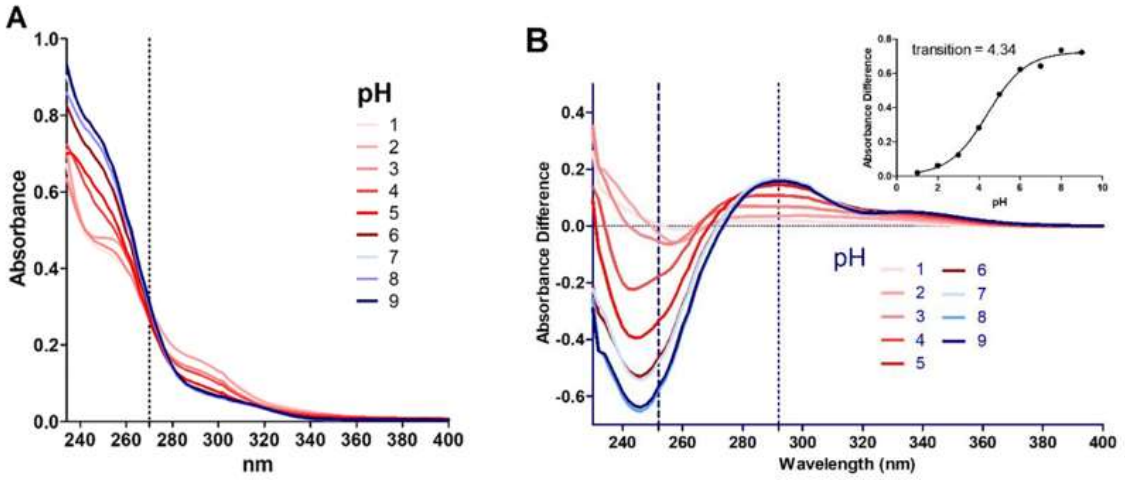

Figure 30. (A) Absorbance spectra of MIDD0301 in aqueous buffered solution with 1% DMSO (B) Plot of spectral difference between solutions of MIDD0301 at different pH values. Inset: plot of absorbance difference versus pH to determine the pH value of the spectrophotometric transition.

nitrogen of 6.15 and 6.04;[64] however, the acid function of MIDD0301 at the 3- position reduces the basicity of the imidazole nitrogen (Figure 31), which is probably similar to the reported pKa of flumazenil (1.7) bearing a carboxylic ester function at the 3-position.[69]

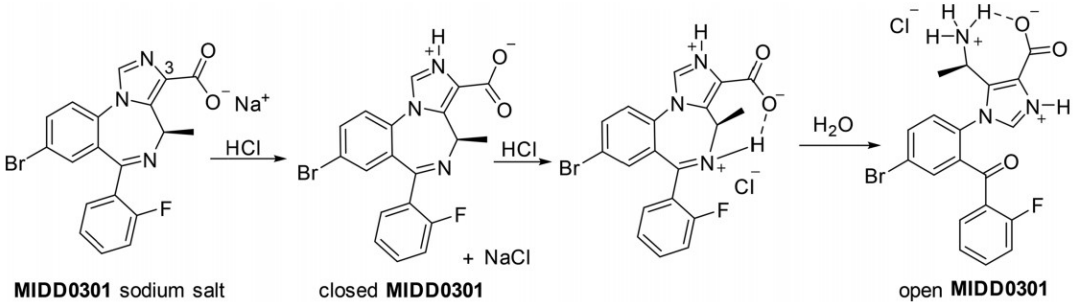

Figure 31. MIDD0301 and its structures at different pH value.

To systematically determine the solubility of MIDD0301 in water at different pH values, we applied a "shake flask" method and determined the concentration using UV absorption. The results are depicted in Figure 32. UV measurements of 50 µM MIDD0301 in buffered water over a pH range of 1−9 after equilibration for 24 h resulted in spectra with an isosbestic point at 270 nm, at which point the structures of MIDD0301 have a similar total absorbance (Figure 30A &

32). Similar pH-dependent absorbance was reported for midazolam with an isosbestic point of

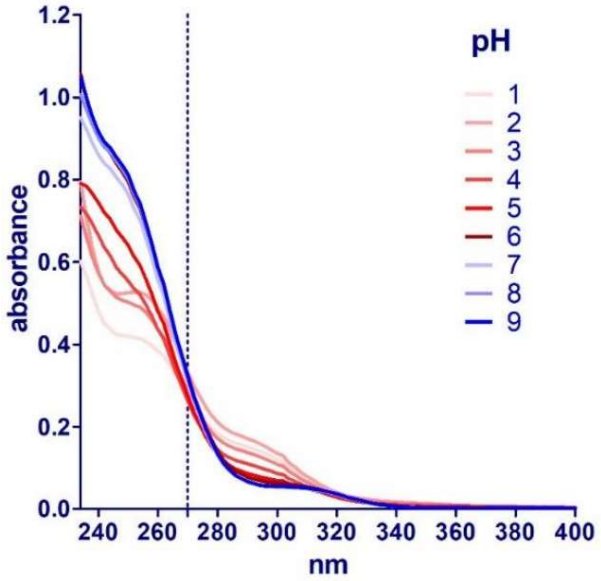

Figure 32. Absorbance spectra of MIDD0301 (Open ring) in aqueous buffered solution with 1% DMSO at 50 µM

255 nm.[64] Subsequently, the aqueous solubility of MIDD0301 at different pH values was determined by a shake flask method using UV absorbance measurements at 270 nm (Figure 33).

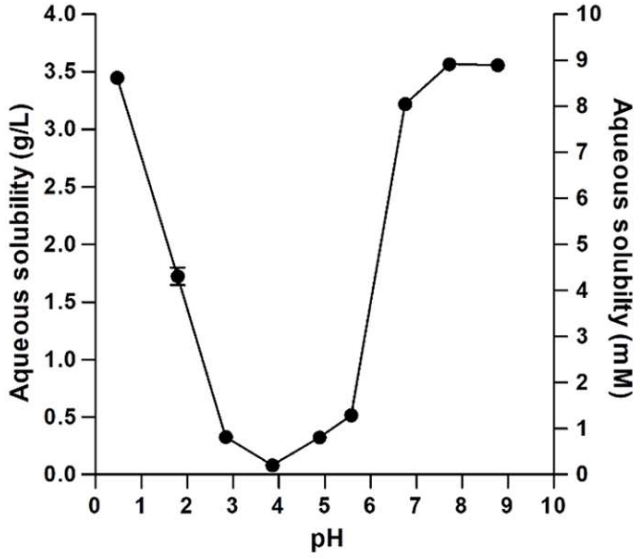

Figure 33. Solubility of MIDD0301 at different pH values in water determined after 24 h in a shake flask using UV absorption at 270 nm.

Excellent solubility of MIDD0301 was observed at neutral pH (>3 g/L); whereas less than a 100 mg/L was soluble at pH 3.9. This behavior is unlike midazolam, which is less soluble at neutral pH

(70 mg/L) but more soluble at lower pH due to the protonation of imidazole nitrogen.[64] In addition to basic imidazole nitrogen, MIDD0301 has a carboxylic acid group, and thus a neutral zwitterionic species is formed at pH 5 (Figure 31). Similar to amino acids, MIDD0301 has its lowest solubility at the isoelectric point.[70]

Mass spectrometry was used to evaluate the possibility that, even under mildly acidic conditions, MIDD0301 converts from a closed to an open form causing a change in absorbance and pKa, consistent with the conversion of an imine to a primary amine (Figure 31). Protonation of the imine is expected to activate the electrophilic carbon center, enabling water to act as a nucleophile. The subsequent carbinolamine is expected to form a ketone after proton transfer and cleavage of the carbon−nitrogen bond. In contrast to the buffered solutions employed for the spectrophotometric analysis of MIDD0301 at different pH values, the solutions of MIDD0301 were adjusted with 0.1 M HCl to minimize ion suppression in MS analysis. After 24 h, the solutions were injected directly into the mass spectrometer to prevent any changes in the equilibrium

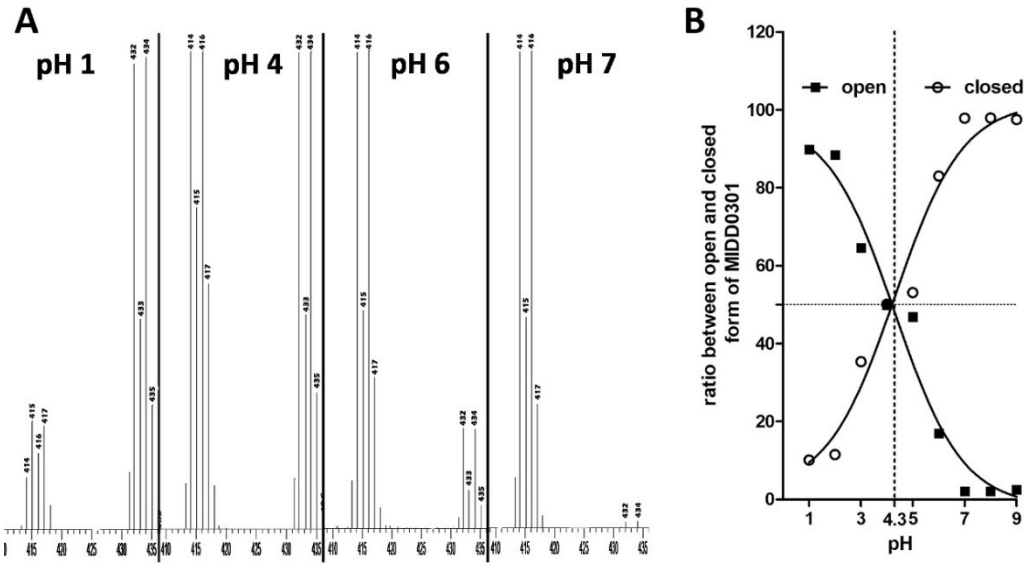

Figure 34. (A) Representative MS spectra of MIDD0301 at different pH values. (B) Ratios of peak heights at 414 m/z (closed MIDD0301) and 432 m/z (open MIDD0301). At pH 4.3, both compounds were present at the same peak height ratio.

caused by liquid chromatography. The MS spectra for representative pH values are depicted in Figure 34A, and the ratios of the peak heights at 414 m/z (closed MIDD0301) and 432 m/z (open MIDD0301) are plotted versus pH in Figure 34B. For the detection of positive ions, closed MIDD0301 has two predominate mass peaks caused by ^{79}Br and ^{81}Br (414 and 416 m/z, respectively). In contrast, open MIDD0301 has two equivalent mass peaks at 432 and 434 m/z. At pH 7 and higher, 414/416 m/z is the main mass signal with only 2% of open MIDD0301. This ratio was observed for *in vivo* quantification of MIDD0301, which included stability assays and pharmacokinetic studies.[71] At pH 6, an increase in open MIDD0301 (17%) was observed after 24 h. This implies that the concentration of H_3O^+ at this pH was high enough to slowly catalyze the hydrolysis of the imine to the amine. The equilibrium between open and closed MIDD0301 in water was observed between pH 4 and 5. A calculated equilibrium pH of 4.3 was similar to the transition determined for the acid titration (4.69) and by UV spectrophotometry (4.34). At pH 3 and lower, open MIDD0301 is the major species; however, even in the presence of 0.1 N HCl after 24 h, 10% of closed MIDD0301 remained.

Next, we investigated the kinetics of the conversion of closed to open MIDD0301 in 0.1 N HCl (gastric pH) and conversion of open to closed MIDD0301 at pH 8 (intestinal pH) using ^1H NMR and UV spectrophotometer. Although kinetic studies using NMR have the advantage of structural identification, the drawbacks are high concentrations, the need for co-solvents to enable high concentrations, and slow acquisition time. To better reflect the conditions of an orally administered drug, spectrophotometry can be carried out at lower concentration, thus omitting the use of co-solvent DMSO and allowing faster acquisition. Based on the absorbance spectra determined for MIDD0301, a wavelength of 246 nm was used to differentiate between closed

and open MIDD0301. Applying first-order kinetics, a k_{acid} of 0.142 min^{-1} and a k_{base} of 0.024 min^{-1} were calculated (Figure 35 A & B). In comparison to the NMR-based analysis, which was carried out by my co-workers, a seven times faster ring opening reaction was observed. Interestingly, both reactions were accelerated at lower concentration in the absence of DMSO, supporting the involvement of a highly charged transition state for this reaction. The half-life for closed MIDD0301 in 0.1 N HCl was 4.8 min, implicating the presence of a significant amount of open

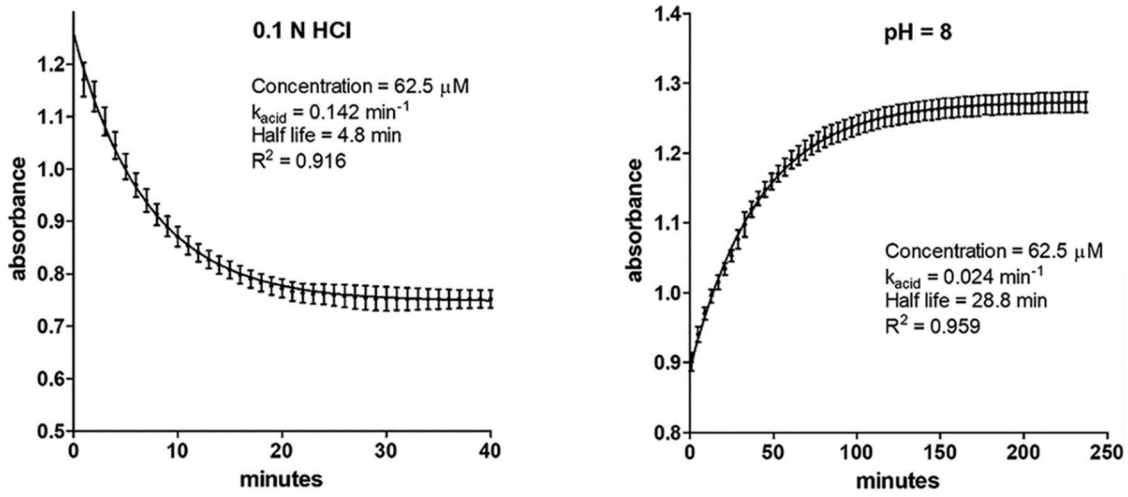

Figure 35. (A) Time-dependent conversion of 62.5 μM closed MIDD0301 in aqueous 0.1 N HCl analyzed by UV absorbance at 246 nm. (B) Time-dependent conversion of 62.5 μM open MIDD0301 in 50 mM aqueous phosphate buffer adjusted to pH 8 analyzed by UV absorbance.

MIDD0301 in the stomach. The half-life of open MIDD0301 at pH 8 was 28.8 min. Identical UV and NMR spectra were obtained using closed or open MIDD0301 at the same pH after the equilibrium was reached.

The bioavailability of MIDD0301 formulated at different pH values was determined. Groups of four Swiss Webster mice were administered 25 mg/kg oral doses of either closed or open MIDD0301. Blood, lung, and brain concentrations of open and closed MIDD0301 were quantified by LCMS/MS 60 min after administration. The results are summarized in Table 3.

Table 3 Concentration of closed and open MIDD0301 60 min after oral administration of MIDD0301 using different formulation

Nr	Compound	Vehicle	Concentration of closed MIDD0301 (nM)[d]			Concentration of open MIDD0301 (nM)[d], % of closed MIDD0301		
			Blood	Lung	Brain	Blood	Lung	Brain
1	Closed MIDD0301	2.5 % PEG400[a] 98 % HPMC[b] (2 % in water)	322±65	287±46	87±27	9±3 3%	5±2 2%	3±1 2%
2	Closed MIDD0301	40 % propylene glycol, 60 % HPMC[b] (2 % in water)	239±37	455±47	104±42	6±2 3%	9±2 2%	3±1 3%
3	Closed MIDD0301 Na^+ salt	10 % PEG400 90 % HPMC(2 % in water)	154±58	306±106	118±58	5±2 3%	5±1 2%	2±1 2%
4	Closed MIDD0301	2.5 % PEG400[a] 98 % HPMC[b](2 % in PBS[c])	413±116	1745±1121	130±24	18±14 4%	28±19 2%	4±3 3%
5	Pretreatment with Omeprazole	100 % HPMC[b] (2 % in carbonate buffered water, pH 9)	516±180	2046±1155	159±33	20±8 4%	32±21 2%	4±2 3%
	Closed MIDD0301	2.5 % PEG400[a] 98 % HPMC[b](2 % in PBS[c])						
6	Open MIDD0301	2.5 % PEG400[a] 98 % HPMC[b](2 % in 0.1 N HCl)	371±104	1792±296	130±42	14±7 4%	35±8 2%	4±2 3%

First, closed MIDD0301 was suspended in polyethylene glycol 400 (PEG400) and diluted further with a 2% solution of hydroxypropyl methylcellulose (HPMC) in water (Table 3, entry 1). This viscous suspension had a pH value of 6.1. One hour after administration of closed MIDD0301 by

gavage at a dose of 25 mg/kg in a volume of 3.3 mL/kg, we observed concentrations of 322 nM in blood and 287 nM in the lung. The concentration of closed MIDD0301 in the non-perfused brain was 30% of the lung concentration, representing good tissue selectivity for an oral asthma drug candidate. The concentration of open MIDD0301 was similar in all samples ranging between 2 and 3% of closed MIDD0301. A 1:1.5 ratio between propylene glycol and a 2.5% solution of HPMC in water gave a clear 18.1 mM solution of closed MIDD0301 with a pH value of 5.9 (Table 3, entry 2). This solution was administered at the same dose and volume as entry 1 and resulted in a lower blood concentration of closed MIDD0301 (239 nM) but a higher lung concentration (455 nM). The concentration of open MIDD0301 did not change significantly among the blood, lung, and brain samples. The sodium salt of closed MIDD0301 when dissolved in a 10% solution of propylene glycol in a 2.5% aqueous solution of HPMC had a pH value of 8.2 (Table 3, entry 3). When administrated at 25 mg/kg, a blood concentration of 154 nM of closed MIDD0301 was detected after 60 min, which was the lowest blood concentration detected among all formulations. The concentration of closed MIDD0301 was 306 nM in the lung and 118 nM in the brain. The concentration of open MIDD0301 was 5 nM in blood, 5 nM in the lung, and 2 nM in the brain. A superior neutral formulation for closed MIDD0301 was achieved by preparing a 2% HPMC solution in phosphate buffered saline (pH 7.4) with the addition of 2.5% PEG400. The viscous mixture exhibited minimal turbidity due to the high solubility of MIDD0301 at that pH (Figure 33). After 1 h, a blood concentration of 413 nM and lung concentration of 2046 nM were detected for closed MIDD0301. Thus, the lung concentration of MIDD0301 was six times higher for the neutral buffered formulation than for the non-buffered formulation. The concentration of closed MIDD0301 in the brain was 7.8% of the lung concentrations representing excellent

tissue selectivity. To further prevent any conversion of closed to open MIDD0301 in the stomach, mice were pretreated with proton pump inhibitor omeprazole (30 mg/kg) to adjust the gastric pH to 6.7 (Table 3, entry 4).[72] Using the same formulation as described in entry 4, a slightly higher concentration of closed MIDD0301 was observed for the blood, lung, and brain. Finally, an acidic formulation using open MIDD0301 was evaluated using 2% HPMC solution prepared in 0.1 M HCl. The pH value of this solution after the addition of 2.5% PEG400 was 1.8 (Table 3, entry 5). One hour after treatment, 371 nM of closed MIDD0301 and 14 nM of open MIDD0301 were detected in blood. Interestingly, all concentrations determined in the blood, lung, and brain were comparable to the neutral formulation of closed MIDD0301 (Table 3, entry 3). The quantification of open MIDD0301 for all formulations agreed with our kinetic investigation of the ring closing reaction that showed that more than 90% of open MIDD0301 is converted to closed MIDD0301 within 1 h at an intestinal pH value of 8 (Figure 35B). Analytical studies have shown that ring opening and closing occur without racemization, enabling selective and rapid interconversion of MIDD0301 to achieve similar concentrations in the blood, lung, and brain regardless of open or closed oral formulation of MIDD0301 are administered.

To demonstrate that the ring opening and closing occurred without racemization, we used method 4 described in chapter 3. At that time, we did not have a method for optical purity determination of MIDD0301. Therefore, we converted MIDD0301 to its ethyl ester for the %ee determination. To simulate the conditions for orally administered MIDD0301, we first dissolved it in 1M HCl and then added a 10% NaOH solution to achieve a pH of 12 followed by the addition of acetic acid. The suspension was centrifuged (2000 x g) and the liquid as was removed. One mL of water was added to the solid and the vial was centrifuged again (2000 x g) after sonication.

The solid was dried under high vacuum after the removal of the water layer. After derivatization to the ethyl ester, the acid-based treated MIDD0301 had the same optical purity compared to non-treated MIDD0301 (Figure 36).

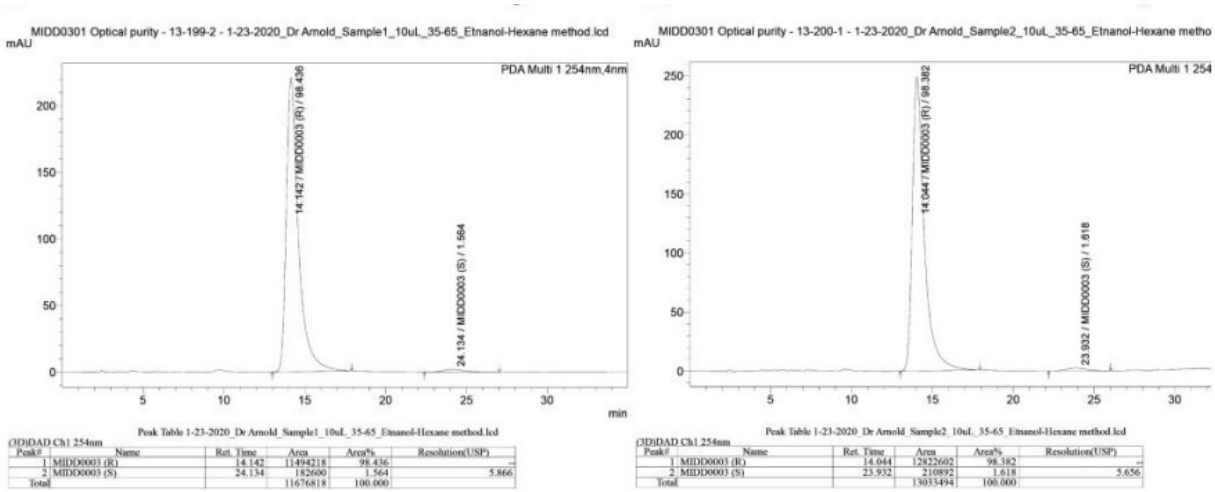

Figure 36. Optical purity analysis of MIDD0301 after conversion to the ethyl ester. A) Before treatment with 1N HCl (97% ee) and B) after treatment with 1M HCl (97% ee) followed by esterification.

2.3 Lipophilicity of MIDD0301

Determination of lipophilicity is another very important parameter of drug molecules. It determines how much of a compound can be absorbed by the intestine. Lipophilicity can be determined with the partition of a compound between a nonpolar and polar phase. A octanol:water solvent system is frequently used to determine lipophilicity as partition coefficient denoted as logP. For an ionizable compound, distribution of species is highly affected by the pH. Therefore, distribution coefficient denoted as logD is used for those compounds, which include MIDD0301. Molecules with logP values of more than 5 usually encounter extensive metabolic turnover whereas molecules with low logP values suffer from low permeability. Therefore,

molecules with a logP value between 1 and 4 are generally anticipated to have optimum ADME properties and considered as good candidate for oral administration. [59]

2.3.1 Experimental

In a screw top vial, 200 µL of a 2.5 mM 1-octanol solution of closed MIDD0301 was added to 300 µL of water-saturated 1-octanol and 500 µL of 1-octanol saturated buffered water at different pH values. The solution was shaken vigorously overnight and allowed to separate for 1 h. Three aliquots of 10 µL of the octanol layer were combined with 70 µL of octanol followed by the determination of absorbance at 270 nm using a 384 well plate (Coring UV star) and a Tecan M1000 microplate reader. Three aliquots of 70 µL of the water layer were combined with 10 µL of corresponding buffer, and the absorbance was determined at 270 nm using a 384 well plate (Coring UV star) and a Tecan M1000 plate reader. Calibration curves for octanol and water were prepared to determine MIDD0301 concentrations. The assay was carried out in triplicate.

2.3.2 Results and Discussion

We determined the partition coefficient logD of MIDD0301 at different pH values, which is important to understand it relates to absorption of orally administered MIDD0301. Here, closed MIDD0301 was dissolved in 1- octanol and partitioned with aqueous buffered solutions in a pH range of 1−9 for 24 h. MIDD0301 concentrations were determined for each layer using spectrophotometry. The results are depicted in Figure 37. The lowest lipophilicity for MIDD0301 was observed at pH 1 due to the formation of open MIDD0301. At pH 8 and higher, closed MIDD0301 carboxylate (Figure 31) exhibited low lipophilicity. This behavior corresponds with the high aqueous solubility of MIDD0301 at those pH values (Figure 33). The highest concentration

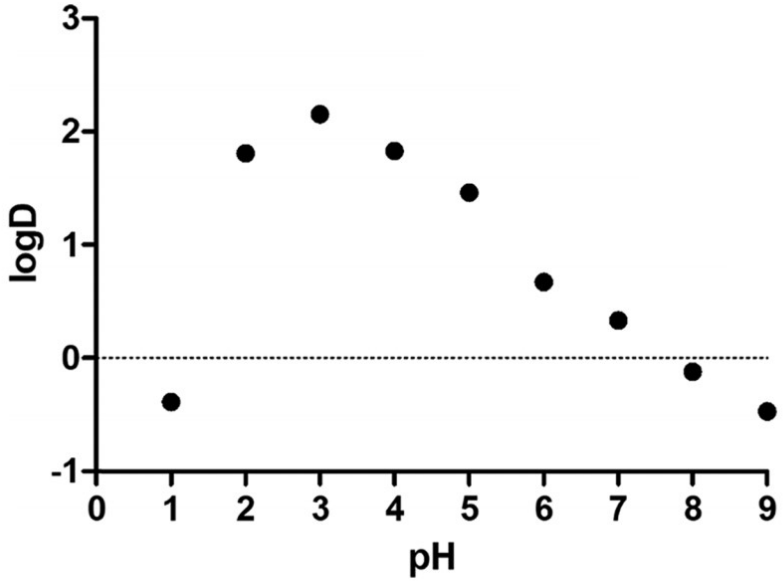

Figure 37. Lipophilicity measurement (log Doct/wat) of MIDD0301 at different pH values. A 2.5 mM solution of closed MIDD0301 in 1- octanol was partitioned with aqueous buffered solutions with different pH values for 24 h. UV absorbance measurements at an isosbestic wavelength of 270 nm were used to determine the concentrations of MIDD0301 in both layers (n = 3).

of MIDD0301 in 1-octanol was observed between pH 2 and 5, which reflects the overall neutral charge of MIDD0301 due to possible hydrogen bond interactions. For this pH range, the lowest aqueous solubility of MIDD0301 was observed (Figure 33).

2.4 Solubility of MIDD0301 in organic solvent

In addition to pH dependent aqueous solubility, solubility of MIDD0301 and its open ring form was evaluated in various organic solvents. The information collected from this study can be useful in future during purification and/or extraction of MIDD0301 from impurity or complex sample matrixes.

2.4.1 Experimental

In a glass vial, about 2-3 mg of closed or open MIDD0301 were added in 300 µl of various organic solvents. The mixture was vortexed, sonicated and kept on shaker overnight. In the case of solvents methanol, DMF, and DMSO several portions of closed and/or open MIDD0301 were

added due to high solubility. After keeping the saturated solution on a shaker overnight, mixtures were centrifuged and three aliquots of 2 µl were diluted in 198 µl of methanol and 80 uL of that solution was transferred into a UV plate for recording. Similar dilutions were made to determine background absorbance. Two separate calibration curves were made for closed and open MIDD0301. Concentrations were determined with calibration curves after subtracting background absorbance.

2.4.2 Results and discussion

Among the 13 solvents tested, closed MIDD0301 has the highest solubility in DMF and DMSO followed by methanol. Inferior solubility was observed for acetonitrile. On the other hand, open MIDD0301 had an overall better solubility than its closed form for most of the solvents that were tested. An especially large difference in solubility was found for methanol. Results are depicted table 4.

Table 4 Solubility of MIDD0301 and its open ring form in organic solvent

Solvents	Solubility (g/L)	
	MIDD0301	Open ring
Ethyl acetate	0.29	0.3
Acetonitrile	0.73	0.28
Acetone	0.8	1.54
Butanol-1	0.87	5.2
DCM	1.83	2.55
Propanol-2	1.92	6.72
Ethanol	5.07	21.34
Methanol	8.1	138.23
MTBE	8.58	0.64

Chloroform	9.64	7.92
THF	24.16	9.32
DMF	119.49	97.41
DMSO	314.2	571.84

Chapter 3: Development of analytical methods for a scale up process of MIDD0301

Manufacturing processes of lead compounds become especially important when the NCE is part of an IND application. Chemistry, manufacturing, and control (CMC) methods are needed to enable consistency between synthesis batches. CMC includes quality control of starting materials, reagents, solvents, catalysts, analytical test methods, purity, stereochemistry, and characterization of impurities. Once the CMC is finalized, different batches can be used for preclinical toxicology study and first in human studies.[67] The development of analytical methods for the scale up synthesis of MIDD0301 was focused to fulfill these recommendations. Here, we will present the development process for each synthesis steps and discuss their influence on the final procedure. All synthesis steps were design to be scalable thus enabling the generation of large amounts of cGMP material. The developed analytical methods will enable us to control the production of MIDD0301 as larger reactors are used.

3.1 Experimental

3.1.1 Method 1 (LC-PDA-MS, Reverse phase)

An HPLC-PDA-MS reverse phase method was created for purity determination for MIDD0002 and MIDD0003. Purity was determined using absolute area percentage. 0.1% formic acid in methanol and 0.1% formic acid in water were used as the mobile phase. High performance liquid chromatography (Shimadzu Nexara series) with a Photo Diode Array detector (PDA, Shimadzu SPD-M30A) and a single quadrupole mass analyzer (LCMS 2020, Shimadzu, Kyoto, Japan) was

used. Analytes were separated using a Restek Pinnacle-C18 (4.6 mm x 50 mm, 5 µm particle size) column with gradient elution at a flow rate of 0.8 mL/min. The time program of mobile phase elution is shown in Table 5. Data were acquired by PDA detection with a range of 190-700 nm.

Table 5 Gradient time program for Method 1

Time (min)	Mobile phase B%
0	40
3.5	55
5.5	55
10	70
11	100
12	100
13	40
15	40

The absorption at a wavelength of 254 nm was used for purity determination. The mass spectrometer was equipped with a DUIS ionization probe (having both ESI and APCI). The mass range was set m/z 200-800 for both positive and negative mode. Scan speed was 5000 u/sec, interface, desolvation line and heat block temperature were 350°C, 250°C and 400°C, respectively. Nebulizing gas flow was 1.5 L/min and drying gas flow was 15 L/min.

3.1.2 Method 2 (LC-PDA-MS, Reverse phase)

A HPLC-PDA-MS reverse phase method was created for purity determination of final product MIDD0301. The purity was determined using absolute area percentage. 0.1% formic acid in methanol and 0.1% formic acid in water were used as the mobile phase. High performance liquid chromatography (Shimadzu Nexara series) with a Photo Diode Array detector (PDA, Shimadzu SPD-M30A) and a single quadrupole mass analyzer (LCMS 2020, Shimadzu, Kyoto, Japan) were used. Analytes were separated using a Restek Pinnacle-C18 (4.6 mm x 50 mm, 5 µm particle size) column with gradient elution at a flow rate of 0.8 mL/min. The time program of mobile phase elution is given in Table 6. Data were acquired by PDA detection with a range of 190-700 nm. The

absorbance at 254 nm was used for purity calculation. The mass spectrometer was equipped with a DUIS ionization probe. The mass range was set m/z 200-800 for both positive and negative mode. Scan speed was 5000 u/sec, interface, desolvation line and heat block temperature were 350°C, 250°C and 400°C, respectively. Nebulizing gas flow was 1.5 L/min and drying gas flow was 15 L/min.

3.1.3 Method 3 (LC-DAD, Normal phase)

For determination of optical purity of compound MIDD0002, an HPLC-DAD normal phase method was optimized. An isocratic mixture of 92% n-hexane and 8% ethanol was used as

Table 6 Gradient time program for method 2

Time (min)	Mobile phase B%
0	40
2.7	80
3.7	100
4.2	100
5	40
7	40

the mobile phase to resolve the R and S enantiomers of MIDD0002. An Agilent 1100 HPLC system consist of a quaternary pump, autosampler and a DAD detector in combination with a Pirkle Whelk-01 column (4.6 mm x 25 cm, 5 µm particle size) was used. A racemic mixture was used for the verification of the method. The (S) enantiomer eluted at 10.12 min and the (R) enantiomer at 11.89 min. The resolution between peaks was 2.8 min. The flow rate was 1 mL/min and DAD wavelength range was set to 200-400 nm. The absorbance at 254 nm was used for relative % area determination and the enantiomeric excess was calculated using % ee = (R-S)/(R+S) x 100.

3.1.4 Method 4 (LC-DAD, Normal phase)

The following HPLC-DAD normal phase method was created for optical purity determination of MIDD0003. An isocratic mixture of 65% n-hexane and 35% ethanol was used as the mobile phase to resolve the (R) and (S) enantiomers of MIDD0003. An Agilent 1100 HPLC system consisting of a quaternary pump, autosampler, and a DAD detector was used in combination with a Pirkle Whelk-01 column (4.6 mm x 25 cm, 5 µm particle size). A racemic mixture enabled the verification of the method. The (R) enantiomer eluted at 13.88 min and the (S) enantiomer at 23.69 min. The resolution between peaks was 5.6 min. The flow rate was 1 mL/min and the DAD wavelength range was set to 200-400 nm. The absorbance at 254 nm was used for relative % area determination and the enantiomeric excess was calculated using % ee = (R-S)/(R+S) x 100.

3.1.5 Method 5 (LC-DAD, Normal phase)

This HPLC-DAD normal phase chromatography method was developed for optical purity determination of MIDD0301. An isocratic mixture of 90% n-hexane and 10% ethanol was used as the mobile phase to resolve the (R) and (S) enantiomers of MIDD0301. An Agilent 1100 HPLC system consisting of a quaternary pump, autosampler, and a DAD detector was used in combination with a Chiralpak IB-N3 (4.6 mm x 15 cm, 3 µm). A racemic mixture was used for the verification of the method. The (R) enantiomer eluted at 9.60 min and the S enantiomer at 12.5 min. The resolution between peaks was 4.9 min. The flow rate was 1 mL/min and the DAD wavelength range was set at 200-400 nm. The absorbance at 254 nm was used for relative % area determination and the enantiomeric excess was calculated using % ee = (R-S)/(R+S) x 100.

3.2 Results and Discussion

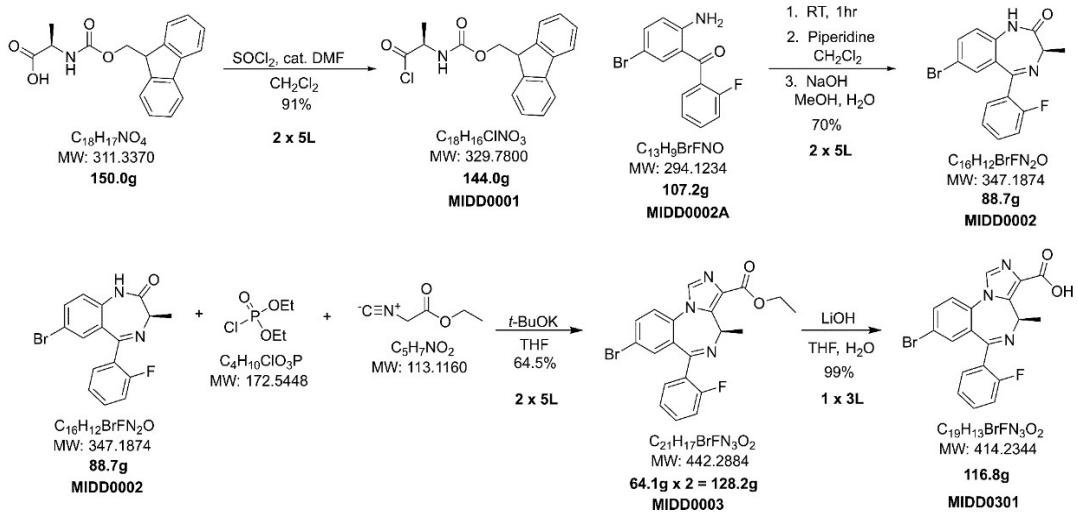

Scheme 1 Initial scale-up reaction scheme for synthesis of MIDD0301.

The initial scale-up synthesis of clinical asthma candidate MIDD0301 is depicted in Scheme 1. F-moc alanine was converted into the corresponding acid chloride and coupled with benzophenone MIDD0002A to yield MIDD0002. The subsequent reaction with diethyl chlorophosphate and ethyl isocyanoacetate under basic conditions yielded MIDD003, which was saponified to give

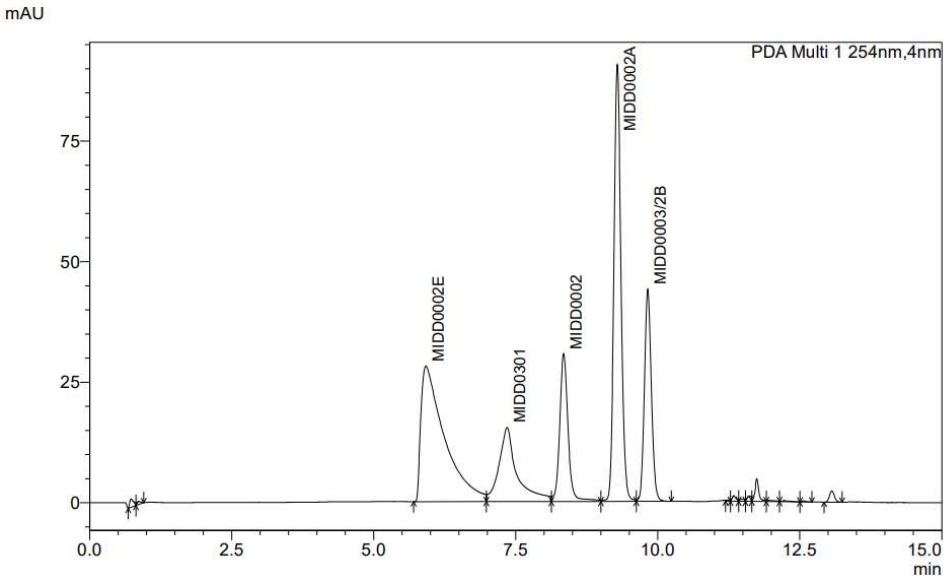

Figure 38. PDA Chromatogram of mixture of starting materials and products of different steps analyzed with method 1.

MIDD0301. The available products were used to develop an analytical method to determine

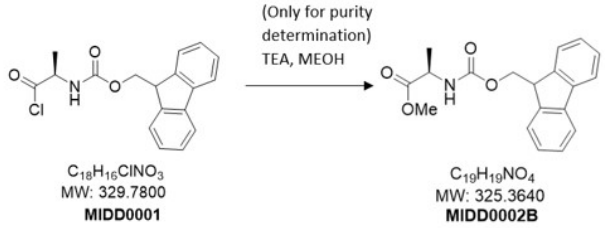

Scheme 2 Derivatization of step 1 purified product MIDD0001 to determine its purity as MIDD0002B using method 1

purity.

It was mentioned in the experimental section 3.1.1 that method 1 was used for purity measurement of MIDD0002 and MIDD0003**.** However, the method was used for all reaction products. In Figure 38, an exemplary chromatogram of the mixture of synthesized products along with some starting materials and intermediates are shown. In this chromatogram MIDD0002B was co-eluting with MIDD0003. MIDD0002B is the derivative of MIDD0001, solely produced to quantify MIDD0001 (Scheme 2). MIDD0002A and MIDD0001 are starting materials for step 2 in Scheme 1. It was very important to achieve baseline separation for MIDD0002A from all other reactants and products as complete consumption of this starting material was never observed. For the deprotection of MIDD0002C, piperidine was used which produced byproduct MIDD0002E

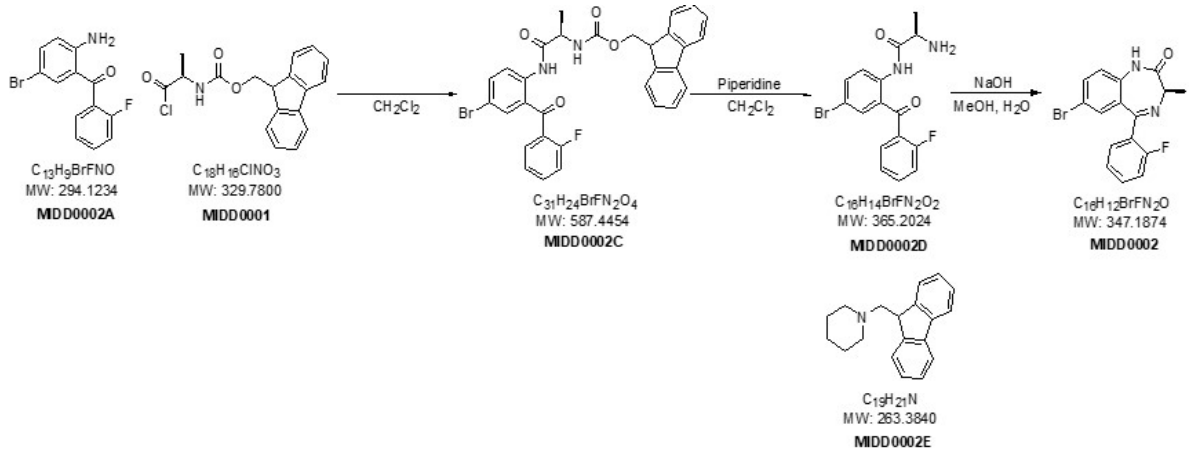

Scheme 3 Synthesis of MIDD0002 from reaction between MIDD0002A and MIDD0001. MIDD0002C was an intermediate after coupling of starting materials. Piperidine was added for deprotection of FMOC from MIDD0002C to form the free amine that eventually cyclized to form MIDD0002 in presence of base. FMOC attached to piperidine produced byproduct MIDD0002E.

(Scheme 3). Thus, it was critical to monitor the presence of MIDD0002A and MIDD0002E after the purification of MIDD0002. Products of the next two steps were MIDD0003 and MIDD0301, which were well resolved with method 1 and can be seen in the Figure 38. However, a non-ideal peak shape for MIDD0301 at higher concentration was observed (Figure 39) which prompted the

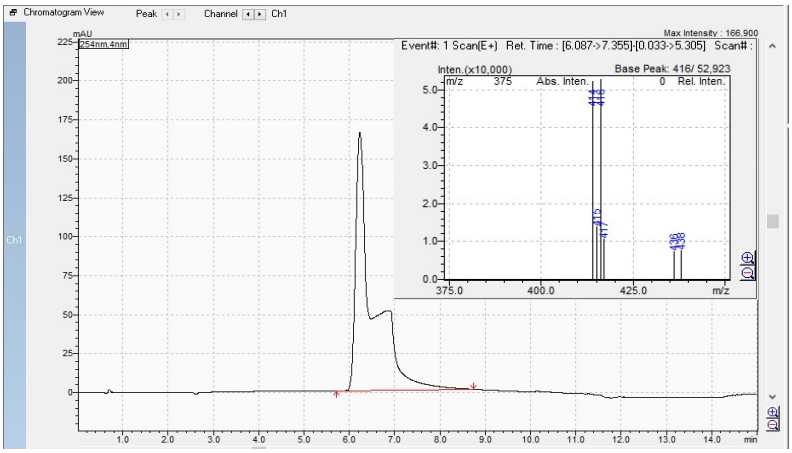

Figure 39. Non-ideal peak shape of MIDD0301 using method 1 at higher concentration (1000 ppm). Mass spectrum in the inset demonstrated peak consist of only MIDD0301 (m/z 414/416) and its sodium adduct m/z 436/438.

development of Method 2 with a steeper gradient. There might be multiple reasons for the non-ideal peak shape. Our column was old, and it is possible that the abnormal shape arose simply due to column deterioration. However, it is more likely that the chemical properties of this molecule caused tailing. It has been reported that trifluoroacetic acid (TFA) can be used as an additive for polar compounds to improve the elution profile, but this additive is not recommended by our mass spec facility for its well-known ion suppression role for ESI.[141] Fortunately, samples with low MIDD0301 concentrations exhibited an acceptable peak shape (Figure 38). A 5 µm particle sized column was chosen to make methods compatible with both HPLC and UPLC system.

The published procedure for MIDD0301 included N,N'- dicyclohexylcarbodiimide (DCC) as the coupling reagent to convert compound **1** (known as MIDD0002A) and Boc-D-alanine (Scheme

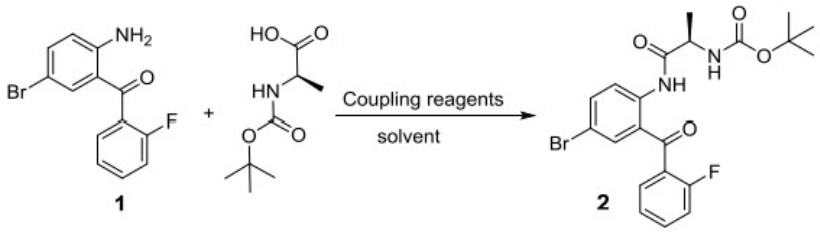

Scheme 4 Reaction between 1 and Boc -D-Alanine.

4).[68] MIDD0002A was not fully consumed during the reaction (204 mmol scale) resulting in 58.6% yield of **2**. To improve the yield of this reaction several attempts were made such as a longer reaction time (48 h), elevated reaction temperature (40 °C), and addition of an increased amount of DCC (2 equiv) and Boc-D-alanine (2 equiv).[69] None of the attempts improved the yield significantly.

Alternatively, F-moc acyl chloride MIDD0001A was used as it has been reported for the synthesis

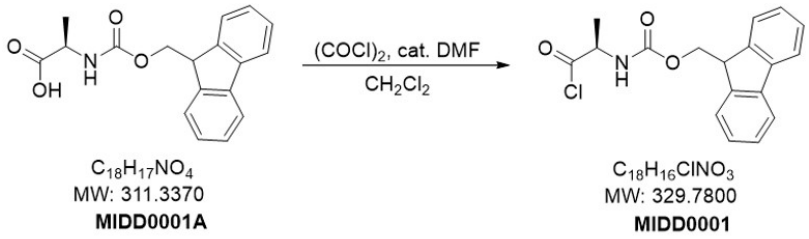

Scheme 5 Synthesis of MIDD0001

of achiral benzodiazepines (Scheme 5).[70-72] 147.5 g of MIDD0001 was generated in 93% yield using this route. The acid chloride was very reactive in the HPLC reverse phase aqueous condition and hydrolyzed back to starting material during purity analysis. Therefore, an aliquot of MIDD0001 was quenched with methanol in the presence of base to form the methyl ester which is MIDD0002B (Scheme 2). This enabled the purity analysis for this compound using the method 1. The reaction between MIDD0002A and MIDD0001 was carried out at room temperature and

complete conversion was observed after 30 min on a 0.4 M scale. Six equivalents of piperidine were added slowly to the reaction mixture for the deprotection of MIDD0002C to form free amine MIDD0002D (Scheme 3). The crude product was dissolved in methanol, followed by the addition of 1.6 M aqueous sodium hydroxide to enable the formation of MIDD0002 after 12 h at room temperature in 68% yield. Unfortunately, we did not discover that the product was racemic at this stage because our optical purity method was under development. Thus, unknowingly, the process was continued to yield 128 g of racemic MIDD0301.

The optimization of a method to separate the (R) and (S) form of MIDD0301 included the

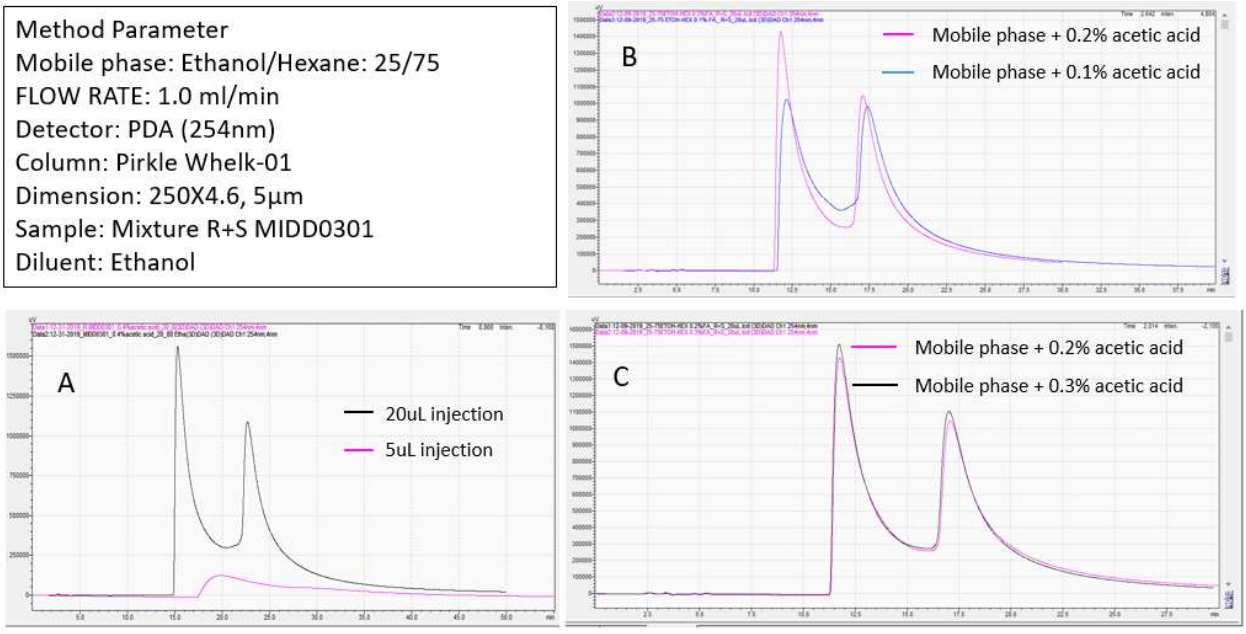

Figure 40. Separation of R and S MIDD0301 enantiomers. Effect of injection volume and mobile phase modifier concentration on separation. A) Comparison of 5 µL vs 20 µL injection volume on peak shape; B) Comparison of chromatograms for modifier's concentration 0.1 vs 0.2%; C) Comparison of chromatograms for modifier's concentration 0.2 vs 0.3%.

screening of available chiral columns. A Regis RR Whelk-O1 column, which according to vendor's manual has good selectivity toward chiral compounds of wide range functional group including amine and carboxylic acid was tried first. Initially a broad single peak was found for the racemate. However, the addition of acetic acid as modifier in the mobile phase and an increased injection

volume resulted in promising separation between two peaks. In Figure 40A, chromatograms resulting from a 20 µL vs 5 µL injection are superimposed. Both injections were made from the same vial under identical conditions. Even though acetic acid was used for both injections, only the higher injection volume demonstrated significant separation. So, an injection volume of 20 µL was used onward for all other trials. Larger amounts of acidic modifier increased the resolution between peaks initially (Figure 40B) but more than 0.2% of acetic acid did not further improve the separation. The chromatogram is similar for 0.2% vs 0.3% acetic acid (Figure 40C). Moreover, adding too much acidic modifier to mobile phase could result in seven-member ring opening of benzodiazepine scaffold. Therefore, 0.2% of acidic modifier was used for all other trials as it provided the maximum effect on separation.

Next, different proportion of mobile phases of ethanol and hexane were used to change the

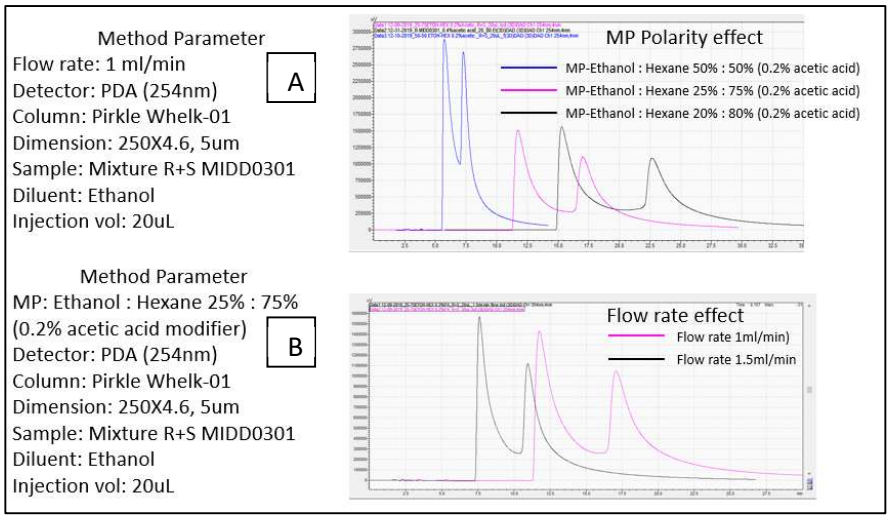

Figure 41. Optimization of R and S MIDD0301. A) Effect of mobile phase polarity; B) flow rate

polarity of mobile phase. Hexane:ethanol mixtures of 50:50 to 80:20 were tested (Figure 41 A). A higher percentage of ethanol shortens the retention times and sharpens the peaks but diminished resolution. On the other hand, a larger percentage of n-hexane increased retention times and improved the resolution. However, the peaks became broader and with 75% hexane

the retention times for the enantiomers differed by several minutes without achieving baseline separation. So, based on peak shape and retention time, a 25:75 mixture of ethanol:hexane was selected. The flow rate had some effect on the peak resolution. A flow of 1.5 mL/min resulted in sharper peaks but without much improvement of the baseline separation (Figure 41 B).

Different mobile phase modifiers were also investigated to explore which one has the most prominent effect on the separation of the enantiomers. Trimethylamine (TEA) was used as basic

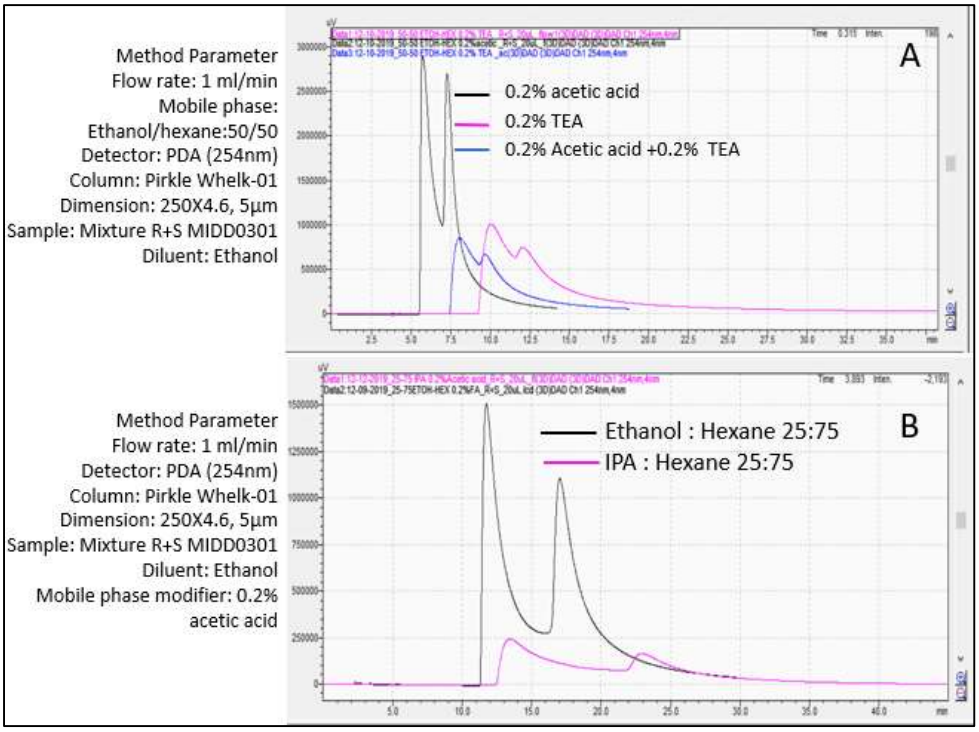

Figure 42. Optimization of R and S MIDD0301; A) Effect of acidic, basic, and mixed modifier on separation and peak shape; B) Switching of strong eluent ethanol with weak eluent isopropyl alcohol.

modifier whereas a combination of acetic acid and TEA were used as mixed modifier. The addition of basic or mixed modifiers to the mobile phase instead of acidic proved to be less effective (Figure 42A). Switching the strong eluent ethanol with a weaker eluent IPA gave broader peaks (Figure 42B). In addition, the intensity of the peaks is lower with IPA as mobile phase. Other combinations of flow rate and mobile phase solvents were investigated, but it was apparent that

a different column is needed to baseline separate the MIDD0301 (R) and (S) form. Although no baseline separation of the racemate was achieved with the Regis RR Whelk-O1 column, two peaks can be clearly distinguishable for the racemic mixture. Thus, this method was sufficient to verify that racemization occurred during the synthesis of MIDD0301 using the presented method. To identify at which synthesis step racemization occurred, we optimized the %ee determination for chiral intermediates. Fortunately, the Regis RR Whelk-O1 column worked very well for the product of step 3 (MIDD0003). Without using any modifier, a isocratic 65:35 hexane:ethanol mobile phase provided a very good separation between optical isomers with ideal peak shape. The retention times for (R) and (S) MIDD0003 were 15.20 min and 25.55 min, respectively (Figure

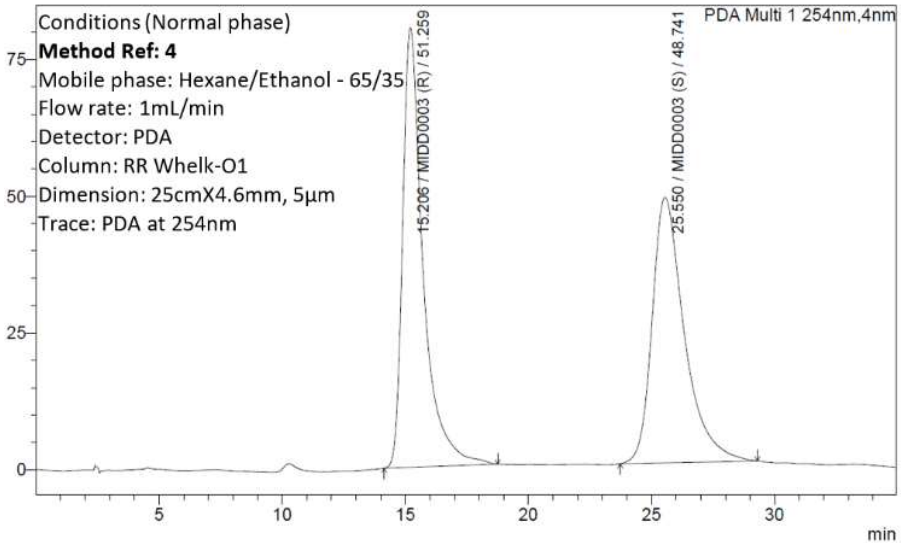

Figure 43. PDA Chromatogram of racemic mixture of MIDD0003 separated using method 4.

43). The analysis of a samples from the large-scale synthesis confirmed that racemization already occurred during the generation of MIDD0003. Next, we investigated the optical purity of MIDD0002. Using the method developed for MIDD003 resulted in low column retention leading

to a fast elution without a baseline separation. However, a change of the polarity of the mobile phase to a 92:08 ratio of hexane:ethanol gave baseline separation for the MIDD0002 enantiomers (Figure 44). The retention times of the isomers were 10.87 min and 13.09 min,

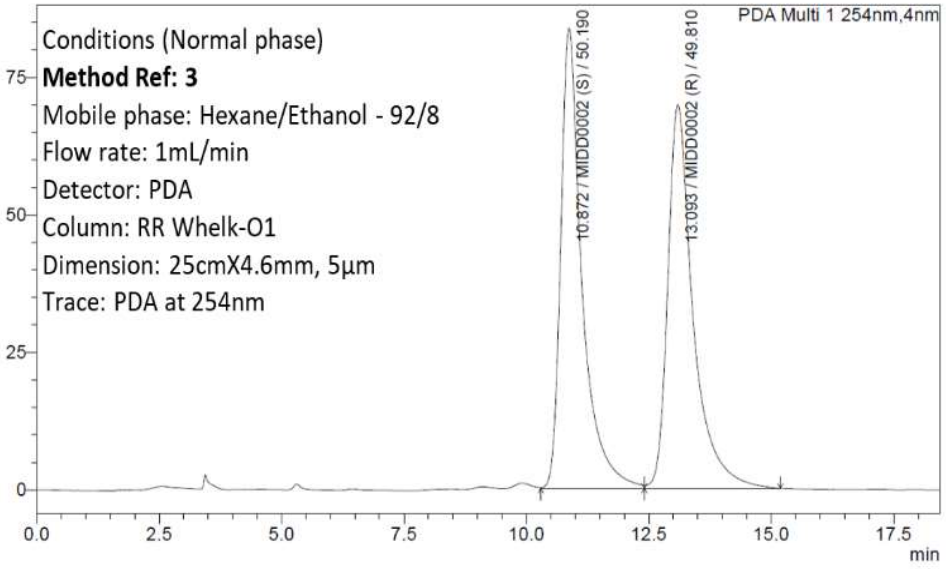

Figure 44. PDA Chromatogram of racemic mixture of MIDD0002 separated using method 3

respectively. Unfortunately, samples from the product of step 2 also appeared as racemic. My co-workers in these project, Dan Knutson and Md Yeunus Mian investigated the cause of racemization which was likely to occur under basic conditions (Scheme 6). It was found that

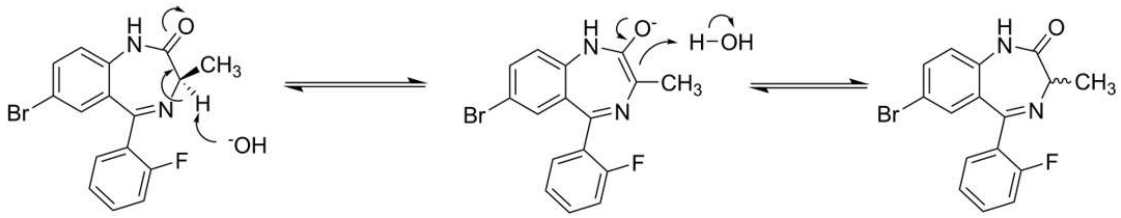

Scheme 6 Proposed mechanisms for epimerization of chiral methyl group in MIDD0002.

epimerization of the chiral methyl group had occurred after the benzodiazepine ring formation in the presence of sodium hydroxide used for the ring closure.

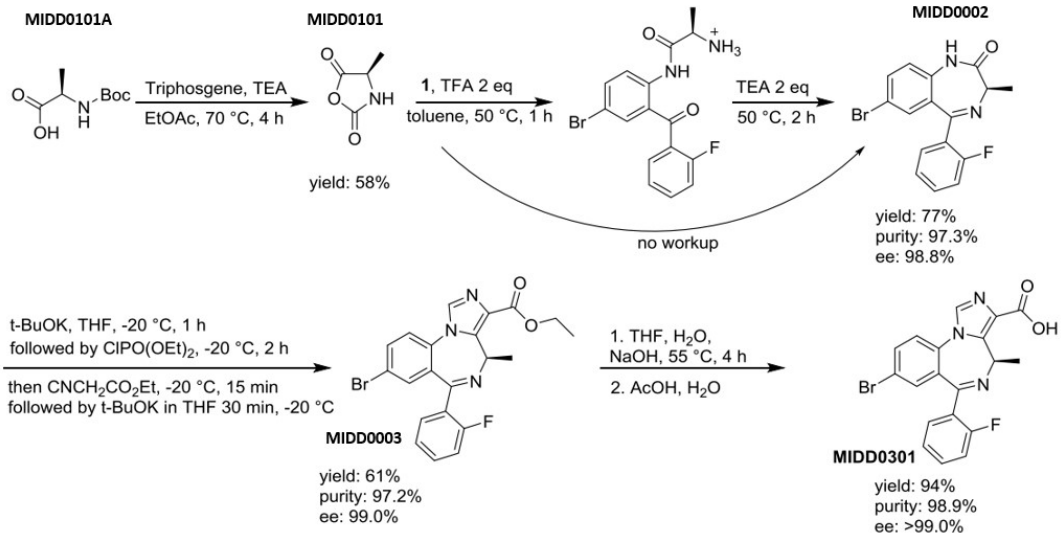

Scheme 7 Final improved scale-up synthesis route.

To overcome the moderate yield and racemization of MIDD0002, a new procedure as developed by Fier and Whitakker[73] using amino acid N-carboxyanhydrides (NCAs) to synthesize optically pure benzodiazepines was adapted (Scheme 7). MIDD0101 was synthesized with triphosgene and triethylamine following a procedure developed by Wilder and Mobashery.[74] Due to the lack of a

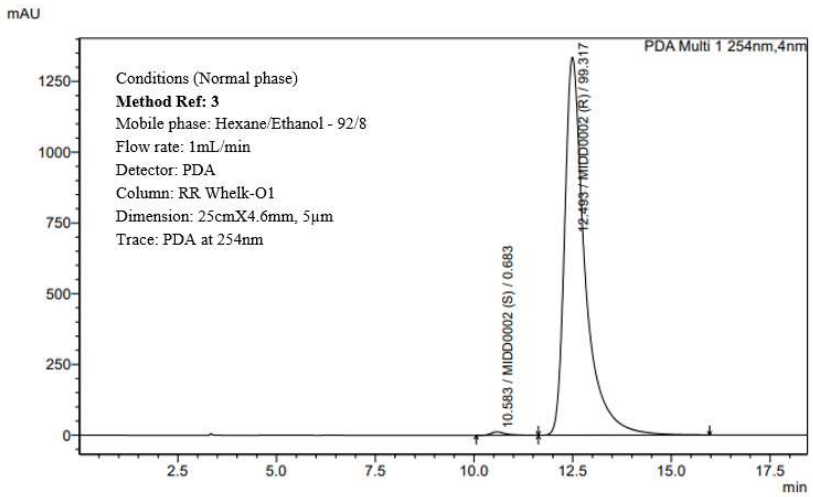

Figure 45. PDA chromatogram of MIDD0002 extracted at 254 nm. Sample was analyzed in normal phase method 3. Purity was found ee 98.8%.

chromophore and instability towards aqueous medium, no suitable purity method for normal

phase or reverse phase was developed. However, good yield (77%) and excellent purity (97.3%) as well as optically purity (ee 98.8%, Figure 45) of product MIDD0002 was observed. The synthesis was continued using the steps already depicted in Scheme 1. Method 3 was used to determine the optical purity of MIDD0002. The reverse phase method 1 was used to analyze purity. Simultaneously, mass analysis was used for impurity identification. All products of step 2,3 & 4,

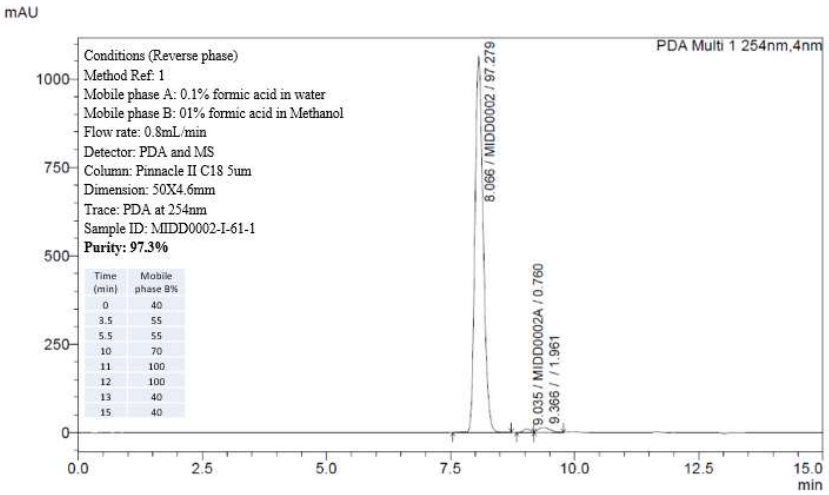

Figure 46. PDA chromatogram of MIDD0002 extracted at 254 nm. Analysis was carried out with reverse phase method 1.

have a bromine substituent. Most of the impurities also contained a bromine atom, which gave a distinct MS signal pattern and simplified our identification. The purity of MIDD0002 was 97.3% along with presence of two impurity peak (Figure 46). The retention time of first and second

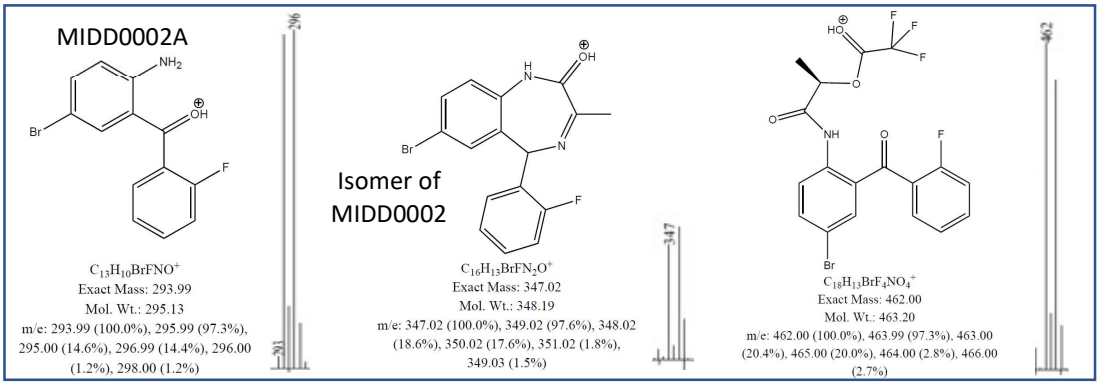

Figure 47. Mass spectrum and proposed structure of MIDD0002 Impurity peak 1 at RT 9.04 min.

impurity peaks were 9.04 min and 9.37 min, respectively. The mass spectrum of the first impurity

peak 1 in Figure 47 suggested that there was co-elution of some starting material MIDD0002A (m/z 294 and 296), a trace amount of the MIDD0002 isomer (m/z 347 and 349), which was formed by a shift of a double bond in 7 membered diazepine ring, and the substitution product of MIDD0002D and TFA (m/z 462 and 464) and its sodium adduct (m/z 484 and 486). The presence of MIDD0002A was confirmed by retention time and mass spectra using an available standard. The identification of the MIDD0002 6H-isomer was new at this point but in later steps of the synthesis, the corresponding regioisomers of MIDD0003 and MIDD0301 were observed. Because more than 1% of those isomers were formed in step 3 and step 4, further structural identification was necessary. Intermediate MIDD0002D was difficult to isolate because of its spontaneous reaction to form MIDD0002. So, instead of TEA, $NaHCO_3$ was added to neutralize MIDD0002D giving a mixture of MIDD0002D (free amine) and MIDD0002 (Figure 48). Impurity

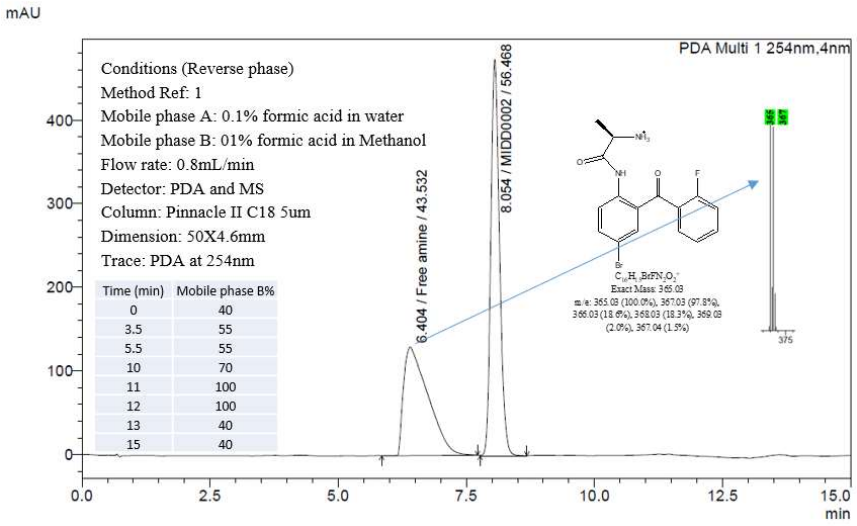

Figure 48. PDA Chromatogram of synthesized free amine intermediate (MIDD0002D). Significant amount already converted to MIDD0002.

peak 2 was identified as an oligomer formed from MIDD002D and the NCA. Its mass was confirmed by both positive and negative ionization mass spectrometry. In positive mode, the m/z

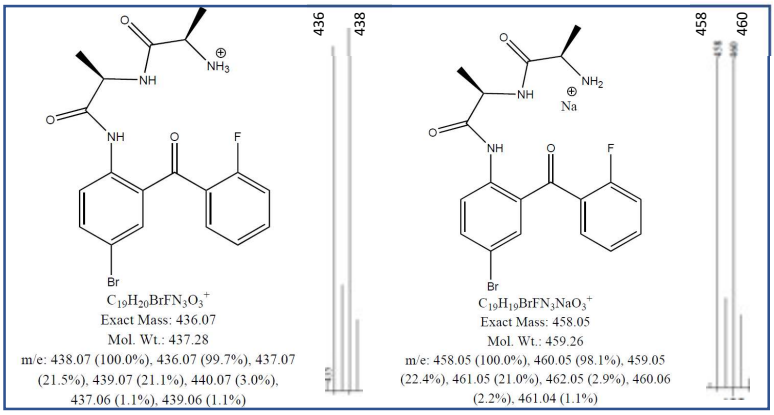

Figure 49. Mass spectrum and proposed structure of MIDD0002 Impurity peak 2 at RT 9.37min

436 and 438 pair along with sodium adduct m/z 458 and 460 was found (Figure 49). In negative mode, m/z 434 and 436 are in agreement with the deprotonated species. In addition to the M-1 species, a M+35/37 (Cl^-) chloride adduct was also found (spectrum is not shown). The impurity accounted for almost 2% of the preparation. The structural confirmation was achieved with the

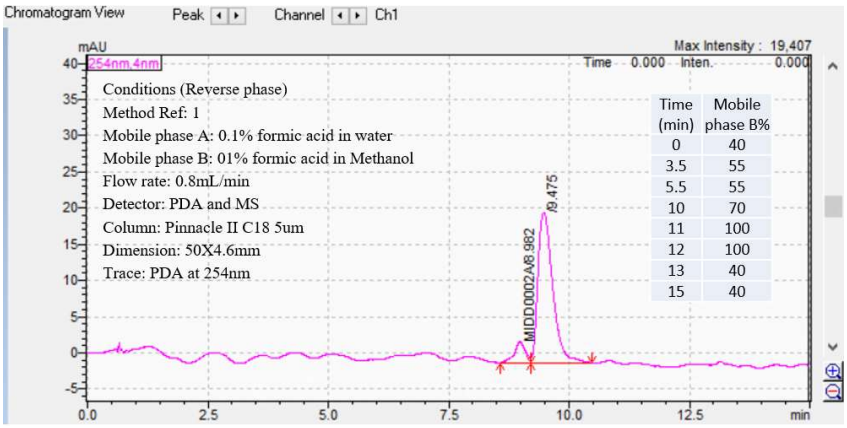

Figure 50. PDA Chromatogram of synthesized oligomer impurity. Retention time and Mass spectrum pattern was matched with impurity.

synthesis of this oligomer and subsequent analysis with same LCMS method (Figure 50). The product of the next step was MIDD0003. Its purity was 97.2% and two impurity peaks were identified (Figure 51). The first impurity peak eluted at 11.24 min and the second at 11.54 min. The mass analysis of first impurity peak corresponded to the *t*-butyl ester of MIDD0301 and the second impurity peak corresponded to the 6H-isomer of MIDD0003. For the first impurity peak,

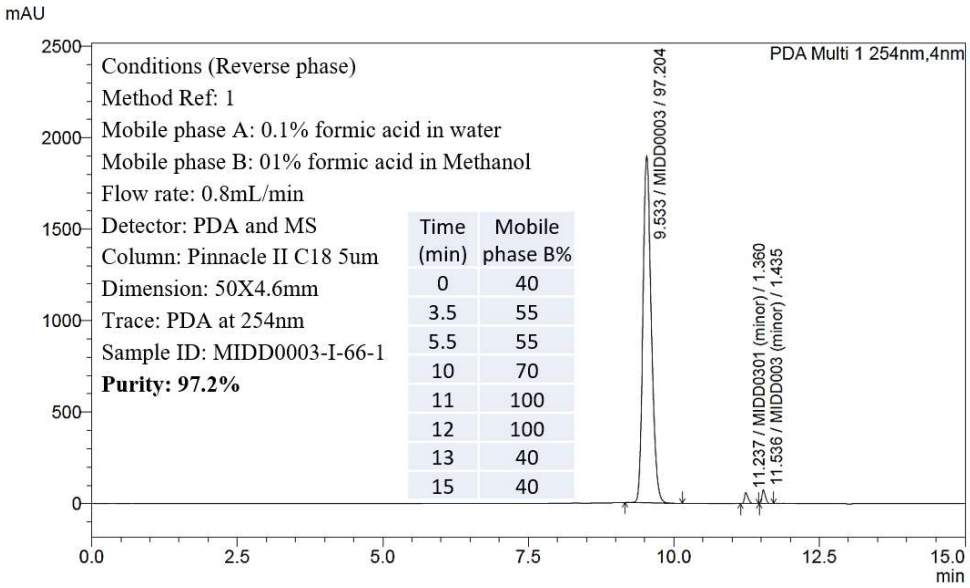

Figure 51. PDA chromatogram of MIDD0003 at 254 nm. The sample was analyzed with reverse phase method 1.

two sets of distinct masses were present which were m/z 414 and 416 and m/z 470 and 472. The m/z 414 and 416 pair could be the final product MIDD0301 or its 6-H isomer bearing an achiral methyl group (Figure 52 left). The mass of m/z 470 and 472 correlated with the *t*-butyl ester of MIDD0301. Potassium *t*-butoxide was used in the 3rd step of the synthesis enabling a transesterification of the ethyl ester to the *t*-butyl ester. Another source of m/z 414 and 416 impurity peak 1 could be the result of an insource fragmentation of the *t*-butyl ester MIDD0301. Thus, several events might be resulted m/z 414 and 416 and m/z 470 and 472 masses of impurity peak 1: a) the t-butyl ester MIDD0301 and corresponding fragmentation product during

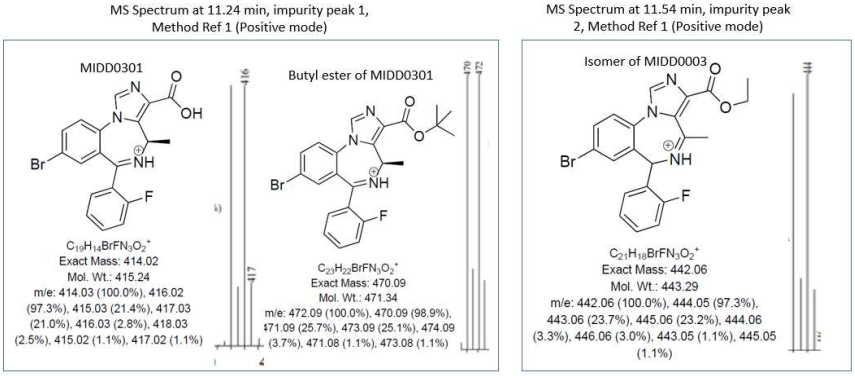

Figure 52. MS spectrum and suggested structure of impurity peaks found in MIDD0003 compound at 11.24 min (left box) and 11.54 min.

ionization, b) a mixture of *t*-butyl ester and MIDD0301 or c) the *t*-butyl ester and the 6H-isomer of MIDD0301. B) was excluded immediately as retention time of MIDD0301 for method 1 was about 7 min and not 11.24 min. For further conformation my coworker Md Yeunus Mian

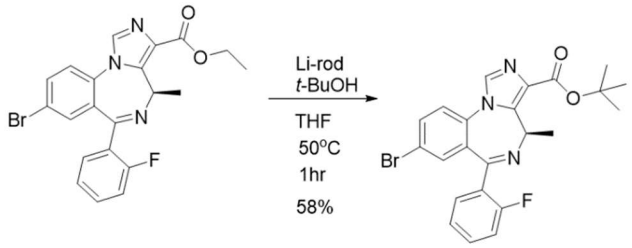

Scheme 8 Synthesis of t-butyl ester from MIDD0003.

synthesized the *t*-butyl ester of MIDD0301 and the 6H-isomer of MIDD0301. Therefore, a transesterification of the ethyl ester was performed in presence of lithium *t*-butoxide as shown in the Scheme 8. The 6H-isomer of MIDD0301 was synthesized in the presence of a sodium hydroxide from the corresponding ethyl ester (Scheme 9). The retention time of 6H-isomer of

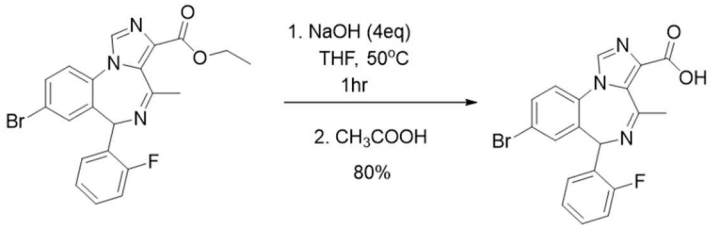

Scheme 9 Synthesis of isomer of MIDD0301.

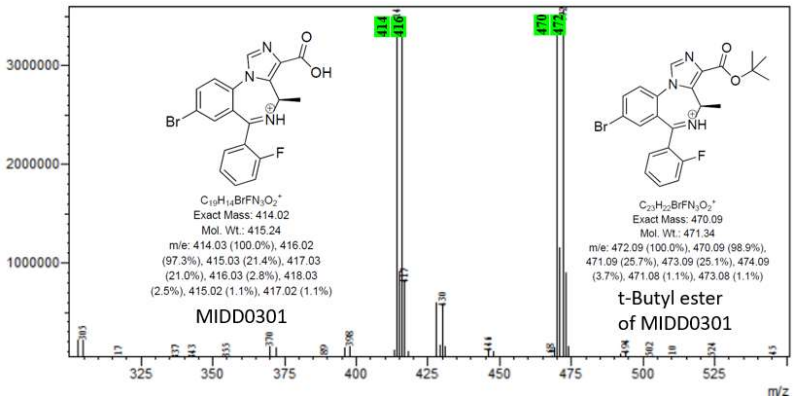

Figure 53. Mass spectrum of synthesized t-butyl ester of MIDD0301. m/z 470/472 represents t-butyl ester MIDD0301 and m/z 414/416 resulted from insource fragmentation.

MIDD0301 was 10.05 min, which did not correspond with the retention time of the impurity at

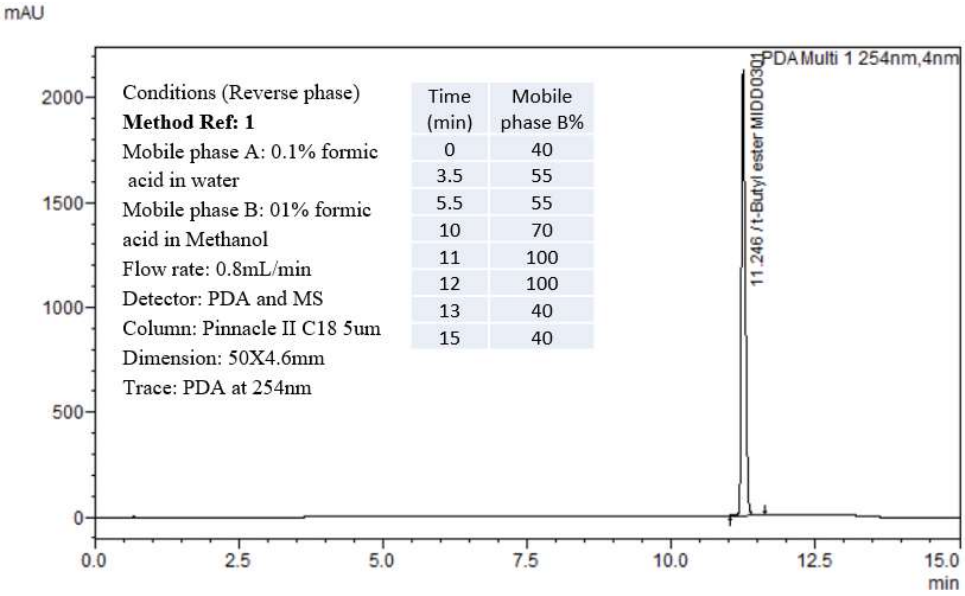

Figure 54. PDA chromatogram of purified t-butyl ester of MIDD0301.

11.24 min. Finally, the synthesized *t*-butyl ester of MIDD0301 was analyzed with same LCMS method. Chromatogram and mass spectrum of the analysis shown in Figure 53 and 54 respectively confirmed the impurity as *t*-butyl ester of MIDD0301, which also formed the acid (m/z 414 and 416) through insource fragmentation. The mass pattern and retention time both

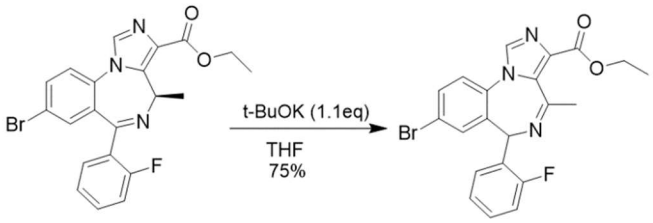

Scheme 10 Synthesis of isomer of MIDD0003 from MIDD0003.

matched with the impurity peak.

The second impurity peak found for the MIDD0003 product was the 6H-isomer of MIDD0003 having an achiral methyl group and retention time of 11.54 min (Figure 51). The percentage of this impurity was found to be more than 1%, so we synthesized it for verification. The olefinic isomer of MIDD003 was synthesized by treating MIDD0003 with potassium *t*-butoxide in THF

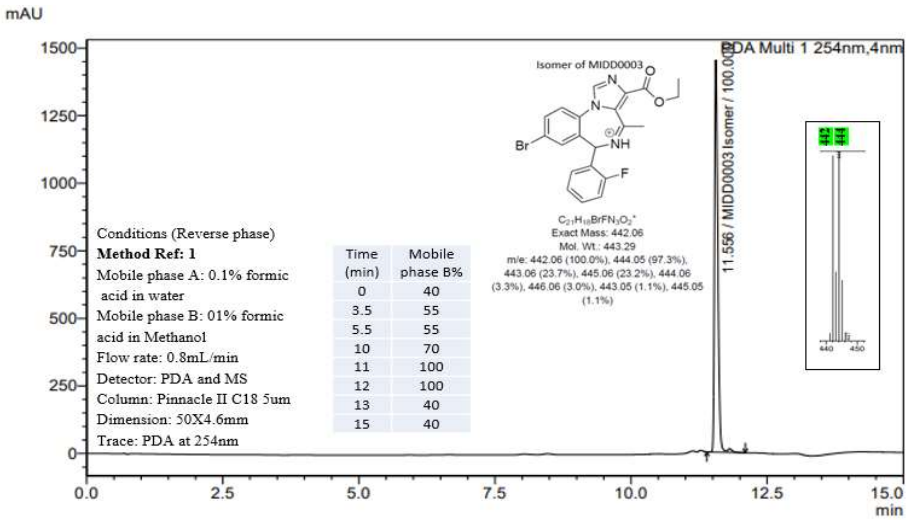

Figure 55. PDA chromatogram of synthesized isomer of MIDD0003 matched with the RT and MS pattern of impurity2 of MIDD0003.

(Scheme 10). A m/z of 442 and 444 pair was found in mass spectrum of synthesized MIDD0003 isomer with a retention time of 11.56 min.-This confirmed that the impurity peak 2 was indeed the 6H-isomer of MIDD0003 (Figure 55). Also, the optical purity of MIDD0003 was determined with method 4. An optical purity of 99.8 % ee was calculated from the chromatogram shown in

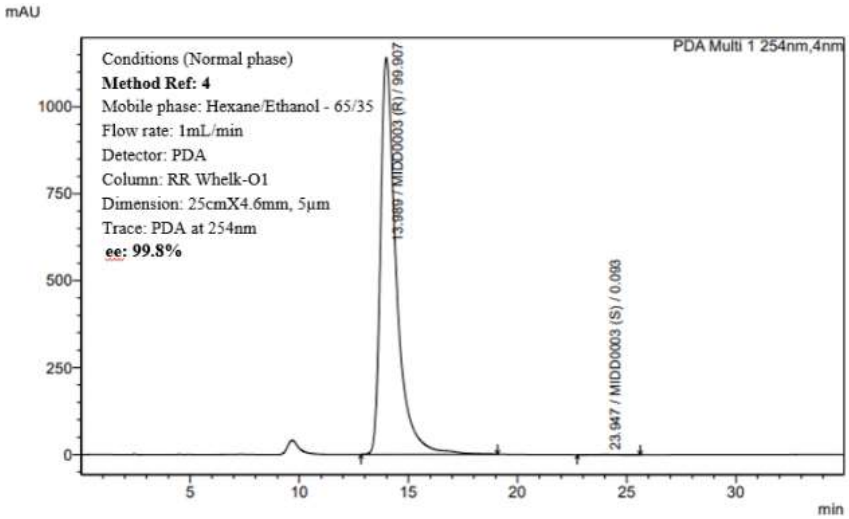

Figure 56. PDA chromatogram of MIDD0003 extracted at 254 nm. The sample was analyzed by normal phase method 4. Purity was found ee 99.8%.

the Figure 56.

Figure 57 showed that only one impurity peak eluted alongside the product peak having the same mass than MIDD0301. Thus, it can be concluded that the impurity is the structural isomer of

MIDD0301. The amount of the impurity was more than 1%. Therefore, MIDD0301 isomer was

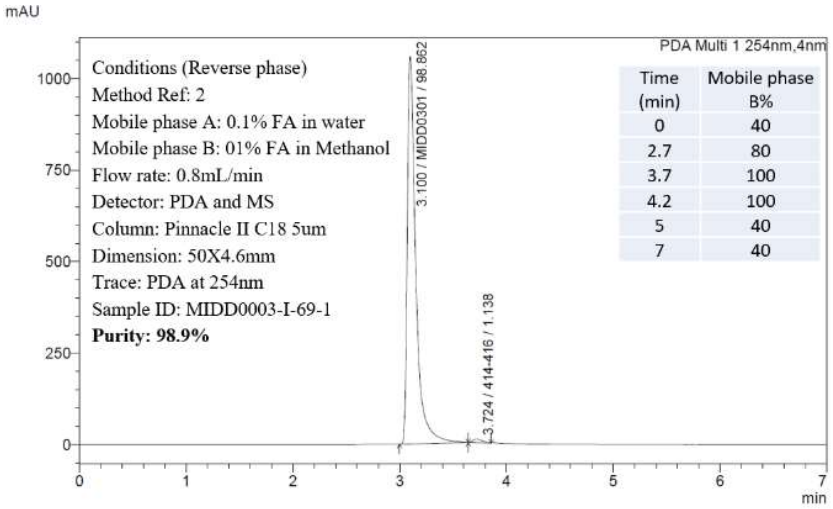

Scheme 57. PDA chromatogram of MIDD0301 at 254 nm. Analysis was carried out with reverse phase method 2.

synthesized (Scheme 9) and analyzed with method 2. The MS pattern and retention time matched the MIDD0301 impurity peak. Purity of the final product was 98.9% (Figure 57).

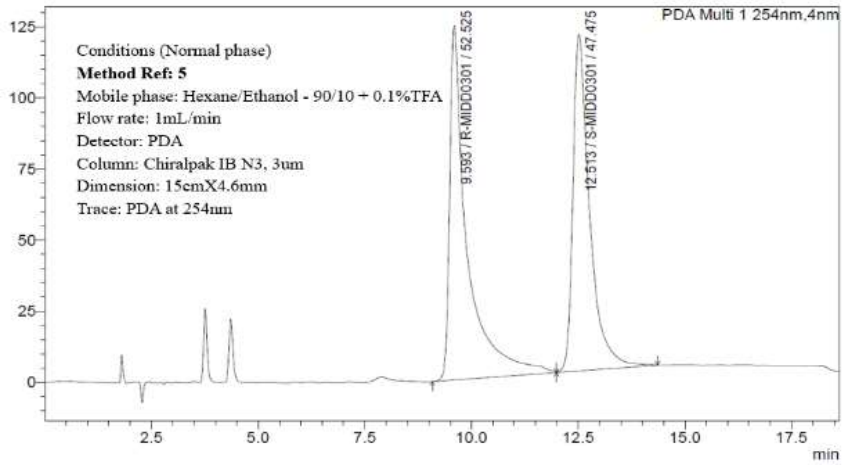

Figure 58. PDA chromatogram of a racemic mixture of MIDD0301 using chiralpak IB N3 column.

However, there was still one last analytical problem namely a suitable method for optical purity determination for MIDD0301. Therefore, a new column was purchased. The application of the Chiralpak IB N3 column resulted of the enantiomeric separation of open MIDD0301 (retention times 3.7 and 4.4 min) and closed MIDD0301 (retention times 9.5 and 12.5 min) (Figure 58).

Although we were able to optimize a method that separated MIDD0301 enantiomers, an acidic modifier had to be used to improve peak shape. Without modifier this column showed excessive

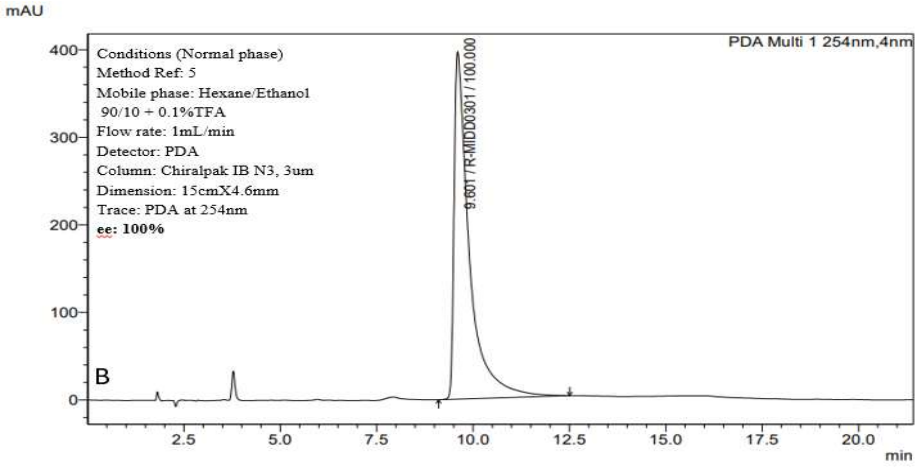

Figure 59. PDA chromatogram of final product MIDD0301 using method 5 for purity determination.

tailing of the MIDD0301 enantiomers without baseline separation. However, the addition of 0.1% TFA resolved this problem and resulted in Method 5. The optical purity of MIDD0301 was found to be 100 % after recrystallization of the final product (Figure 59).

Chapter 4: Drug metabolism and pharmacokinetic analysis

The identification of metabolites of clinical drug candidates is essential to understand potential safety liabilities, especially for drugs with significant human metabolism. This analysis is of particular significance for metabolites that reach >10% of the area under the curve exposure.[75] Metabolites can occur via phase I and phase II processes. A simplified version of phases I & II

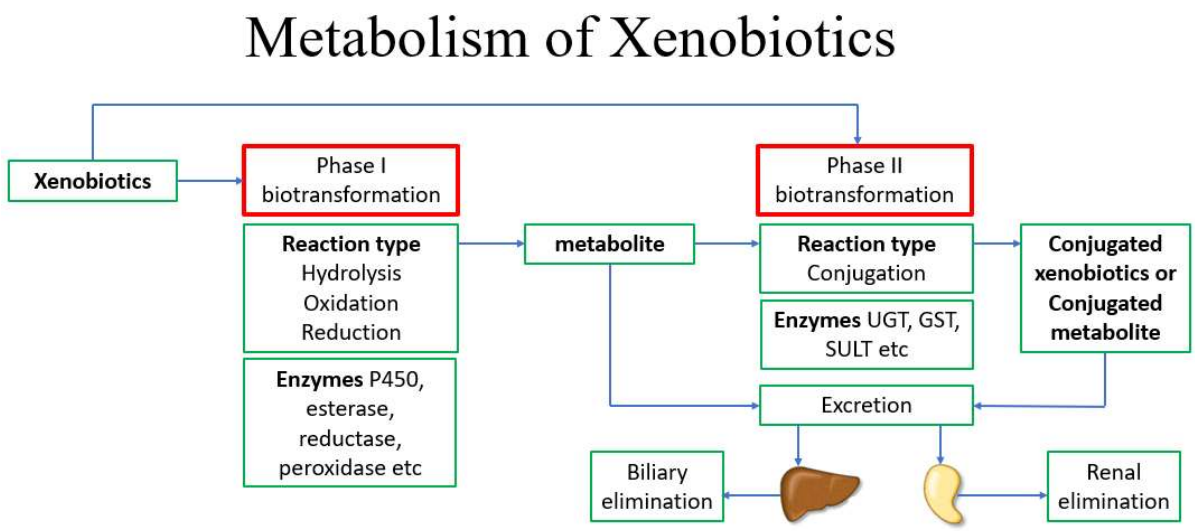

Figure 60. Simplified representation of xenobiotics in vivo metabolism.

metabolism is depicted in Figure 60. The majority of xenobiotic phase I metabolites are formed by cytochrome P450 oxidases.[76] Other phase I modifications can be formed by monooxygenases,[77] dehydrogenases,[78] peroxidase,[79] reductase,[80] esterase,[81] amidases and epoxyhydrolases.[82] Phase II xenobiotic metabolism, or conjugation, is catalyzed predominately by transferases that include UDP-glucosyltransferases,[83] N-acetyltransferase,[84] methyltransferase,[85] glutathione transferase,[86] and sulfotransferases.[87] Conjugation with amino acids or taurine occurs via activation by acyl CoA synthetase,[88] followed by conjugation catalyzed by the corresponding N-acyltransferase.[89]

MIDD0301 is a clinical drug candidate being developed for asthma symptom control that was shown to attenuate airway hyperresponsiveness and reduce lung inflammation in rodents when administered orally[22] or nebulized.[11] The drug acts via binding to gamma aminobutyric acid receptors ($GABA_ARs$)[90] that are expressed on airway smooth muscle[18] and inflammatory cells.[91] Relaxation of contracted human airway smooth muscle in the presence of MIDD0301 has been shown to occur within minutes using *ex vivo* tissue.[23] MIDD0301 did not cause any adverse effects or suppress systemic T cell dependent antibody responses following repeated high dose exposure in rodents.[24] The compound contains a carboxylic acid and is highly solubility in water at neutral pH.[92] There is very little brain absorption and no observed central nervous system effects at high single or repeated dosing.[22]

In this study, we describe the metabolism and excretion of MIDD0301. The compound is based on a benzodiazepine scaffold, which has been the subject of several decades of medicinal chemistry research to modify $GABA_AR$ binding selectivity and pharmacokinetic properties. The substitution of the N-methyl amide by an imidazole ring impacted the sensitivity to demethylation.[93] Introduction of a chiral methyl group prevented C3-hydroxylation.[94] Finally, the introduction of a carboxylic acid group did not only create tissue selectivity but also prevented further phase I metabolism.[95] Phase I and II metabolic stability studies of MIDD0301 are presented using microsomes from various species. Furthermore, MIDD0301 metabolites were identified, and corresponding analytical standards synthesized to enable detection and quantification by LC-MS/MS. An analytical method was developed to quantify all currently known MIDD0301 metabolites with one LC-MS/MS method using urine and feces samples. Additionally,

blood, lung, and brain concentrations of MIDD0301 were determined following oral, intraperitoneal, and intravenous drug administration.

4.1 Experimental

4.1.1 Experimental animals

5-10 week-old female Swiss Webster mice (Charles River Laboratory, Wilmington, MA) were used for *in vivo* studies. Animals were housed under specific pathogen-free conditions, under standard conditions of humidity, temperature, and a controlled 12 h light and dark cycle and had *ad libitum* access to food and water. All animal experiments were conducted in compliance with the University of Wisconsin-Milwaukee or Columbia University Institutional Animal Care and Use Committees (IACUC).

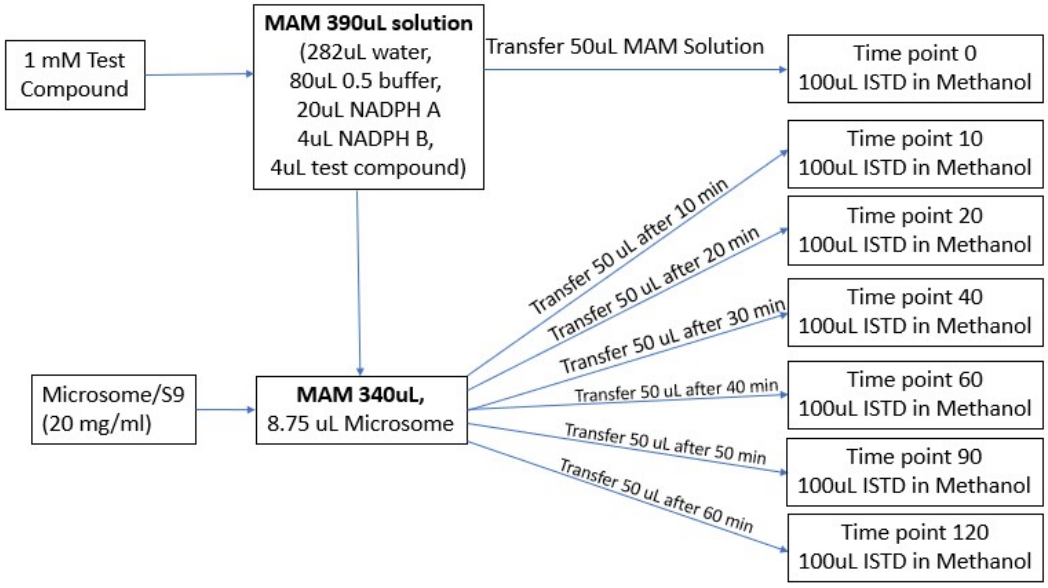

Figure 61. Schematic diagram of a typical microsomal stability assay.

4.1.2 Phase I microsomal stability assay

4 µL of 1 mM MIDD0301 in DMSO was added to a mixture of 282 µL water, 80 µL phosphate buffer (0.5 M, pH 7.4), 20 µL NADPH Regenerating System Solution A (BD Bioscience, San Jose,

CA), and 4 µL NADPH Regenerating System Solution B (BD Bioscience). The assay concentration of MIDD0301 was 10 µM. The solution was pre-incubated at 37°C for 5 min using a digital heating shaking dry bath (Fischer Scientific, Pittsburgh, PA) followed by removal of 50 µL at the 0 min time point, which was added to 100 µl methanol that contained 10 µM 4,5-diphenylimidazole as internal standard (IS). The reaction was initiated by addition of 8.8 µL of human, mouse, rat, or dog liver microsomes (each from Xenotech, Kansas City, KS), resulting in a protein concentration of 0.5 mg/mL. 50 µL aliquots were taken at 10, 20, 30, 60, and 120 minutes. Like the 0 min time point, each aliquot was transferred to 100 µL of cold methanol containing 10 µM IS. This was followed by sonication for 10 sec and centrifugation at 11,000 x g for 5 min. The supernatant was transferred into a spin-X HPLC filter tube (Corning Inc., Corning, NY) and centrifuged at 11,000 x g for 30 sec. The filtrate was diluted 20-fold and subsequently analyzed by LC-MS/MS with Shimadzu LCMS 8040 mass spectrometer, (Shimadzu, Kyoto, Japan). The ratio of the peak areas of the internal standard and MIDD0301 was calculated for every time point and the natural log of the area ratio of % remaining at any time point (T_t) compared to start time (T_0) were plotted against time to determine the linear slope (k) and half-life (0.693/k). All determinations were carried out on two different days in triplicate.

4.1.3 Phase II microsomal stability assay (glucuronidation and glucosidation)

4 µL of 1 mM MIDD0301 in 50:50 water:acetonitrile was added to a mixture of 222 µL water, 80 µL phosphate buffer (0.5 M, pH 7.4), 40 µL substrate (50 mM of UDP-glucuronic acid or UDP glucose), 40 µL inhibitor (50 mM of sacharic-1,4-lactone or gluco-1,5-lactone), 4 µL 100 mM $MgCl_2$, and 1.8 µL 5 mg/ml alamethicin in dimethyl sulfoxide. The assay concentration of MIDD0301 was 10 µM. The solution was pre-incubated at 37°C for 5 min using a digital heating

shaking dry bath (Fischer Scientific, Pittsburgh, PA) followed by removal of 50 µL as 0 min time point, which was added to 100 µl acetonitrile that contained 5 µM compound 2[13] as internal standard (IS). The reaction was initiated by addition of 8.8 µL of either human or mouse liver S9 fraction or mouse kidney S9 fraction (each from Xenotech, Kansas City, KS) resulting in a protein concentration of 0.5 mg/mL. Aliquots of 50 µL were taken at time intervals of 10, 20, 30, 60, 90, and 120 minutes (for short assay) or 1, 2, 4, 8, and 24 hours (for long assay). Like the 0 min time point, each aliquot was transferred into 100 µL of cold acetonitrile containing 5 µM IS. The solution was sonicated for 10 sec and centrifuged at 16,000 x g for 5 min. The supernatant was transferred into a 0.22 µm nylon spin-X HPLC filter tube (Corning Inc., Corning, NY) and centrifuged at 16,000 x g for 30 sec. The filtrate was diluted 10-fold (for short assay, no dilution for long assay) and subsequently analyzed by LC-MS/MS with a Shimadzu LCMS 8040 mass spectrometer, (Shimadzu, Kyoto, Japan). The ratio of the peak areas of the internal standard and MIDD0301 was calculated for every time point and the natural log of the area ratio of % remaining at any time point (T_t) compared to start time (T_0) were plotted against time to determine the linear slope (k) and half-life (0.693/k) in the short assay. For the long assay, area ratios of internal standard and MIDD0301 glucuronide (or MIDD0301 glucoside) were plotted against time and first order kinetics were used to determine rate constant k. All determinations were carried out in triplicate.

4.1.4 Identification of MIDD0301 metabolites

To identify metabolites, urine and feces were collected for a mouse using a metabolic cage (Techniplast, Varese, IT) after 24 h of MIDD0301 IP administration. The sample preparation was conducted as follows. For urine samples: 200 µL of sample was taken in an Eppendorf tube and

200 µL methanol was added, vortexed, centrifuged at 11,000 x g for 10 min and filtered through a 3000 molecular weight cutoff filter (Amicon) before analysis. For feces samples: Whole feces pellets were collected over 24 h and were added to a 50 mL tube containing 10 mL of 50:50 water:methanol. The mixture was homogenized with a handheld homogenizer (Cole Palmer LabGen 7B Homogenizer) and centrifuged for 20 min. 500 µL of the supernatant was transferred into a different tube and filtered with 3000 MW cut-off filter (Amicon) before analysis. Three different types of mass spectrometry analyses were carried out to identify MIDD0301 metabolites.

4.1.4.1 Full scanning

Using single quadrupole LCMS (LCMS 2020, Shimadzu, Japan), the mass range was set 150 to 1200 Da both in positive and negative modes. Water and methanol mobile phases contained 0.1% formic acid. The gradient started at 20% methanol and reached 99% methanol within 22 min. After a hold of 3 min, the mobile phase returned to 20% within 1.5 min and was kept at that composition for 3.5 min to attain column equilibration for the next injection. An Agilent RRHD Extend-C18 (2.1 mm x 50 mm, 1.8 µm particle size) column at a flow rate of 0.5 mL/min was used. Drying gas and nebulizing gas flow were 15 and 1.5 L/min respectively; heat block temperature and desolvation line temperature were 400°C and 250°C, respectively.

4.1.4.2 Neutral loss scanning

A triple quadrupole LCMS (LCMS 8040, Shimadzu, Japan) was used for this analysis. All parameters were the same as described in 4.1.4.1 except the nebulizing gas flow which was set to 2 L/min. Scanning range was 300 – 800 Da. Neutral loss molecules that were investigated

included glucuronic acid (194 Da), glucuronic acid -H_2O (176 Da), glucose (162 Da), taurine (107 Da).

4.1.4.3 Precursor ion search

During the precursor ion search, MIDD0301 products ions containing ^{81}Br were used resulting in the following product ions m/z 304.90, 371.95 and 397.95 in three different events (each event constituted a search based on one product ion). Mobile phases were water and methanol both having 0.1% formic acid. The flow rate was 0.6 mL/min and the mobile phase was comprised of 20% methanol and increased to 70% within 2 min. During a period of 4 min, the mobile phase was increased to 99% which was continued for 4 min. Finally, the composition was reduced to 20% methanol over a period of 0.75 min. Data were recorded for 15 min. Interface parameters were the same as 4.1.3.2.

4.1.5 Quantification of MIDD0301 and MIDD0301 metabolites in urine and feces

Urine and feces were collected for each mouse individually using a metabolic cage (Techniplast, Varese, IT) at the indicated time periods (24 and 48 h) after MIDD0301 administration. The change of body weights and food and water consumption were recorded. Mice had *ad libitum* access to water and ground diet. Samples were stored at -20°C. Three different routes of administration were investigated in this study. *Oral*: vehicle; 2% polyethylene glycol and 98% of 2% aqueous hydroxypropyl-methyl cellulose; dose: 7.5 mg/mL; injection volume: 100 µL and total administered amount 750 µg. *Intraperitoneal*: 50% propylene glycol and 50% phosphate buffered saline pH 7.2; dose: 3.25 mg/mL; injection volume: 200 µL and total administered amount 750 µg. *Intravenous:* phosphate buffered saline pH 7.2; dose: 5 mg/mL; injection volume: 50 µL and total administered amount 250 µg. Stored urine samples were thawed on ice, vortexed for 5 sec,

and a 200 µL aliquot was combined with 200 µL cold acetonitrile containing compound 2[13] as internal standard (IS1). The IS1 concentration was 0.5 ppm for the 24 h period and 0.05 ppm for the 24 - 48 h period. Samples were vortexed for 15 sec and centrifuged at 11,400 x g for 10 min. The supernatant was transferred into a clean tube, diluted ten times with 80:20 water:acetonitrile. 400 µL was separated by size exclusion filtration (Amicon Ultra-0.5, 3000 NMWL centrifuge filter, Millipore, St. Louis, MO) at 16,000 x g for 30 min. 100 µL of filtrate was transferred into a HPLC vial with 200 µL glass insert and 10 µL of 0.5 ppm XHE-III-74A[12] in acetonitrile was added as a second internal standard. Feces samples were collected during the 0 - 24 h and 24 – 48 h time period in 50 ml Eppendorf tubes and diluted with 20 mL (50:50 solution of acetonitrile with 2.5 ppm IS1) and 10 mL (50:50 solution of acetonitrile with 0.25 ppm IS1), respectively. The samples were homogenized with a handheld homogenizer (Cole Palmer LabGen 7B Homogenizer) and centrifuged at 2700 x g for 20 min at 4 °C. 100 µL of supernatant was diluted with 900 µL of an 80:20 solution of water:acetonitrile. 400 µL of this solution was separated by size exclusion filtration (Amicon Ultra-0.5, 3000 NMWL centrifuge filter, Millipore, St. Louis, MO) at 11,000 x g for 30 min at 4°C. 100 µL of filtrate was transferred into a HPLC vial with a 200 µL glass insert and 10 µL of 0.5 ppm XHE-III-74A[12] in acetonitrile added as second internal standard. High performance liquid chromatography (HPLC) was performed with Shimadzu Nexera X2 LC30AD series pumps (Shimadzu, Kyoto, Japan) using a 5 µL injection volume. Separation was achieved by reverse phase chromatography using an Agilent RRHD Extend-C18 (2.1 mm x 50 mm, 1.8 µm particle size) column with gradient elution at a flow rate of 0.5 mL/min. The mobile phase was methanol and water (both containing 0.1% formic acid). Program: 35% B (0 min) → 50% B (0.75 min), hold at 50% B (1.75 min), → 62% B (3.5 min) → 99% B (0.5 min), hold at 99% B (1 min),

return to 35% B (0.25 min), hold at 35% B (2.25 min); column temperature: ambient. Analytes were monitored under positive mode multiple reaction monitoring (MRM) using a Shimadzu 8040 triple quadrupole mass analyzer (Shimadzu, Kyoto, Japan) with electrospray and atmospheric pressure ionization run in dual (DUIS) mode. Ion pairs for MIDD0301 were m/z 415.95 > 304.90, m/z 415.95 > 397.95, m/z 413.95 > 302.90, m/z 413.95 > 395.95; XHE-III-74A[12] m/z 314.10 > 368.10, m/z 314.10 > 278.10; compound 2[27] m/z 360.20 > 249.10, m/z 360.20 > 273.10, m/z 360.20 > 342.15, m/z 360.20 > 301.10; MIDD0301 glucoside m/z 578.10 > 416.05, m/z 578.10 > 414.05; MIDD0301 glucuronide m/z 592.10 > 416.05, m/z 592.10 > 305.00, m/z 590.10 > 342.15, m/z 590.10 > 303.00, MIDD0301 taurine m/z 523.10 > 398.05, m/z 523.05 > 356.95, m/z 521.10 > 396.05, m/z 521.05 > 354.95, MIDD0301 glycine m/z 473.00 > 398.00, m/z 471.00 > 396.00, m/z 473.00 > 356.80, m/z 471.00 > 354.80. Collision energy was optimized for each transition to obtain optimal sensitivity. The mass spectrometer was operated with the heat block temperature set at 400 °C, drying gas flow of 15 L/min, desolvation line temperature of 250 °C, nebulizing gas flow of 1.5 L/min, and both needle and interface voltages of 4.5 kV. Data acquisition and data processing were performed using LabSolutions software. Standard curves were generated with analytical standards and fitted by a linear regression. Concentrations were calculated with calibration curves of that day. The mean and standard deviation were calculated accordingly.

4.1.6 Pharmacokinetic studies in mice

Six-week-old female Swiss Webster mice received MIDD0301 doses of 25 mg/kg by intra-gastric gavage, 25 mg/kg by intraperitoneal injection, or 1 mg/kg by tail vein injection using formulations described in 4.1.5. *Quantification of MIDD0301 and MIDD0301 metabolites in urine and feces*. At

10, 20, 40, 60, 120, 240, 480, and 1,440 min, blood was collected via cardiac puncture and placed into heparinized tubes. Lung and brain were harvested and stored in liquid nitrogen until analysis (n = 4). Blood was thawed on ice, vortexed for 10 sec, and a 100 µL aliquot was combined with 400 µL cold methanol containing 300 nM XHE-III-74A^{12} IS. Samples were vortexed for 30 sec and centrifuged at 16,000 x g for 10 min at 4 °C. The supernatant layer was then transferred into clean tubes and evaporated using a Speedvac concentrator. The residue was reconstituted with 400 µL methanol and spin-filtered through a 0.22 µm nylon centrifugal filter units (Costar, Glendale, AZ). After reconstitution, the samples were diluted if needed and 4,5-diphenylimidazole was added as instrument standard. The injection volume was 5 µL (LC–MS/MS, Shimadzu 8040). Brain and lung tissue samples were thawed, weighed, and homogenized directly into 400 µL or 600 µL methanol, respectively, containing 300 nM XHE-III-74A^{12} (IS) using a Cole Palmer LabGen 7B Homogenizer. Samples were centrifuged for 10 min at 16,000 x g at 4 °C. The supernatants were then spin-filtered through 0.22 µm nylon centrifugal filters (Costar) and evaporated using a Speedvac concentrator. After reconstitution with 200 µL or 400 µL of methanol for brain and lung respectively, 4,5-diphenylimidazole was added after spin-filtration through 0.22 µm nylon centrifugal filters. The injection volume was 5 µL (LC–MS/MS, Shimadzu 8040). High performance liquid chromatography (HPLC) was performed with Shimadzu Nexera X2 LC30AD series pumps (Shimadzu, Kyoto, Japan). Analytes were separated with an Agilent RRHD Extend-C18 (2.1 mm x 50 mm, 1.8 µm particle size) column with gradient elution at a flow rate of 0.5 mL/min. The mobile phase was methanol and water (both containing 0.1% formic acid). Time program: 20% B (0 min) → 45% B (2 min) → 99% B (4 min), hold at 99% B (4.75 min), return to 20% B (5 min), hold at 20% B (1.5 min); column temperature: ambient. Analytes were monitored under positive mode

by a Shimadzu 8040 triple quadrupole mass analyzer (Shimadzu, Kyoto, Japan) using electrospray and atmospheric pressure ionization run in dual (DUIS) mode as described under 4.1.5. *Quantification of MIDD0301 and MIDD0301 metabolites in urine and feces*. The following transitions were monitored in MRM mode. Ion pairs for MIDD0301 were m/z 416.10 > 304.95, m/z 416.1 > 397.95, m/z 416.10 > 372.05, XHE-III-74A:22 m/z 314.10 > 368.10, m/z 314.10 > 278.10, m/z 314.10 > 296.15. Transition pairs for 4,5-diphenylimidazole were m/z 220.80 > 193.10, m/z 220.80 > 166.90, m/z 220.80 >151.95 and m/z 220.80 > 116.10. Data were analyzed with PK solution 2.0 using a two compartment PK model. Half-lives were calculated based on elimination rates.

4.2 Results and Discussion

First, we investigated the metabolic stability of MIDD0301 in the presence of liver microsomes

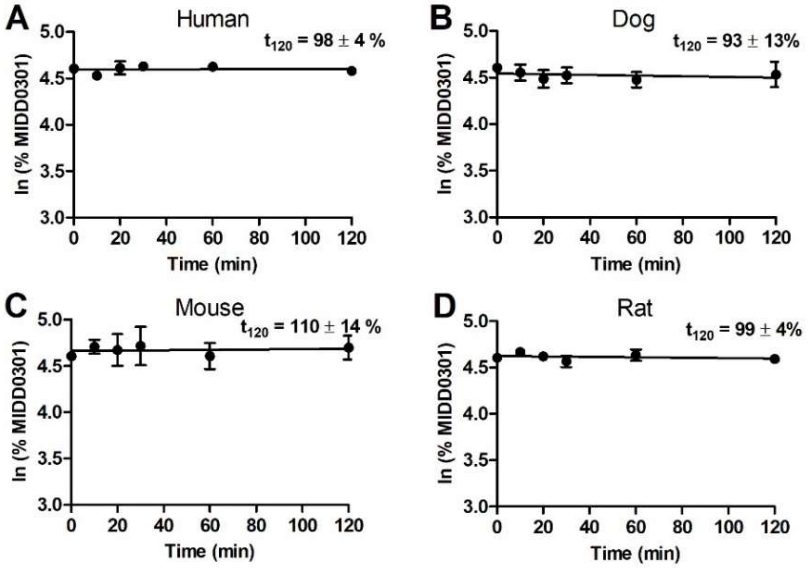

Figure 62. In vitro phase I metabolism of MIDD0301 in the presence of A) human liver S9 fraction; B) beagle dog liver microsomes; C) mouse liver microsomes; D) rat liver microsomes. All assays were performed as two independent assays with an n = 3. Data are presented as averages with standard deviations. Percent MIDD0301 remaining at the 120-minute time point is shown on each graph.

and S9 fractions derived from different species. The results are depicted in Figure 62. In the

presence of human, dog, mouse and rat liver fractions, metabolic conversion of MIDD0301 over a period of two hours was not observed. A similar compound SH-053-2'F-R-CH_3 bearing an ester group instead of an acid group was metabolized fully within four hours, whereas the corresponding amide (MP-III-022) was stable during this time period.[96] Thus, the carboxylic acid group of MIDD0301 in contrast to the ester resulted in resistance to conversion by microsomal enzymes that use NADHP as cofactor. In addition to the method described in the experimental section 4.1.2 for phase I microsomal stability assay, a higher microsome concentration, extended

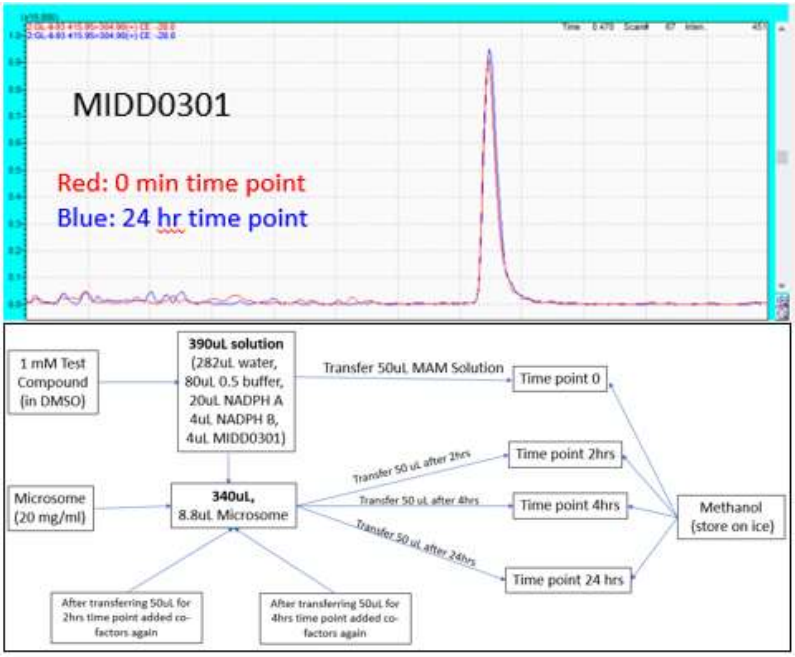

Figure 63. Extended incubation time and additional co-factors used for a modified phase I microsomal stability assay. Figure shows a comparison of MIDD0301 sample signal in mass chromatogram for 0 min vs 24 hours (top panel) and schematic diagram of the assay (bottom panel).

incubation time and multiple addition of co-factors to incubation solution were investigated to detect any phase I biotransformation. But none of the attempts manifested any sign of significant reduction of the initial concentration of MIDD0301 (Figure 63).

In order to evaluate drug-drug interactions, MIDD0301 was incubated with recombinantly expressed CYP3A4 and a substrate that fluoresces once oxidized and cleaved. No significant inhibition of the enzymatic reaction was found in the presence of MIDD0301 in comparison with

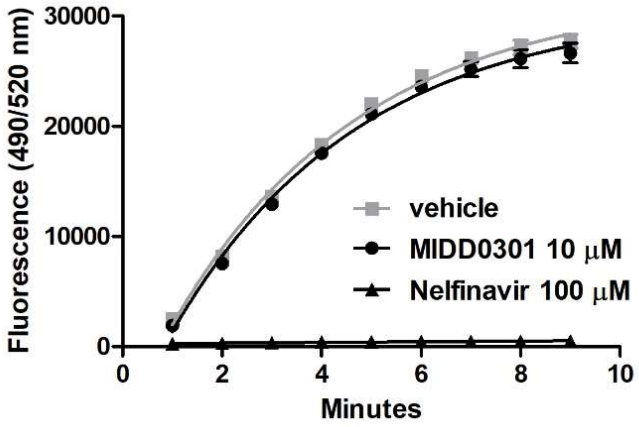

*Figure 64. CYP3A4 inhibition assay. Recombinantly expressed CYP3A4 enzyme was incubated in the presence of NADPH, fluorescent substrate, and MIDD0301 (10 μM) or vehicle. Fluorescence intensity was determined over time and depicted as mean with standard deviation and rates were determined by non-linear regression (first-order kinetics). % inhibition was defined as (1-((X-B)/(A-B)))*100, A is the rate observed for vehicle, B is the rate observed in the presence Nelfinavir. MIDD0301 inhibition of CYP3A4 was less than 1%.*

Nelfinavir (Figure 64). 10 μM MIDD0301 inhibited less than 1% activity of CYP3A4, a P450 enzyme that metabolizes more than 50% of all drugs. In contrast, nelfinavir at 100 μM completely inhibited the CYP3A4 activity. Accordingly, MIDD0301 does not inhibit phase I metabolism meditated by CYP3A4, consistent with the observed resistance of MIDD0301 to metabolism by liver microsomes. Furthermore, we expect the absence of drug-drug interactions for MIDD0301, which occurs when a co-administered drug alters the metabolism of a primary drug. Next, we investigated MIDD0301 phase II metabolism. Therefore, urine and feces of treated mice were analyzed using mass spectrometry. For this purpose, MIDD0301 was administered IP and mice were placed in cages to collect urine and feces. The problem with this method was that urine and feces samples cross-contaminated each other. To circumvent this problem, a metabolic cage

Figure 65. A) Techniplast metabolic cage for single mouse; B) urine and feces deposited in the separate collection containers after keeping the mouse for 24 h in the upper chamber of the cage; C) collected urine during 24 h; D) collected feces over 24 h.

(Techniplast, Varese, IT) for a single mouse (Figure 65) was applied. With this metabolic cage, urine and feces can conveniently be collected without cross-contamination. Initially MIDD0301 glucuronide and methyl ester were identified through full scanning of mouse urine. These metabolites were anticipated due to carboxylic acid function of MIDD0301. Molecules bearing an amine, alcohol or carboxylic acid group are usually subject to glucuronidation. Enzymatic formation of the methyl ester via methylation such as N-methylation is possible but the methanol which was used for sample preparation might have reacted with MIDD0301 conjugates. The analytical method was verified with the synthesized methyl ester of MIDD0301. We were wondering if the esterification of MIDD0301 took place during extraction with methanol or during chromatography using methanol as mobile phase. Three MIDD0301 solutions were prepared. One contained methanol, the other one 0.1% formic acid in methanol and the third one acetonitrile. The solutions were kept at room temperature overnight. Next day, all three samples

along with a synthesized methyl ester of MIDD0301 and a urine sample were analyzed with LCMS.

No sign of conversion of MIDD0301 was observed in methanol or 0.1% formic acid in methanol

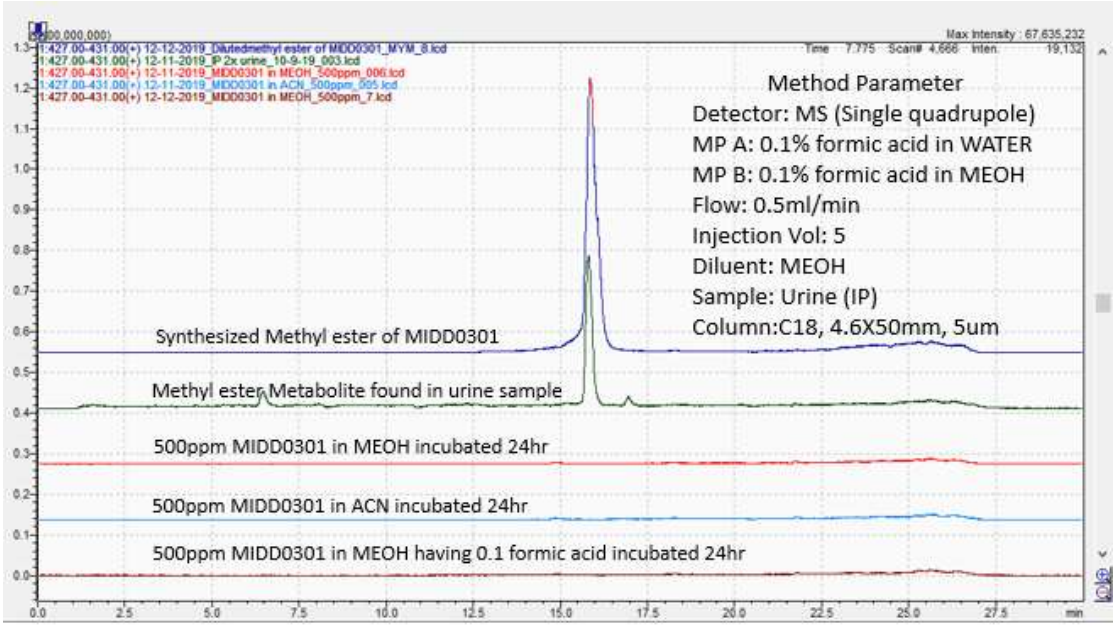

Figure 66. Extracted mass chromatogram at mass range 427-431 m/z to investigate the methyl ester MIDD0301 peak whose m/z is 428 and 430. No sign of esterification of MIDD0301 in methanol even after 24 h.

solution (Figure 66). Thus, the methyl ester is not formed directly from MIDD0301 during the sample preparation and analysis. At a later stage of study, a higher dose of MIDD0301 was

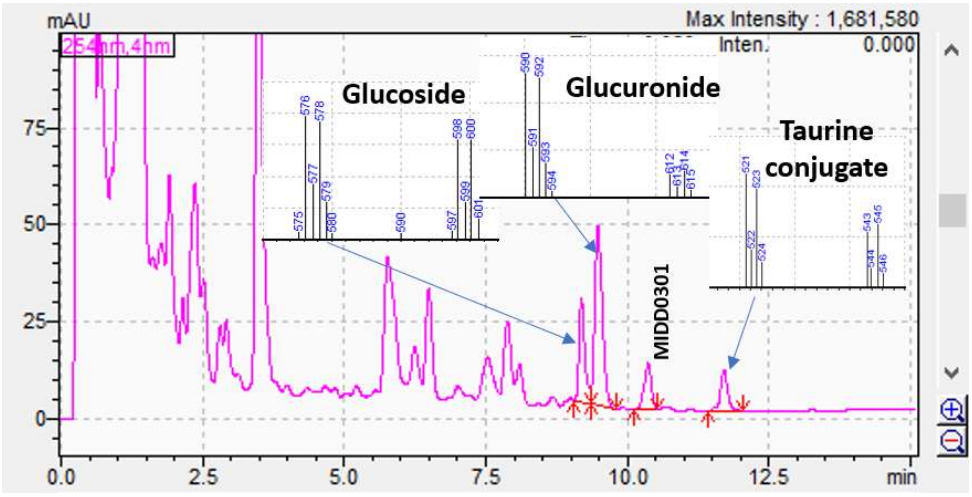

Figure 67. PDA chromatogram of urine sample for IP administered MIDD0301. (Inset) mass spectra of metabolite peaks.

administered via IP and an improved sample clean-up that included the use of a Amicon 3000 MW cut-off filter instead of 0.22 µm nylon spin X filter was applied. The use of a UPLC column

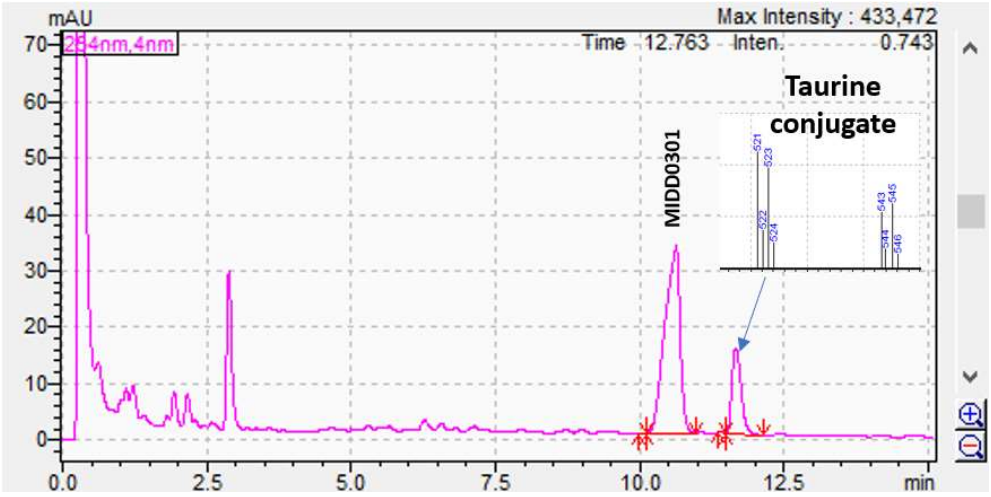

Figure 68. PDA chromatogram of feces sample after IP administered MIDD0301. (Inset) mass spectra of metabolite peaks.

(Agilent RRHD Extend-C18, 2.1 mm x 50 mm, 1.8 µm particle size) gave proper separation among the metabolites in full scanning mode (Figures 67 & 68). Each metabolite showed the characteristic two isotopes of ^{79}Br and ^{81}Br. The ions found for the metabolites in full scan mode were confirmed by neutral loss scanning and precursor ion search scanning. Especially the precursor ion search turned out later to be the one of the best predictors for phase II conjugates.

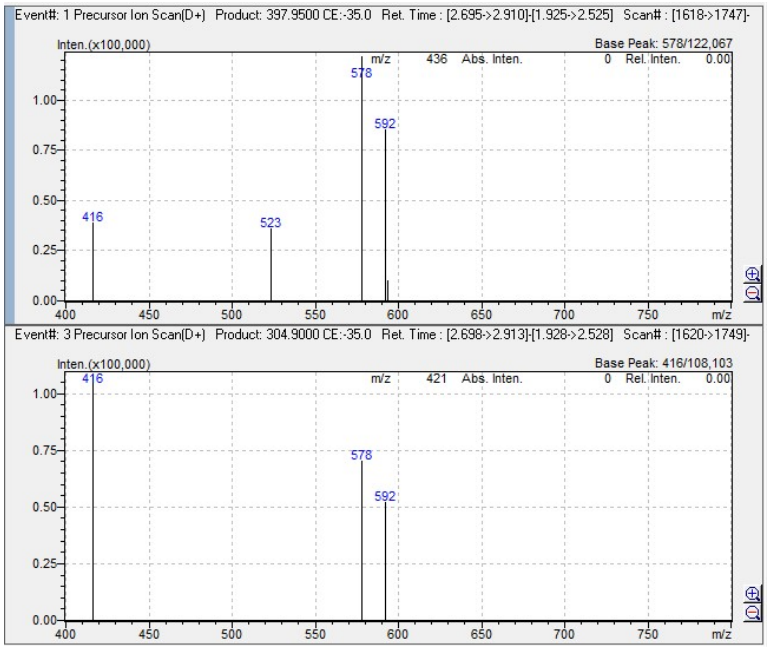

Figure 69. Precursor ion search in urine sample for IP administered MIDD0301. Mass spectra at peak region 2.69 to 2.91 min. Mass spectra based on product ion m/z 397.95 (Top pane) and m/z 304.90 (bottom panel).

For the precursor ion search, precursor ions which produce m/z 398 and 305 product ions, were m/z 523, 578, 592 along with 416 in urine sample (Figure 69). For feces samples, precursor ion search scanning provided m/z 523 and 416. The masses of 523, 578 and 592 m/z were identified as taurine conjugate, glucoside, and glucuronide, respectively, and confirmed with the corresponding synthesized compounds. Neutral loss scanning for m/z 176, resulted in m/z 590 and 592, which correspond to MIDD0301 glucuronide. However, neutral loss for glucose or taurine was not found. To achieve a better signal for neutral loss scanning, the collision energy needed to be optimized. Usually, a lower collision energy generates a better signal for neutral

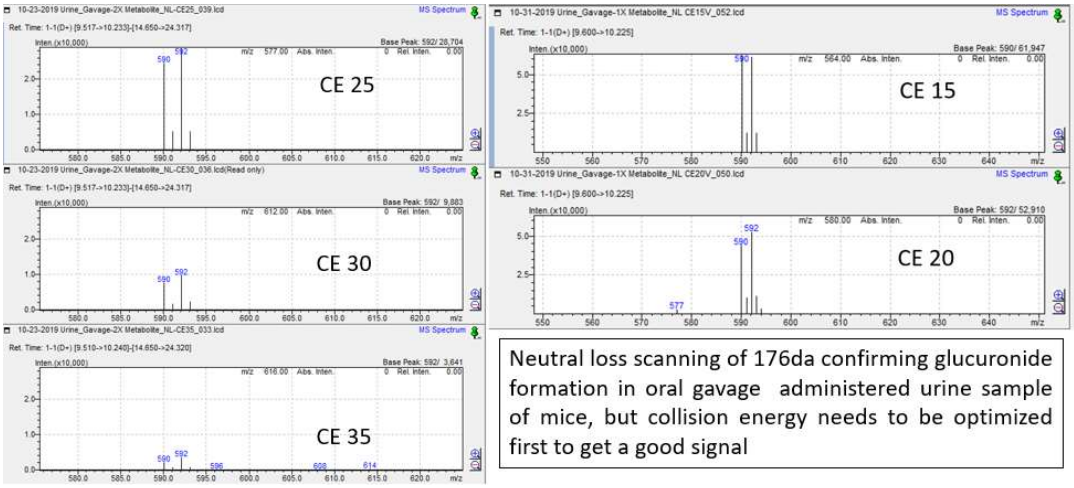

Figure 70. Neutral loss scanning of oral administered urine sample. Collision energy varied from 35 to 15 eV. Maximum intensity was 3641 at 35 eV and increased to 61947 at 15 eV.

loss scanning (Figure 70). For MIDD0301 conjugates identified in urine and feces, we optimized *in vitro* phase II metabolism assays for glucuronidation and glucosidation to determine the kinetics of these reactions. For the analysis of the phase II glucuronidation assay, the mass of the methyl ester of MIDD0301 was found along with the MIDD0301 glucuronide. The assay was repeated with deactivated microsomes but no formation of MIDD0301 glucuronide or methyl ester was observed. At this point we realized that the transesterification of glucuronide in presence of methanol might form the methyl ester of MIDD0301. When acetonitrile was used

instead of methanol for stopping the *in vitro* phase II metabolism reaction, no sign of the methyl ester MIDD0301 was found. We also prepared urine samples with acetonitrile or methanol and incubated the samples at room temperature for 24 h before analysis and only found the methyl

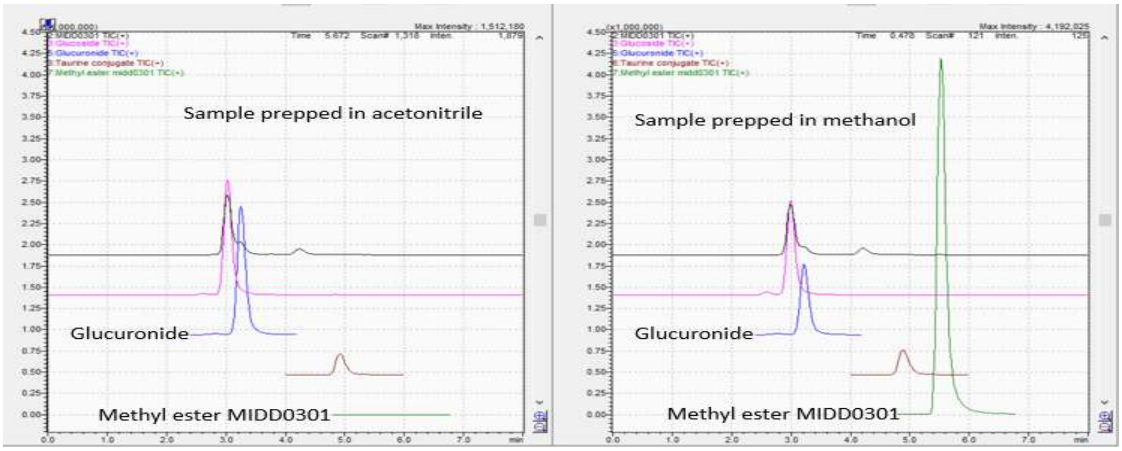

Figure 71. Sample extraction in acetonitrile and methanol for urine samples collected for IP administered MIDD0301. After sample preparation, samples were kept in room temperature for 24 hours before analysis. A significant methyl ester MIDD0301 peak was only found for methanol exacted samples. MRM method that was optimized for the quantitative analysis of MIDD0301 and its metabolites was used to analyze this sample.

ester in the methanol extracted sample (Figure 71). Later, we found that the glucoside is also susceptible to transesterification like the MIDD0301 glucuronide, however, MIDD0301 taurine was stable under these conditions. Therefore, the extraction solvent was changed from methanol to acetonitrile even though solubility of the metabolites were superior in methanol. However, before switching to acetonitrile, ethanol and 2-propanol were used as extraction solvent prompted by a report that showed that ethanol promoted only 10% conversion to the ethyl ester and 2-propanol resulted in only 0.1% transesterification.[101] It was found that ethanol and propanol-2 were more prone to transesterification compared to methanol in our case.

To identify and quantify phase II metabolic products of MIDD0301 using LC-MS/MS, MIDD0301 glycine, glucuronide, glucoside, and taurine conjugates were synthesized as outlined in Scheme

11. MIDD0301 taurine was generated by conversion of MIDD0301 to the corresponding acid

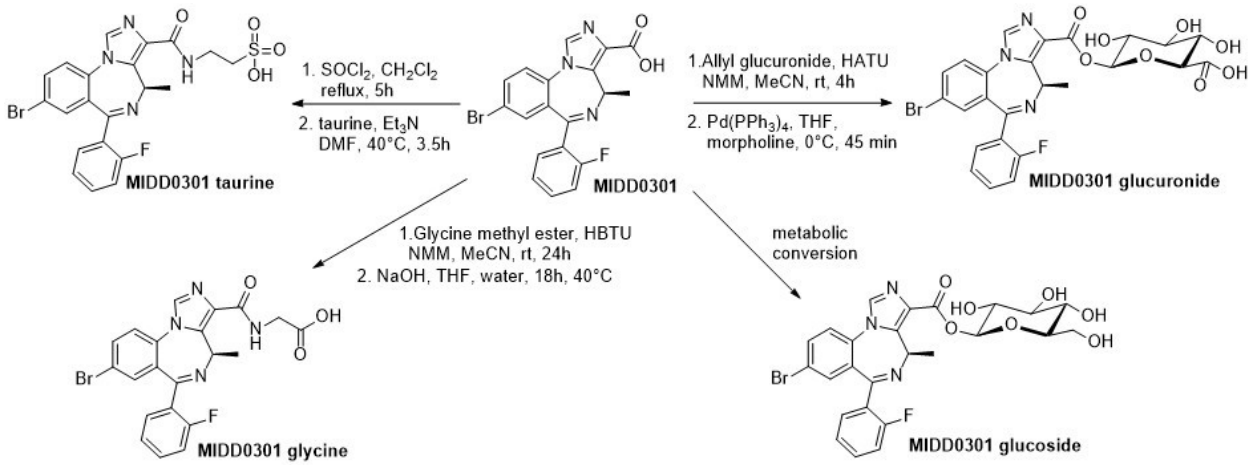

Scheme 11 Synthesis of possible MIDD0301 phase II metabolites

chloride using thionyl chloride followed by the addition of taurine in the presence of trimethylamine. The glycine methyl ester was coupled with MIDD0301 in the presence of O-(benzotriazol-1-yl)-N,N,N',N'-tetramethyluronium hexafluorophosphate (HBTU) in excellent yield followed by hydrolysis in the presence of sodium hydroxide to yield MIDD0301 glycine. MIDD0301 glucuronide was synthesized by adopting a procedure developed by the Stachulski group using allyl glucuronide.[97] After the coupling step in the presence of 1-[Bis(dimethylamino)methylene]-1H-1,2,3-triazolo[4,5-b]pyridinium 3-oxid hexafluorophosphate (HATU), the MIDD0301 allyl glucuronide was converted to MIDD0301 glucuronide in the presence of $Pd(PPh_3)_4$ and morpholine. Several attempts to synthesize MIDD0301 glucoside were unsuccessful, but enzymatic conversion of MIDD0301 in the presence of mouse kidney S9 fractions and uridine 5'-diphosphoglucose (UGT-Glc) yielded enough material to develop a LC-MS/MS selective reaction monitoring method for this metabolite. At this point it was unclear whether the mobile phase should be changed to acetonitrile. Therefore, the urine sample extracted with acetonitrile was analyzed with the usual water:methanol mobile phase in which

both having 0.1% formic acid. No sign of MIDD0301 methyl ester formation was found (Figure

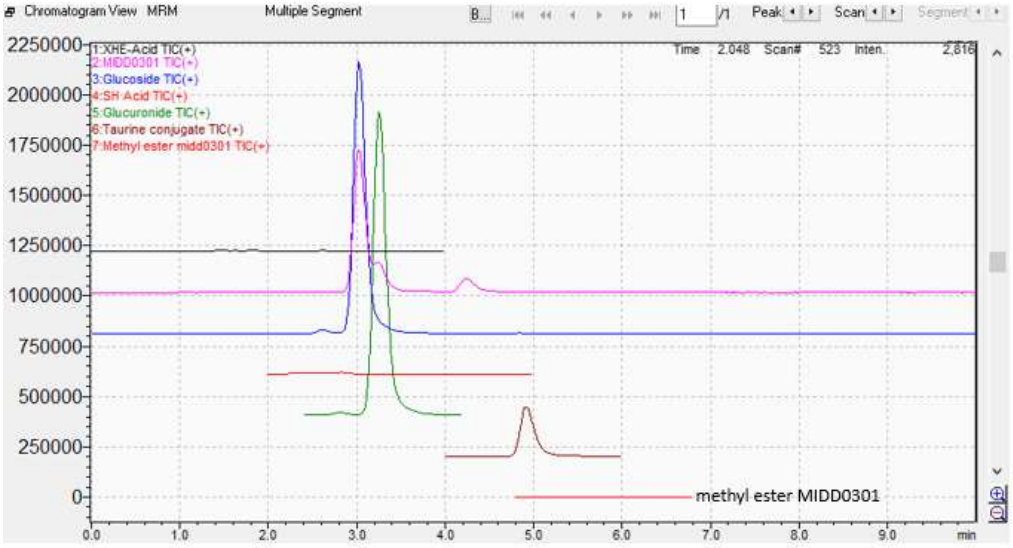

Figure 72. Mass chromatogram of an acetonitrile extracted urine sample demonstrated no sign of methyl ester MIDD0301.

72). The run time of the method is only 10 min and the acidic condition of mobile phase might suppress the transesterification during the analysis. Thus, the initial method using methanol as mobile phase was not changed.

Another difficulty to quantify MIDD0301 glucuronide was insource fragmentation of these

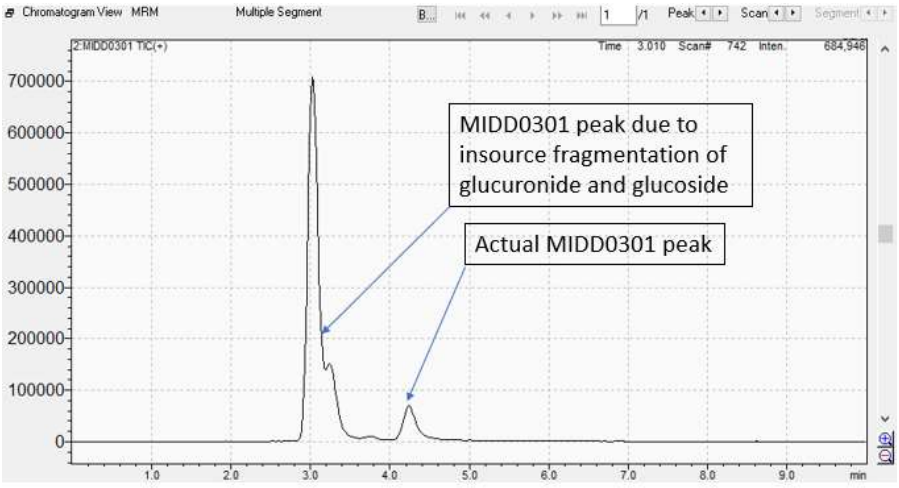

Figure 73. MRM mass chromatogram of MIDD0301 for urine sample. Additional MIDD0301 peak eluted earlier than 4 min is due to insource fragmentation of glucuronide and glucoside metabolite peaks.

particular metabolites. In source fragmentation means the breakdown of a molecule during

ionization. In our case, metabolites deconjugated during ionization giving the parent molecule mass at a different retention time (Figure 73). These peaks of MIDD0301 have to be baseline separated in order to quantify MIDD0301 glucuronide and glucoside. Otherwise, the analysis would result in an overestimated MIDD0301 concentration. Transesterification in presence of alcohol as extraction solvent and insource fragmentation made it very difficult to find metabolites at the beginning of our study. Along with the glucuronide, glucoside, and taurine conjugate, a minor metabolite was detected with represented the glycine conjugate of MIDD0301. The concentration was below the limited of detection for the full scanning mode. However, with the

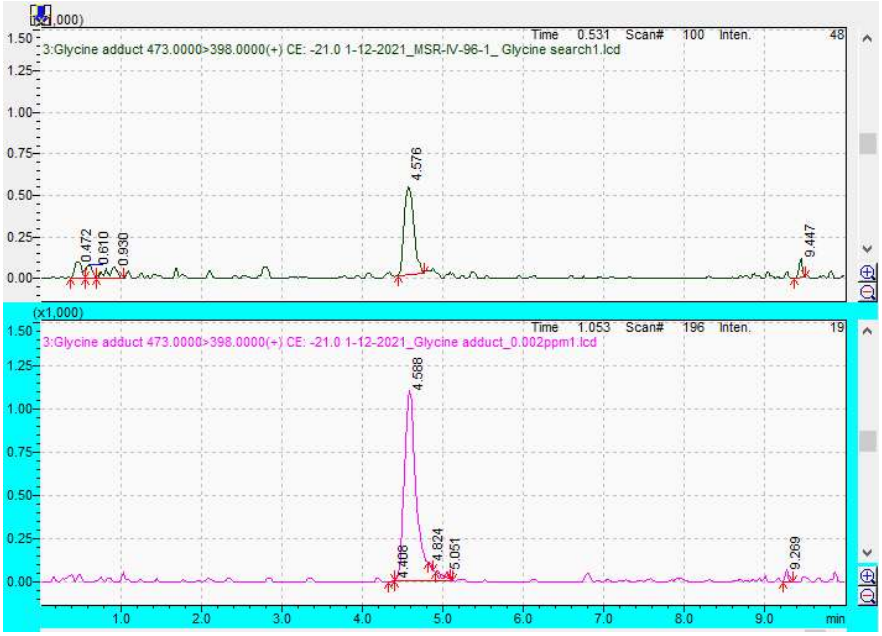

Figure 74. MRM mode mass chromatogram enabled detection of MIDD0301 glycine conjugates peak urine sample (top panel) and mass chromatogram of 0.002 ppm MIDD0301 glycine adduct standard (bottom panel).

MIDD0301 glycine standard available, a MRM event for MIDD0301 glycine was optimized allowing the detection of this metabolite in the urine sample (Figure 74).

In vitro assays using liver and kidney S9 fraction were conducted in the presence of appropriate co-factors to determine phase II metabolism kinetics. The results are depicted in Figure 75. In the

presence of human or mouse liver S9 fractions, conversion of MIDD0301 was observed in the presence of uridine 5'-diphosphoglucuronic acid (UGT-GlcUA) with half-lives of 240 and 143 min,

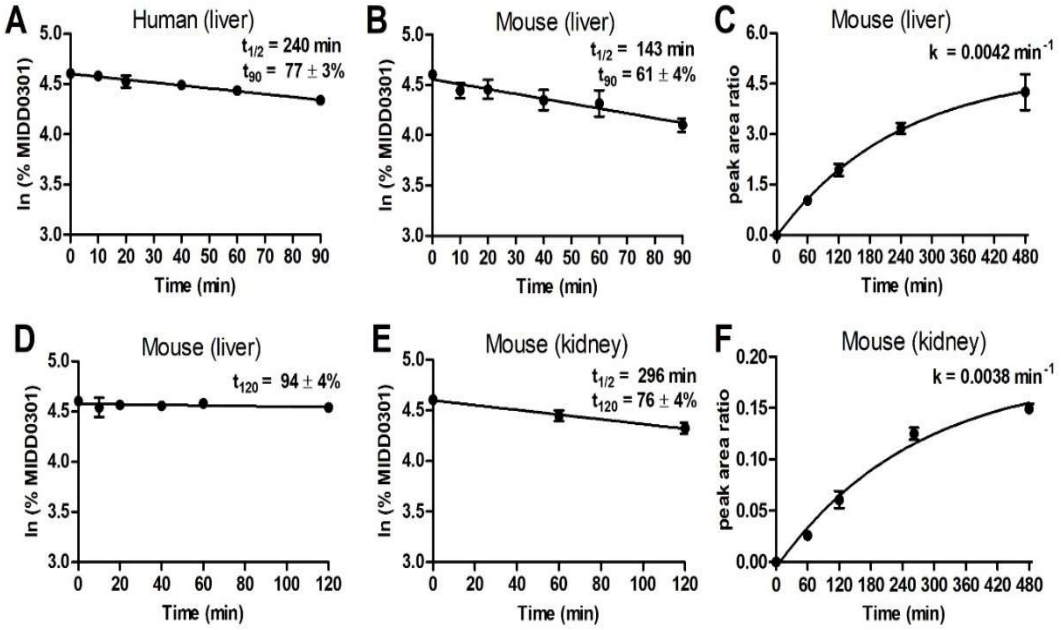

Figure 75. In vitro phase II metabolism of MIDD0301. Glucuronidation of MIDD0301 was determined in the presence of A) human liver S9 and B)/C) mouse liver S9. For C) peak area ratios of internal standard and MIDD0301 glucuronide were plotted versus time and first order kinetic analysis used to determine rate constant k. Glucosidation of MIDD0301 was determined in the presence of D) mouse liver S9 and E)/F) mouse kidney S9. For F) peak area ratios of internal standard and MIDD0301 glucoside were plotted versus time and first order kinetic analysis used to determine rate constant k. All assays were performed as two independent assays with n = 3. Data are presented as averages with standard deviations.

respectively (Figure 75 A and B). The reaction was carried out in the presence of alamethicin[98] and β-glucuronidase inhibitor saccharolactone.[99] Similar to the conversion of MIDD0301, the formation of MIDD0301 glucuronide was by quantified by LC-MS/MS. The reaction was monitored for eight hours resulting in a reaction rate of 0.0042 min^{-1} when analyzed by a first order kinetic equation (Figure 75C). Thus, MIDD0301 is readily converted by liver UDP-glucuronosyltransferases (UGT) and the formed MIDD0301 glucuronide is stable under physiological conditions for at least eight hours. It has been reported that benzoic acid acyl-glucuronides are more stable than aliphatic acyl-glucuronides, which can undergo intramolecular rearrangement and protein alkylation.[100]

Conjugation of xenobiotics by UGTs using uridine 5'-diphosphoglucose (UGT-Glc) has been reported infrequently and usually occurs to a lesser extent.[83] We used mouse liver S9 fraction initially but did not observe conversion of MIDD0301 (Figure 75D). However, in the presence of mouse kidney S9 a pronounced conversion of MIDD0301 was observed (Figure 75E). Glucoside

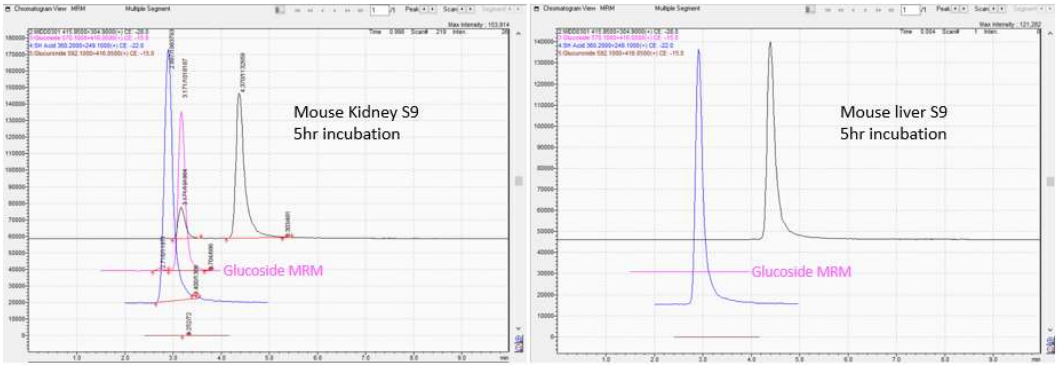

Figure 76. MRM mass chromatogram of phase II glucosidation assay in presence of kidney S9 (left) and liver S9. MIDD0301 was incubated for 5 hours before quenched in acetonitrile. Pink line representing glucoside MRM. A glucoside peak was visible in mouse kidney S9 sample but not in the mouse liver s9 sample confirming glucosidation only occurred in the kidneys.

formation was confirmed with MRM mass chromatogram monitoring (Figure 76). The half-life of MIDD0301 in mice for the glucosidation was significantly longer ($t_{1/2}$ = 296 min) than the glucuronidation ($t_{1/2}$ = 143 min). MIDD0301 glucoside was identified by LC-MS/MS, bearing the signature bromine isotope ratio. Quantification relative to an internal standard enabled us to analyze the formation of MIDD0301 glucoside, which occurred with a reaction rate of 0.0038 min^{-1} (Figure 75F), thus slower than the corresponding glucuronidation reaction. The tissue selective glucosidation reaction of MIDD0301 could be mediated by UGT3A2.[83] This specific UGT uses UGT-Glc and UGT-xylose instead of UGT-GlcUA and is not expressed in liver.

To investigate the extent of MIDD0301 conjugation *in vivo*, we quantified phase II metabolites in feces and urine from mice following oral administration. The results are summarized in Table 7.

Table 7 Excretion of MIDD0301 and its metabolites after oral administration.

	0-24 hours		24-48 hours		0-48 hours
	Feces (%)[1]	Urine (%)[1]	Feces (%)[1]	Urine (%)[1]	Feces & Urine (%)[1]
MIDD0301	54.3 ± 5.2	0.1 ± 0.01	0.7 ± 0.4	<LOD	55.1 ± 5.7
MIDD0301 taurine	2.7 ± 0.7	0.2 ± 0.04	<LOD	<LOD	2.9 ± 0.8
MIDD0301 glucoside	<LOD	2.5 ± 0.1	<LOD	0.3 ± 0.3	2.8 ± 0.5
MIDD0301 glucuronide	<LOD	5.8 ± 0.4	<LOD	0.6 ± 0.3	6.4 ± 1.1
Total	57.0 ± 5.9	8.6 ± 0.55	0.7 ± 0.4	0.9 ± 0.6	67.2 ± 7.45

[1]% is based on moles of MIDD0301 administered; LOD, limit of detection.

After 24 hours, 54.3% of unconjugated MIDD0301 was observed in feces, whereas 0.1% of unconjugated MIDD0301 was found in urine. The major metabolite was MIDD0301 glucuronide followed by MIDD0301 taurine and glucoside. MIDD0301 glucuronide and glucoside were exclusively excreted in urine, whereas MIDD0301 taurine was predominately found in feces. During the 24-48-hour sample collection period, only 0.7% of MIDD0301 was recovered in feces and very low concentrations of MIDD0301 glucuronide and glucoside in urine. Overall, 67.2 ± 7.5% of the initial dose of MIDD0301 was recovered, thus, other metabolites such as MIDD0301 amino acid conjugates might be formed. However, MIDD0301 glycine was detected at less than 0.01% in urine and feces.

Next, we investigated the metabolic fate of MIDD0301 when administered intravenously. The results are summarized in Table 8.

Table 8 Excretion of MIDD0301 and its metabolites after IV injection.

	0-24 hours		24-48 hours		0-48 hours
	Feces (%)[1]	Urine (%)[1]	Feces (%)[1]	Urine (%)[1]	Feces & Urine (%)[1]
MIDD0301	30.4 ± 3.4	0.4 ± 0.1	1.2 ± 0.2	<LOD	32.0 ± 3.7
MIDD0301 taurine	7.0 ± 3.1	0.6 ± 0.1	<LOD	<LOD	7.6 ± 3.2
MIDD0301 glucoside	<LOD	44.0 ± 3.4	<LOD	2.0 ± 0.7	46.0 ± 4.1
MIDD0301 glucuronide	<LOD	2.5 ± 0.5	<LOD	0.1 ± 0.04	2.6 ± 0.54
Total	37.4 ± 6.5	47.5 ± 4.1	1.2 ± 0.2	2.1 ± 0.74	88.2 ± 11.54

[1] % is based on moles of MIDD0301 administered; LOD, limit of detection.

The recovery of unconjugated MIDD0301 during the first 24 hours was 30.4% in feces and 0.4% in urine. In contrast to oral administration of MIDD0301, MIDD0301 glucoside was the major metabolite, followed by taurine and glucuronide. We established that glucosidation occurs exclusively in the kidney, thus the absence of first pass liver metabolism might be responsible for more pronounced glucosidation. However, the formation of MIDD0301 taurine was still more than twice as high as in feces in comparison to oral administration. For IV administration, the recovery of MIDD0301 and its metabolites were below 4% for the 24-48 hour sample collection period. Interestingly, 88.2% of the initial dose was recovered as unconjugated MIDD0301 and MIDD0301 metabolites implying that formation of unknown MIDD0301 metabolites occurred to a lesser degree for IV administered MIDD0301. Because 32.0% of the initial IV dose was excreted as unconjugated MIDD0301 in comparison to 55.1% when given orally, bioavailability of MIDD0301 could be as high as 77%.

The recovery of MIDD0301 and formation of MIDD0301 conjugates were also investigated following intraperitoneal injection of MIDD0301 (Table 9).

Table 9 Excretion of MIDD0301 and its metabolites after IP injection.

	0-24 hours		24-48 hours		0-48 hours
	Feces (%)[1]	Urine (%)[1]	Feces (%)[1]	Urine (%)[1]	Feces & Urine (%)[1]
MIDD0301	43.2 ± 5.9	0.3 ± 0.2	0.3 ± 0.1	0.1 ± 0.04	43.9 ± 6.24
MIDD0301 taurine	16.2 ± 0.9	0.4 ± 0.1	<LOD	<LOD	16.6 ± 1.0
MIDD0301 glucoside	<LOD	13.9 ± 7.1	<LOD	2.4 ± 0.2	16.3 ± 7.3
MIDD0301 glucuronide	<LOD	2.8 ± 1.2	<LOD	0.3 ± 0.2	3.1 ± 1.4
Total	59.4 ± 6.8	17.4 ± 8.6	0.3 ± 0.1	2.8 ± 0.44	79.9 ± 15.94

[1] % is based on moles of MIDD0301 administered; LOD, limit of detection.

After IP injection of MIDD0301, 43.2% of unconjugated MIDD0301 was found in feces, whereas 0.3% was detected in urine. In contrast to oral and IV administration, MIDD0301 taurine was the main metabolite for IP injected MIDD0301 followed by MIDD0301 glucoside and glucuronide. Similar to oral and IV injected MIDD0301, MIDD0301 taurine was predominately found in feces. Total MIDD0301 glucoside was five-fold greater than the glucuronide, much less than the 17.6-fold difference for IV injected MIDD0301. Also, the percentage of MIDD0301 taurine was twice as high as for IP injected MIDD0301. Less than 4% of unconjugated MIDD0301 and its metabolites were detected during the 24–48 hour sample collection period, which was consistent for all routes of administration. Total recovery of the MIDD0301 initial dose following IP administration was 79.9%, which was greater than oral administration but less than IV injection.

Next, we determined the blood concentrations of MIDD0301 for oral, IP and IV administration. The blood concentrations were determined over a period of 24 h and are depicted in Figure 77.

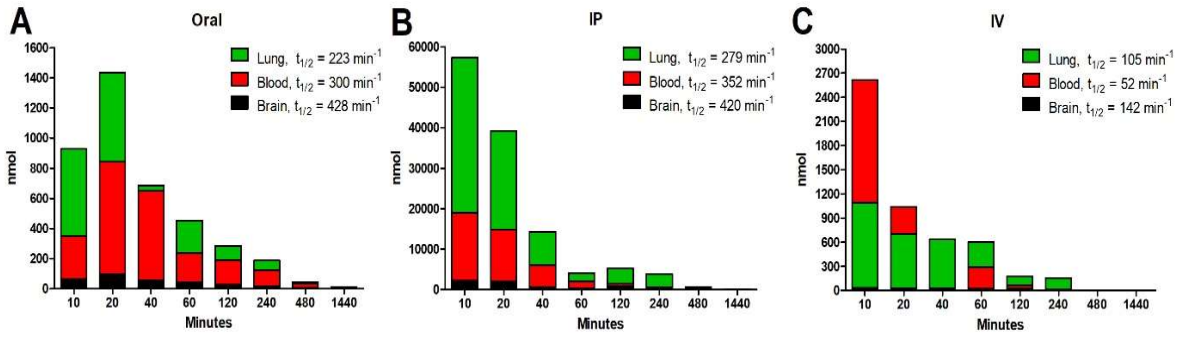

Figure 77. Pharmacokinetic data for MIDD0301. A) 25 mg/kg by oral gavage; B) 25 mg/kg by IP injection; C) 1 mg/kg by tail vein injection. Animals were scarified at indicated time points and concentrations of MIDD0301 were quantified by LC-MS/MS. Data are shown as means (n = 4 for oral, n = 8 for IP 10 and 20 min/rest n = 4, and n = 8 for IV) and fitted to a two-compartment body equation to determine half-life (t1/2) based on calculated elimination constants.

For the oral administration of MIDD0301, we observed a t_{max} of 20 min (Figure 77A). Even at 10 min the blood and lung concentrations of MIDD0301 exceeded receptor affinity (EC_{50} = 72 nM) at a dose of 25 mg/kg. Thus, orally administered MIDD0301 was absorbed very quickly. Based on calculated elimination rates, MIDD0301 half-lives for blood and lung were 4-5 h. MIDD0301 concentrations in the non-perfused brains were very low, usually less than 7% of the corresponding blood concentrations. After 24 h, lung and brain MIDD0301 concentrations were less than 3 nM, whereas 12 nM MIDD0301 was still found in blood. Intraperitoneal administration of the same dose of MIDD0301 in a 50:50 mixture of phosphate buffered saline and polypropylene glycol resulted in very high lung and blood concentrations of MIDD0301 during the first 40 min (Figure 77B). Mice exhibited no signs of toxicity throughout the study. Half-lives for MIDD0301 in blood, lung, and brain for IP injections were similar to oral administration. Tail vein injections of an aqueous MIDD0301 solution (1 mg/kg) were well-tolerated without signs of irritation at the injection side. Half-lives of MIDD0301 were shorter (1-2 h) for this administration

(Figure 77C), probably due to the rapid formation of MIDD0301 glucoside in urine that was observed for this the route of administration (Table 8).

Recently we reported that MIDD0301, in addition to its ability to reduce asthma symptoms by oral administration, it also rapidly reduced bronchoconstriction when delivered by inhalation.[11] The onset of action and effective doses were comparable to BAA albuterol in allergen-induced

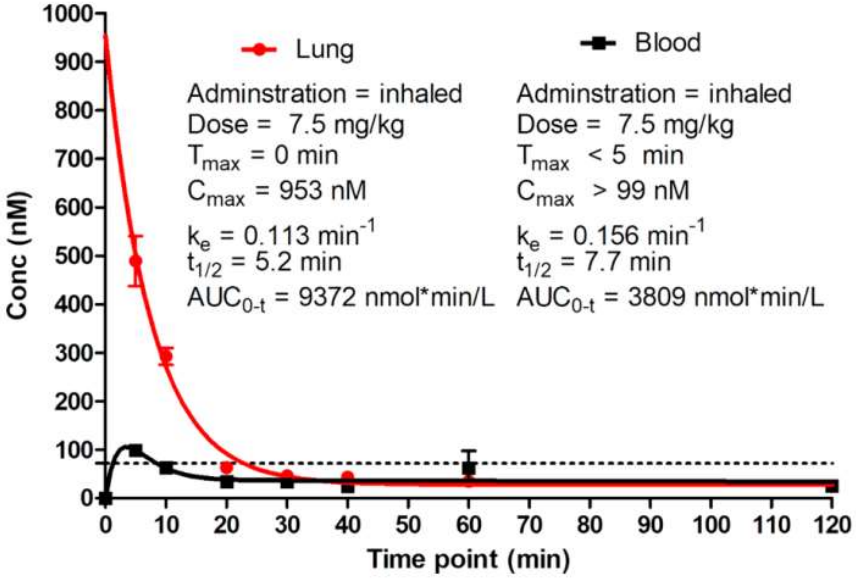

Figure 78. Pharmacokinetics of nebulized MIDD0301 in Swiss Webster mice. Groups of four mice were dosed with 20 µL of nebulized MIDD0301 (7.5 mM in water pH 7.5). Tissues were harvested at indicated time periods and MIDD0301 quantified by LCMS/MS. Data are depicted as means ± SD. Data were analyzed with PK Solution 2.0.

murine asthma models. Repeated inhaled nebulized doses of MIDD0301 achieved bronchodilation at doses lower than single treatments. Cardiovascular, CNS, and respiratory toxicity studies confirmed the safety of inhaled MIDD0301 at exposure 50-fold greater than its therapeutic dose. Exponential one-phase nonlinear regression reflected a lung concentration of 953 nM at t = 0 (Figure 78). The half-life of MIDD0301 in the lung was 5.2 min. MIDD0301 has a binding affinity of 72 nM for the $GABA_AR$; thus, therapeutic concentrations for receptor activation were maintained at this level for at least 25 min.

In conclusion, MIDD0301 is metabolized solely via conjugation, with no observable phase I oxidation due to the presence of an acid group on the diazepine structure. The route of administration significantly influences the ratio of MIDD0301 and its metabolites, indicating that the sequence of tissue exposure, including first pass metabolism, affects the formation and rates of discrete phase II metabolites. However, the elimination rates of MIDD0301 for oral and IP administration are similar. More detailed studies are necessary to quantify the *in vivo* conjugation rates for all identified MIDD0301 metabolites as well as their rates of excretion into feces and urine. It is possible that concentrations of MIDD0301 conjugates is higher in the blood than observed in feces and urine due to the lability of glucuronides and glucoside conjugates in aqueous media.[101] Deconjugation can occur enzymatically or via hydrolysis at elevated temperatures. We demonstrated that MIDD0301 metabolites can be synthesized and used to development accurate LC-MS/MS methods for identification and quantification.

Chapter 5: Comparative study of R and S MIDD0301

Chirality can be found in many drugs despite drug development efforts to reduce the number of chirality centers through iterative chemistry approaches.[102] One reason for this effort is to reduce production costs because optical pure starting materials are usually more expensive, racemic resolutions steps reduce the amount of compound by at least 50%, and enantio- or diastereoselective reactions rarely proceed with high stereoselectivity. Furthermore, the distomer is considered an impurity and special guidelines have to be followed to comply with FDA drug approval.[103] However, drug targets such as receptors and enzymes consist of chiral amino acids that in turn create asymmetric building sites. Therefore, chiral centers are sometimes part of drug molecule that enables high affinity binding. Usually, optical pure drugs exhibit significantly better binding than their corresponding enantiomer. For instance β-adrenoreceptor antagonists such as propranolol and atenolol are more potent with a (S) alcohol configurations.[104] Another drug class includes dihydropyridine based calcium channel blockers such as amlodipine and nimodipine, where the (S) enantiomer is more potent than the (R) form.[104] Most of these older drugs are marketed as racemates, whereas newer drugs are usually marketed optically pure such as ACE inhibitor captopril as (S,S) enantiomer.[105] Development of an optical pure compound avoids the possibility that a distomer has undesired pharmacological effects such as the (R) enantiomer of clopidogrel inducing severe neurotoxicity.[106] Extension of a patent can be achieved for drugs that have been marketed as racemates by offering a single enantiomer (chiral switching).[107] Enantiomers that demonstrate an almost identical pharmaceutical activity are very rare and include flecainide, a sodium channel blocker used to treat heart arrhythmia.[108] Another example is antidepressant fluoxetine, a serotonin uptake inhibitor.[109] Chirality can also influence

the administration, distribution, metabolism and excretion (ADME). For oral administration, D-amethopterin showed a significant higher Cmax and AUC than L- amethopterin.[110] There are also many chiral drugs with different volume of distribution for their enantiomers such as ketorolac and methadone.[111, 112] Most chiral drugs, however, show significant differences in the their phase I and II metabolism.[113] For instance, the (S) enantiomer of anticoagulant acenocoumarol is metabolized more quickly by CYP2C19 than the corresponding (R) isomer, which contributes most of the pharmacological effects.[114] For glucuronidation, (S) enantiomer of β-adrenoreceptor antagonist propranolol, is more quickly conjugated by UGT1A9, whereas UGT1A10 has a preference for (R) propranolol.[115] Finally, the secretion of metabolized chiral drugs can be different due to differentiation by chiral transporters. For example, the (R) enantiomer of the 1-hydroxy O-glucuronide of carvedilol is quicker eliminate by biliary secretion for oral and IV dosing than its (S) enantiomer.[116]

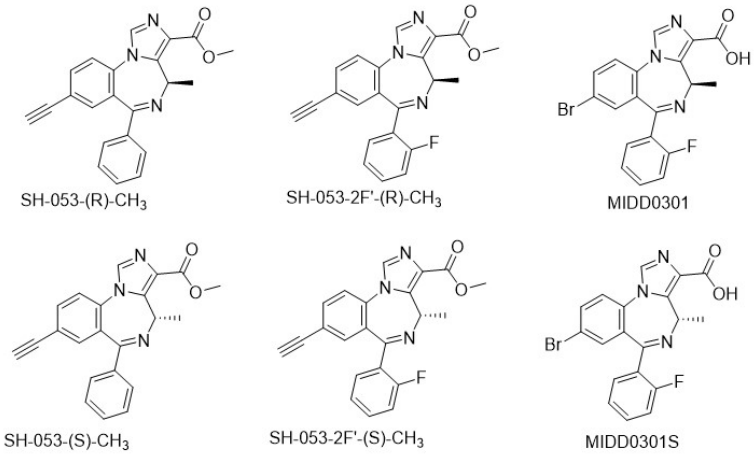

Figure 79. Examples of chiral imidazodiazepines

Chiral and achiral allosteric modulators have been developed for the gamma aminobutyric acid A receptor ($GABA_AR$), a pentameric ligand gated chloride ion-channel that is predominately expressed on neurons. For imidazodiazepines, significant receptor binding differences for

enantiomers has been reported.[17] For instance SH-053-(R)-CH3 potentiated only the $\alpha_5\beta_3\gamma_2$ $GABA_AR$, whereas SH-053-(S)-CH3 additionally potentiated the $\alpha_{2/3}\beta_3\gamma_2$ $GABA_ARs$ (Figure 79).[117] The overall binding affinity of the (R) and (S) enantiomer of SH-053-(R)-CH3 for $GABA_ARs$ expressed in the rat brain was 379 nM and 111 nM, respectively.[118] Significant differences were also observed in respect to metabolism. For instance, only 2.3 % of the original amount of SH-053-2F'-S-CH3 was observed after 30 min in the presence of human liver microsomes, whereas the (R) enantiomer was stable.[119] Our group has recently introduced a new class of imidazodiazepines with the inability to cross the blood brain barrier (BBB).[120] The lead compound MIDD0301 bearing a methyl substituent in the (R) configuration has been shown to relax ex vivo human, guinea pig and mouse airway smooth muscle,[22, 23] which has been reported to express $GABA_AR$.[18] *In vivo* studies have demonstrated that MIDD0301 is alleviating airway hyperresponsiveness in several rodent asthma models when delivered orally[22] and nebulized.[11, 23] However, the corresponding S enantiomer (MIDD0301S) has not been evaluated yet. Here, we report the evaluation of both enantiomers, in respect to binding, metabolism and pharmacokinetics.

5.1 Experimental

5.1.1 Microsomal stability assay (Phase I)

To 0.282 mL water, 0.080 mL phosphate buffer (0.5 M, pH 7.4), 0.020 mL NADPH Regenerating System Solution A, and 0.004 mL NADPH Regenerating System Solution B (BD Bioscience, San Jose, CA) was added 0.004 mL of a 1 mM DMSO (dimethyl sulfoxide) solution of MIDD0301S or MIDD0301. The final assay concentration was 10 µM. During the preincubation of the solution at

37°C using a heating shaking dry bath (Fischer Scientific, Pittsburgh, PA), a 0.05 mL aliquot was removed and quenched with 0.1 ml of cold methanol that contained 10 µM 4,5-diphenylimidazole as internal standard (IS). This aliquot was removed before addition of 8.8 µL of human or mouse liver microsomes (Xenotech, Kansas City, KS). The protein concentration was 0.5 mg/mL. Further aliquots were taken after 10, 20, 30, 60, and 120 minutes after the addition of microsomes and quenched with 0.1 mL of cold methanol containing 10 µM IS. The samples were sonicated for 10 sec, centrifuged at 11,000 x g for 5 min, filtered using a spin-X HPLC filter tube (Corning Inc., Corning, NY), and centrifuged at 11,000 x g for 30 sec. For the analysis by LC-MS/MS (Shimadzu 8040, Kyoto, Japan), the samples were diluted 20-fold. Peak areas ratios between the analytes and internal standard were calculated and graphed as ln(%) compared to the starting concentration against time to determine the linear slope (k) and half-life (0.693/k). The experiments were carried out in triplicate.

5.1.2 Microsomal stability assay (Phase II) (glucuronidation and glucosidation)

To 0.282 mL water, 0.080 mL phosphate buffer (0.5 M, pH 7.4), 0.04 mL of a 50 mM of UDP-glucuronic acid or UDP glucose in water, 0.04 mL of a 50 M solution of inhibitor sacharic-1,4-lactone or gluco-1,5-lactone in water, 0.004 mL of a 100 mM $MgCl_2$ solution in water, and 0.0018 mL of a 5 mg/ml alamethicin in dimethoxy sulfoxide (DMSO). The final compound assay concentration was 10 µM. During the preincubation of the solution at 37°C for 5 min using a heating shaking dry bath (Fischer Scientific, Pittsburgh, PA), a 0.05 ml aliquot was removed and quenched with 0.1 ml of cold methanol that contained 5 µM compound 2[13] as IS. The first aliquot was removed before addition of 8.8 µL of either human or mouse liver S9 fraction or mouse kidney S9 fraction (each from Xenotech, Kansas City, KS). The protein concentration was 0.5

mg/mL. Further aliquots were taken after 10, 20, 30, 60, and 120 minutes and quenched with 0.1 mL of cold acetonitrile containing 5 µM IS. The samples were sonicated for 10 sec, centrifuged at 11,000 x g for 5 min, filtered using a 0.22 µm nylon spin-X HPLC filter tube (Corning Inc., Corning, NY), and centrifuged at 11,000 x g for 30 sec. For the analysis by LC-MS/MS (Shimadzu 8040, Kyoto, Japan), the samples were diluted 10-fold. Peak areas ratios between the analytes and internal standard were calculated and graphed as ln(%) compared to the starting concentration against time to determine the linear slope (k) and half-life (0.693/k). The experiments were carried out in triplicate.

5.1.3 Pharmacokinetic study

The following vehicles were used for oral and intravenous administration. *Oral*: vehicle; 2% polyethylene glycol and 98% of 2% aqueous hydroxypropyl-methyl cellulose; dose: 100 mg/kg. *Intravenous:* phosphate buffered saline pH 7.2; dose: 5 mg/mL. Thirty-two Swiss Webster mice received intra-gastric gavage of MIDD0301 or MIDD0301S formulated in mentioned oral vehicle. At 10, 20, 40 60,120, 240, 480, and 1440 minutes animals were sacrificed, the blood (collected into heparinized tubes), lungs and brain were harvested, and samples were stored in liquid nitrogen until analysis. Another group of 32 Swiss Webster mice were given intravenous administration of MIDD0301 and after 10, 20, 30, 40, 60, 120, 240 and 480 min time points, groups of four animals were sacrificed and blood collected via cardiac puncture into heparinized tubes. Lungs and brain were collected and stored in liquid nitrogen until analysis. Blood samples were thawed on ice and vortexed for 10 sec. 200 µL blood was combined with 400 µL cold acetonitrile containing 0.1 ppm compound 2[13] as internal standard (I.S.1). Samples were vortexed for 10 sec, sonicated for 2 min, and centrifuged at 11,000 x g for 20 min at 4 °C. The supernatant

was then transferred into a new tube and spin-filtered through 0.22 µm nylon centrifugal filter unit (Costar). For the analysis, 100 µL of each filtrate was combined with 10 µL of a 0.5 ppm XHE-III-74A[12] as second internal standard in a HPLC vial having a 150 µL insert. After vortexing the vial for 10 sec the sample was ready for analysis. Whole brains were placed in wide bottom 2 mL Eppendorf tube and weighed. 400 µL of 0.1 ppm compound 2[13] in acetonitrile was added and homogenized with a handheld homogenizer (Cole Palmer LabGen 7B Homogenizer). After centrifugation for 30 min at 11,000 x g, the supernatant was filtered with a 0.22 µm nylon spin X centrifuge filter tube (Costar) and centrifuged again for 5 min at 11,000 x g. A 100 µL aliquot of the filtrate was placed in a vial insert and 10 µL of 0.5 ppm XHE-III-74A[12] was added. The vial was vortexed before analysis. Ultra-high performance liquid chromatography was enabled with Shimadzu Nexera X2 LC30AD series pumps (Shimadzu, Kyoto, Japan). The injection volume was 5 µL (LC–MS/MS, Shimadzu 8040). Analytes were separated with an Agilent RRHD Extend-C18 (2.1 mm x 50 mm, 1.8 µm particle size) column with gradient elution at a flow rate of 0.5 mL/min. The mobile phase was methanol and water (both containing 0.1% formic acid). Program: 35% B (0 min) → 50% B (0.75 min), hold at 50% B (1.75 min), → 62% B (3.5 min) → 99% B (0.5 min), hold at 99% B (1 min), return to 35% B (0.25 min), hold at 35% B (2.25 min); column temperature: ambient. Analytes were monitored under positive mode multiple reaction monitoring (MRM) using a Shimadzu 8040 triple quadrupole mass analyzer (Shimadzu, Kyoto, Japan) with electrospray and atmospheric pressure ionization run in dual (DUIS) mode. Ion pairs for MIDD0301 were m/z 415.95 > 304.90, m/z 415.95 > 397.95, m/z 413.95 > 302.90, m/z 413.95 > 395.95; XHE-III-74A[12] m/z 314.10 > 368.10, m/z 314.10 > 278.10; compound 2[13] m/z 360.20 > 249.10, m/z 360.20 > 273.10, m/z 360.20 > 342.15, m/z 360.20 > 301.10; MIDD0301 glucoside

m/z 578.10 > 416.05, m/z 578.10 > 414.05; MIDD0301 glucuronide m/z 592.10 > 416.05, m/z 592.10 > 305.00, m/z 590.10 > 342.15, m/z 590.10 > 303.00, MIDD0301 taurine m/z 523.10 > 398.05, m/z 523.05 > 356.95, m/z 521.10 > 396.05, m/z 521.05 > 354.95, MIDD0301 glycine m/z 473.00 > 398.00, m/z 471.00 > 396.00, m/z 473.00 > 356.80, m/z 471.00 > 354.80. Collision energy was optimized for each transition to obtain optimal sensitivity. The mass spectrometer was operated with the heat block temperature set at 400 °C, drying gas flow of 15 L/min, desolvation line temperature of 250 °C, nebulizing gas flow of 1.5 L/min, and both needle and interface voltages of 4.5 kV. Data acquisition and data processing were performed using LabSolutions software. Standard curves were constructed with analytical standards and fitted by a linear regression and concentrations were calculated to the calibration curve of that day. The mean and the standard deviation were calculated accordingly. PK solution 2 was used to construct the AUC curve.

5.1.4 Determination of plasma protein binding

1 mM MIDD0301 and 500 nM of 4,5-diphenylimidazole were prepared in methanol. Mouse plasma was thawed on ice and 495 µl was dispensed into an Eppendorf tube together with 5 µl of 1 mM MIDD0301. 400 µl of this solution was transferred into the red marked retainer well of a rapid equilibrium dialysis device (Thermo Scientific). 600 µl PBS buffer was added to the adjacent buffer chamber. This was repeated three times at different locations in the plate. The plate was sealed with tape and placed into a shaker for 4 h at an orbital shaking rate of 250 rpm. 50 µl of sample from the red well was transferred to an Eppendorf tube and combined with 50 µl PBS. 50 µl of sample from the buffer well was transferred to an Eppendorf tube and combined with 50 µl mouse plasma. 300 µl of ice cold methanol was added to each of the tubes to

precipitate proteins. The tubes were vortexed and incubated for 30 min on ice followed by centrifugation for 10 min at 10,000 x g. 50 µl of supernatant was added to a new Eppendorf tube and combined with 25 µl of a 500 nM 4,5-diphenyl imidazole solution as ISTD followed by the addition of 425 µl of methanol. The samples were analyzed by LCMS/MS using a Shimadzu 8040 instrument. Quantifications was achieved by using a calibration curve. The assay was repeated three times.

5.1.5 28 days 200 mg/kg/day repeated dose study

MIDD0301 was formulated in 100 mg of peanut butter at a dose of 100 mg/kg. Twice a day, mice were taken from their cages and put in separate plastic containers that contained 100 mg of peanut butter or 100 mg of compound formulated peanut butter. The animals were left in the container during the feeding and returned after 10 min to their cage. During that time, all the peanut butter was consumed. Three groups of mice were given peanut butter formulated MIDD0301. Group 1 (n=4) were sacrificed on the 14^{th} day without any administration on the day of sacrifice. Group 2 (n=7) and group 3 (n=4) were sacrificed on 28^{th} day. Group 2 mice did not receive MIDD0301 on the day of sacrifice while group 3 mice were administered MIDD0301 one hour before euthanasia. Blood was drawn by cardiac puncture and placed into heparinized cryo-tubes. Brains were harvested and placed in cryotubes. All tubes were stored in liquid nitrogen until analysis as described in section 5.1.3

5.2 Results and discussion

Binding of MIDD0301 and MIDD0301S to $GABA_AR$s expressed in the rat brain was determined

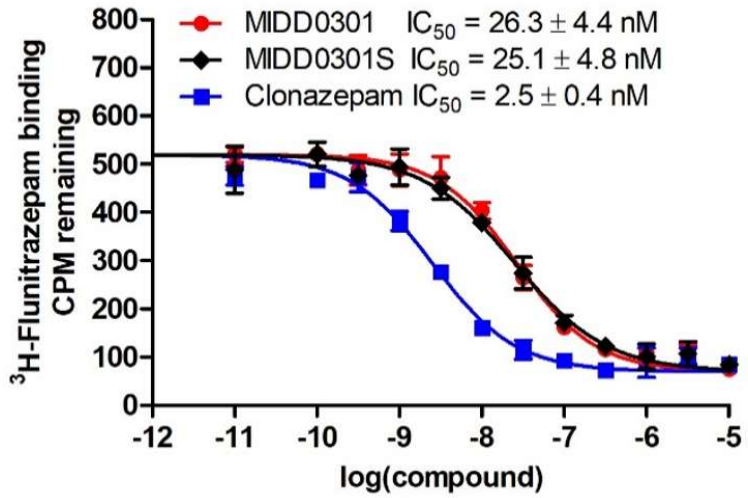

Figure 80. $GABA_AR$ binding of MIDD0301 and MIDD0301S. Radioactive competition with 3H-flunitrazepam using rat brain extract. Experiments were carried out as two independent studies in triplet. IC_{50} values were determined by non-linear regression.

with an inhibition assay using ^{3}H-flunitrazepam (Figure 80) in collaboration with the PDSP. $GABA_AR$ subtypes with two α and two β subunits and one γ or δ subunit that bind to flunitrazepams include to $\alpha_{1\text{-}3,5,6}\beta_{1\text{-}3}\gamma_{1\text{-}3}/\delta$ $GABA_ARs$.[121-124] The extra synaptic $GABA_ARs$ expressed in the brain consist of 43% $\alpha_1\beta_2\gamma_2$, 15% $\alpha_2\beta_3\gamma_2$ + 8% $\alpha_2\beta\gamma_1$, 10% $\alpha_3\beta_3\gamma_2$, 6% $\alpha_4\beta\gamma/\delta$, 4% $\alpha_5\beta_3\gamma_2$, and 4% $\alpha_6\beta_2\gamma_2/\delta$.[125] Thus, compounds binding $\alpha_{1\text{-}3}\beta_{2\text{-}3}\gamma_{1\text{-}2}$ $GABA_ARs$ such as positive control compound clonazepam exhibit excellent IC_{50} values in this assay.

We have reported that MIDD0301 interacts strongly the $\alpha_{1\text{-}5}\beta_3\gamma_2$ $GABA_ARs$.[22] For the binding affinity towards $GABA_AR$ expressed in the rat brain, we observed an IC_{50} value of 26.3 nM. In contrast to other chiral imidazodiazepines such as SH-053-CH3, MIDD0301S has almost the same IC_{50} value than MIDD0301. We have shown that MIDD0301 adopts two different stable conformations and can undergo hydrolysis to form an open keto form at very low pH.[92] The two

stable conformations can be detected by ^{1}H-NMR. For MIDD0301, the potential energies of the

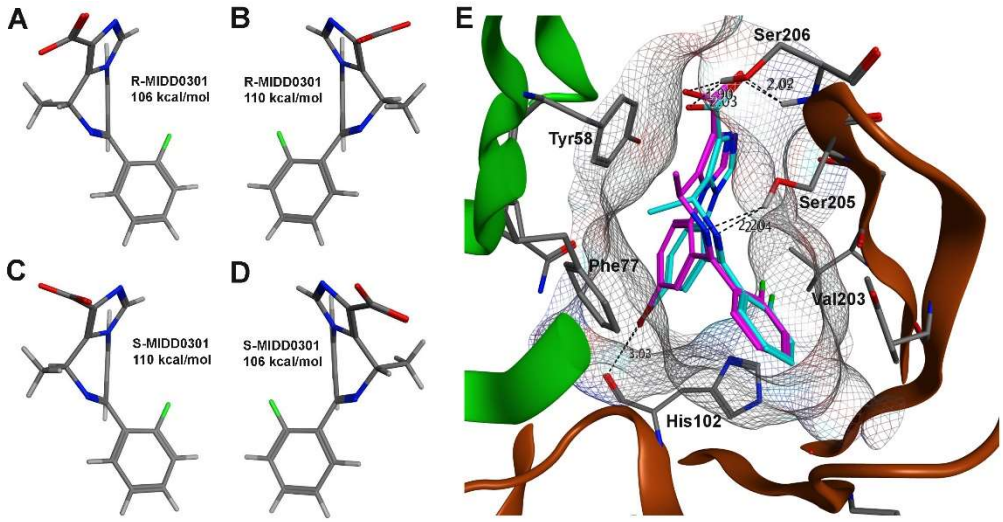

Figure 81. Configuration and binding of MIDD0301 and MIDD0301S. A-B) Most stable conformations of MIDD0301 calculated by molecular dynamics simulation (Born model); C-D) Most stable conformations of MIDD0301S calculated by molecular dynamics simulation (Born model); E) Overlay of docked conformations of MIDD0301 (cyan) and MIDD0301S (magenta) in the complex with the $\alpha_1\beta_3\gamma_{2L}$ $GABA_A$ receptor using structure 6HUO.[126] The $\alpha1^+/\gamma2^-$ interface is indicated as α_1 (green) and γ_2 (brown). Hydrogen and halogen bonds are indicated as dashed lines.

conformers are 106 kcal/mol and 110 kcal/mole, respectively (Figure 81). Interestingly, the high energy conformation of MIDD0301 overlays well with the low energy structure of MIDD0301S and the high energy conformation of MIDD0301S overlays well with the low energy structure of MIDD0301 (Figure 81, A-D). When superimposed, the orientation of the methyl group reflects the (R) and (S) stereochemistry. To determine the preferred conformation for $GABA_AR$ receptor binding, both conformation of the MIDD0301 enantiomers were docked into the binding site of alprazolam for the $\alpha_1\beta_3\gamma_{2L}$ $GABA_AR$ reported by Masiulis et al (Figure 81E).[126]

The best fit for the $GABA_AR$ $\alpha1^+/\gamma2^-$ interface was observed for the low energy conformer of MIDD0301 and high energy conformer of MIDD0301S. Halogen bonding between bromine and His102 were similar than the chlorine-His102 interaction observed for alprazolam. Possible strong hydrogen bonding between the carboxylate of MIDD0301/MIDD0301S and Ser206 positioned both compounds to enable hydrogen bonding with Ser205. For this binding mode,

both enantiomers were accommodated with similar docking scores, revealing that receptor binding stabilizes the high energy conformation of MIDD0301S, which is supported by the similar binding affinity of both enantiomers. Ester or amide analogs of MIDD0301 such as SH-053-2F'-R-CH3 would clash with Ser206 and are therefore predicted to move further into the $\alpha1^{+}/\gamma^{2-}$ interface, which in turn is likely to results in an enantiomeric differentiation due to interaction with Phe77.

Next, other receptors and channels mostly expressed in the CNS were investigated at a 10 μM concentration with MIDD0301 and MIDD0301S. The results are summarized in Table 10. All values are given as % inhibition at 10 μM concentration.

Table 10 Binding data of MIDD0301 and MIDD0301S to receptors and channels.

Receptor	5- Hydroxytryptamine receptor											Histamine Receptors		
Subtype	1A	1B	1D	1E	2A	2B	2C	3	5A	6	7A	H2	H3	H4
(R)-MIDD0301	3.1 ±6.7	-10.1 ±2.5	2.5 ±5.3	-7.4 ±9.8	-7.4 ±8.4	1.7 ±15.2	2.1 ±1.2	-9.1 ±9.9	-7.3 ±15.0	-9.0 ±17.2	3.3 ±4.8	7.3 ±5.9	-16.7 ±16.1	-13.8 ±21.3
(S)-MIDD0301	-2.8 ±4.3	2.1 ±12.6	-2.0 ±5.9	-1.7 ±5.7	-5.2 ±9.0	4.7 ±5.7	5.7 ±3.5	-7.3 ±6.8	-8.9 ±11.6	3.0 ±5.6	2.8 ±4.2	-3.8 ±6.6	-13.1 ±11.5	-26.1 ±13.0

Receptor	Adrenergic receptors						Muscarinic acetylcholine receptors					Opioid Receptor		
Subtype	α1A	α1B	α1D	α2A	β1	β2	M1	M2	M3	M4	M5	δ	μ	κ
(R)-MIDD0301	-24.5 ±10.3	3.8 ±12.2	8.5 ±9.1	-3.9 ±6.5	1.3 ±9.4	-2.3 ±7.7	-11.0 ±4.7	-13.3 ±3.6	-16.1 ±5.9	-9.9 ±4.4	-17.3 ±8.3	-6.3 ±14.5	-12.3 ±7.9	52.3 ±26.4
(S)-MIDD0301	-23.2 ±8.6	2.1 ±12.8	11.1 ±8.1	0.7 ±8.1	-0.5 ±9.0	-1.2 ±11.6	-7.3 ±4.0	-19.2 ±10.8	-12.5 ±7.2	-2.7 ±10.4	-1.7 ±9.4	-0.4 ±21.3	-2.0 ±2.6	62.8 ±13.4

Receptor	Dopamine receptor					Neurotransmitter receptor			Sigma Receptor			
Subtype	D1	D2	D3	D4	D5	DAT	NET	SERT	1	2		

(R)-MIDD 0301	16.3 ±11.0	-2.4 ±12.1	-11.0 ±8.7	-26.1 ±8.7	-4.9 ±7.5	-9.5 ±20.2	-2.5 ±20.7	-4.8 ±4.8	4.5 ±7.3	-15.5 ±10.7	
(S)-MIDD 0301	3.1 ±12.5	-9.6 ±17.2	-9.4 ±7.1	-15.8 ±2.6	1.2 ±12.3	-17.1 ±25.0	-6.1 ±9.6	-4.7 ±4.8	-2.9 ±15.6	-19.5 ±30.4	

Receptor	$GABA_A$ receptor	Benzodiazepine site (rat brain)	Peripheral benzodiazepine receptor
(R)-MIDD0301	34.6 ±10.9	91.9 ±3.5	18.3 ±8.7
(S)-MIDD0301	42.4 ±11.6	95.3 ±4.8	23.3 ±8.5

Among the 41 channels and receptor screened, only the benzodiazepine site assayed with $GABA_AR$ ligand ^{3}H-flunitrazepam showed appreciable competition. As shown in Figure 80, 26.3 nM and 25.1 nM binding was observed for MIDD0301 and MIDD0301S, respectively. Interactions at very high concentrations were observed for the κ opioid receptor resulting an IC_{50} values of >10 µM. Interesting, very weak interactions were determined for the GABA binding sites of $GABA_AR$, probably due to the acid function of MIDD0301 and the nitrogen atom in the gamma position (imine). However, *in vivo* blood concentrations of MIDD0301 and MIDD0301S are unlikely to reached levels high enough to result in biological effects mediate by those pathways. Different rates of metabolic conversion have often been described for enantiomers of chiral

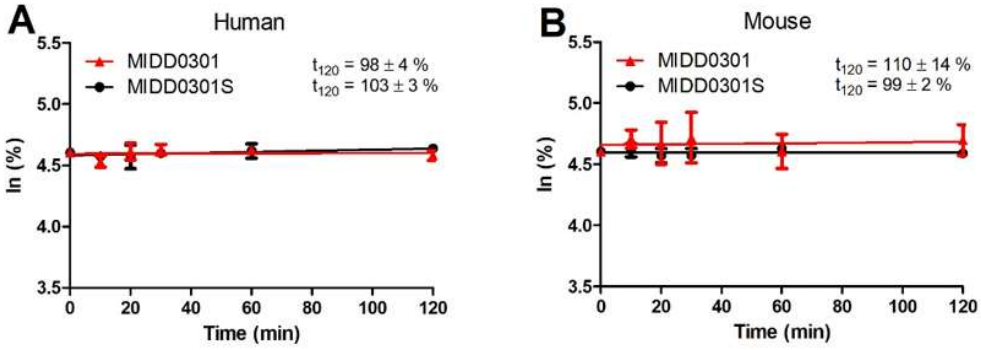

Figure 82. In vitro microsomal stability of MIDD0301 and MIDD0301S. A) Enzymatic oxidation in the presence of human liver S9; B) Enzymatic oxidation in the presence of mouse liver S9.

drugs. Here, microsomal stability in respect phase I and phase II metabolism of MIDD0301 and

MIDD0301S was investigated and presented in Figure 82, 83 and 84. Both enantiomers are stable in the presence of human and mouse liver S9 for at least two hours (Figure 82). Many years of compound development have enabled us to remove metabolic liabilities common to benzodiazepines by introducing an imidazole ring with non-basic nitrogens due to a carboxylic acid substituent. The insertion of a methyl group prevented C3-hydroxylation.[94] Carboxylic acid containing drugs are known to undergo glucuronidation and a chiral center close to this function have been reported to influence the rate of this transfer.[127] For both MIDD0301 and MIDD0301S,

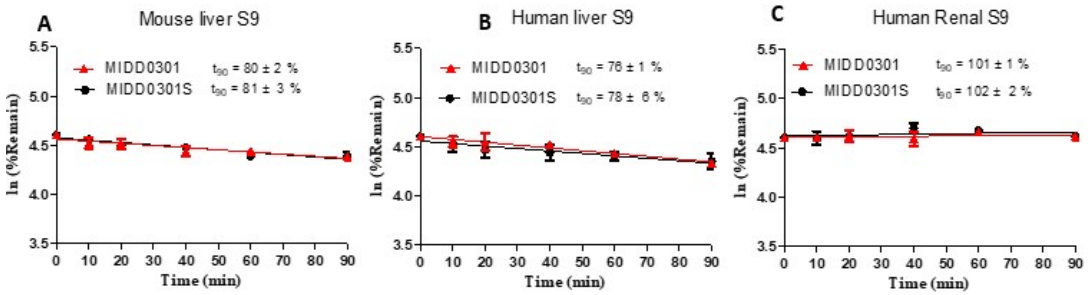

Figure 83. In vitro phase II microsomal stability of MIDD0301 and MIDD0301S (Glucuronidation). A) Mouse liver S9; B) human liver S9, and C) human kidney S9.

we observed the same glucuronidation rate in presence of mouse and human liver S9 (Figure 83A and B). After two hours, about 80% of each enantiomer was still present resulting in a half-life of around 300 min. Glucuronidation was not observed for both enantiomers in presence of human kidney S9 (Figure 83C). MIDD0301 glucoside was identified as one of three major metabolites in mouse urine in addition to MIDD0301 glucuronide. In fact, the glucoside adduct was found to be the dominant metabolite for the *intravenous* administration of MIDD0301. The identification of these metabolites is discussed in chapter IV. Interestingly, the rate of glucosidation for MIDD0301 and MIDD0301S in the presence of mouse kidney S9 was different (Figure 84A). In contrast to MIDD0301, MIDD0301S did not form the corresponding glucose adduct. Thus, glucuronosyltransferase UGT3A2,[83] which utilizes uridine 5'-diphosphoglucose instead of uridine

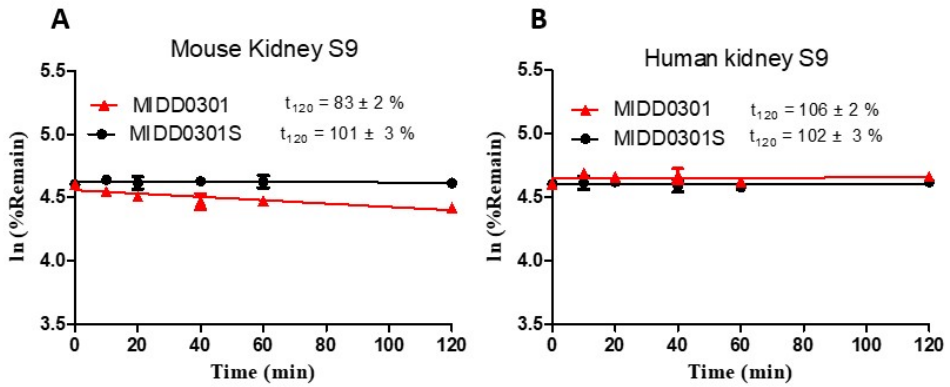

Figure 84. In vitro phase II microsomal stability of MIDD0301 and MIDD0301S.Glucosidation Assay in presence of - A) Mouse kidney S9; B) Human kidney S9.

5'-diphosphoglucuronic acid preferred MIDD0301 bearing the R-methyl as substrate in presence of mouse kidney S9. Neither MIDD0301 nor MIDD0301S formed glucoside adducts in presence of human kidney S9 (Figure 84B). It was reported by Meech at el. that in contrast to mice, human UGT3A2 is mainly expressed in thymus with very little expression in liver or kidney.[128]

MIDD0301 taurine was the only metabolite found in feces, whereas MIDD0301 glucoside, glucuronide and taurine were found in urine. Here, we quantified parent compounds MIDD0301 and MIDD0301S as well as their metabolites in blood. The results are summarized in Figure 85. MIDD0301 and MIDD0301S reach the highest blood concentration after 20 min with the c_{max} of MIDD0301S being more than threefold higher than MIDD0301. Thus, MIDD0301S is better absorbed than MIDD0301, whereas compound clearance is almost the same with half-lives of 47.8 min and 50.2 min, respectively. The major metabolites of MIDD0301 and MIDD0301S in blood were their corresponding glucuronides. The c_{max} of MIDD0301S glucuronide is threefold higher than the c_{max} of MIDD0301 glucuronide. The t_{max} occurred between 20 min to 30 min. A significant blood concentration of parent compounds and glucuronides were already observed at 10 min. The half-lives of the glucuronides were 17.9 min and 21.7 min, respectively. Thus, in

PK parameters

Compound	T_{max} (min)	C_{max} (nM)	K_e (min^{-1})	$t_{1/2}$ (min)	AUC (ng*min/mL)
MIDD0301	20	273	0.015	47.8	43223
MIDD0301S	20	896	0.014	50.2	201418
MIDD0301 Glucuronide	30	5415	0.025	27.9	415282
MIDD0301S Glucuronide	20	14293	0.032	21.7	1181000
MIDD0301 Taurine	20	345	0.004	158.9	52106

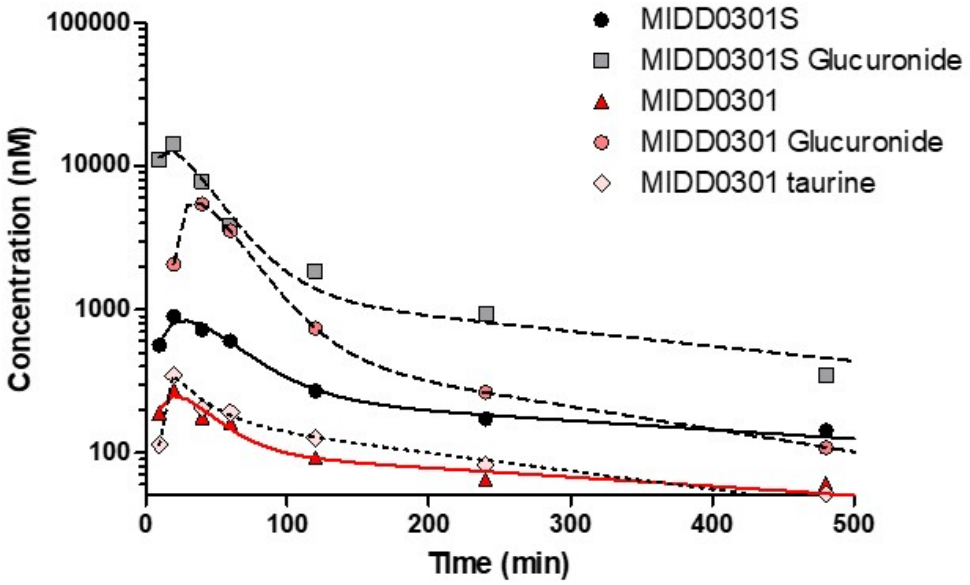

Figure 85. Pharmacokinetic analysis: Distribution of MIDD0301 and MIDD0301S and their metabolites in blood.

respect to the results obtained for the *in vitro* microsomal stability studies, the metabolism *in vivo* is significantly faster for both compounds. The fast rate of glucuronidation in the liver might be supported by an active carrier mediated transport of the glucuronides. Another reason behind discrepancy between the *in vitro* and *in vivo* glucuronidation rate might be attributed to the hydrolysis of the glucuronide forming the parent molecule. Non-perfused brain concentrations of MIDD0301 enantiomers and their corresponding metabolites were determined and presented in the Figure 86. Concentration of glucuronides in the brain compared to blood were 2% for MIDD0301S and 10% for MIDD0301. I can assume that these metabolites were present in the residual blood in the brain because these compounds are too polar to cross the blood brain

PK parameters

Compound	T_{max} (min)	C_{max} (nM)	K_e (min^{-1})	$t_{1/2}$ (min)	AUC (ng*min/mL)
MIDD0301	10	140	0.016	42.1	18362
MIDD0301S	20	108	0.011	61.7	8258
MIDD0301 Glucuronide	10	276	0.034	20.1	43390
MIDD0301S Glucuronide	20	230	0.030	23.4	22936

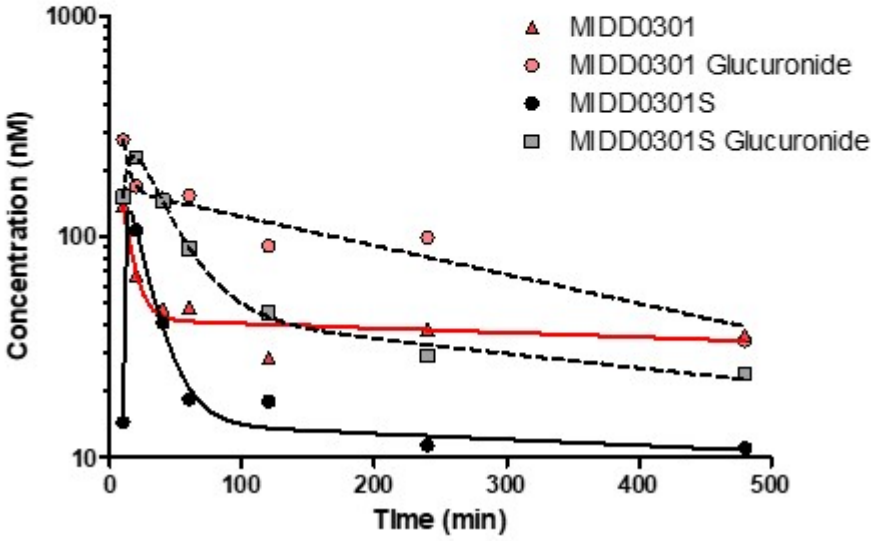

Figure 86. Pharmacokinetic analysis: Distribution of MIDD0301 and MIDD0301S and their metabolites in non-perfused brain.

barrier by passive diffusion. The c_{max} for both MIDD0301 and MIDD0301S was more than 100 nM which is larger than the therapeutic concentrations, however, no sensorimotor impairment was observed visually. It was evident from a separate study that a 10 times higher dose than used in the current study did not induce any sign of sensorimotor impairment. So taken together, the presence of glucuronides and corresponding parent compounds in the brain can be largely attributed to the blood as these were non-perfuse brain.

Next, we investigated the difference of absorption for oral vs IP MIDD0301 administration observed in previous PK investigations discussed in chapter IV. We hypothesized that efflux and first pass metabolism reduced the circulating concentrations of orally administered MIDD0301.

It was found that glucuronidation also occurs in the presence of microsomes derived from mouse intestine (Figure 87). Most of the glucuronide that is formed in the intestine is probably transported back into the intestine followed by deconjugation in the gut. The rates of

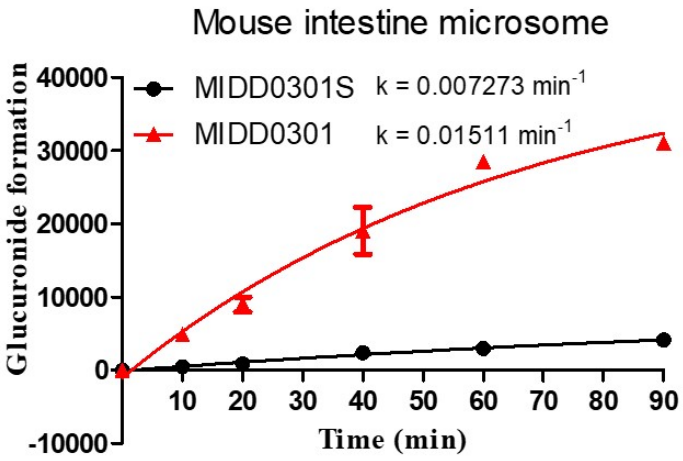

Figure 87. Peak areas of glucoside were plotted against time and first order kinetic analysis used to determine rate constant k.

glucuronidation were determined for both enantiomers and plotted against time (Figure 87). It was found that the MIDD0301 glucuronide formation rate was at least twice as fast as the rate for MIDD0301S. Thus, the lower blood concentrations of MIDD0301 and MIDD0301 glucuronide might partially be due to pronounced glucuronidation in the intestine after oral administration. Interestingly, the taurine adduct was only observed for MIDD0301 at blood concentrations similar to the parent compound. Although we demonstrated *in vitro* glucosidation for MIDD0301 and MIDD0301S and reported large amounts of MIDD0301 glucoside in mouse urine for *intravenous* administration, blood concentrations of this conjugate were below the limit of detection for oral administration. In contrast, for *intravenous* administrated MIDD0301, MIDD0301 glucoside was found in blood although at a lower AUC than MIDD0301 glucuronide (Figure 88). The high concentration of MIDD0301 glucoside in urine for the metabolic study but

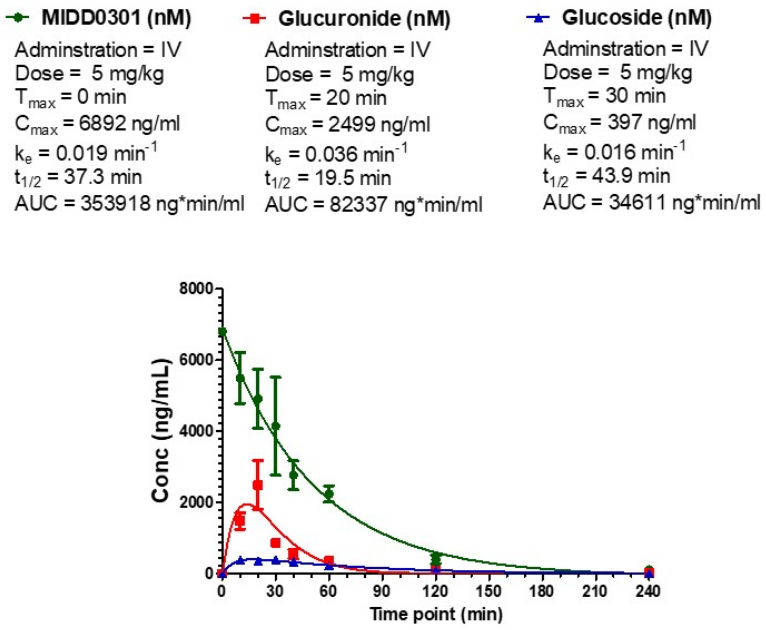

Figure 88. PK study of IV administered MIDD0301 demonstrated lower amount of glucoside compared to glucuronide. In our metabolic study we actually got 45% glucoside metabolite urine.

low blood concentration, indicates that MIDD0301 is undergoing glucosidation in kidney, followed by secretion without any significant reabsorption.

We discussed plasma protein binding of MIDD0301 in chapter 2. Here, we evaluated and compared the protein binding of MIDD0301 with its enantiomer MIDD0301S. The equilibrium dialysis method was adapted from ThermoFisher as described in chapter 2. The results are depicted in Table 11.

Table 11 Concentration of % free drug determined in human and mouse plasma for MIDD0301 enantiomers

		%Free drug			
		In Human Plasma	Average ± SD	In Mouse Plasma	Average ± SD
MIDD0301	Sample 1	4.39	4.3±0.1	11.09	11.3±0.5
	Sample 2	4.30		11.90	
	Sample 3	4.21		11.00	
MIDD0301S	Sample 1	1.08	1.3±0.2	27.78	23.6±4.3
	Sample 2	1.32		19.22	
	Sample 3	1.46		23.80	

For MIDD0301 and MIDD0301S, the amount of free drug was lower for human plasma compared to mouse plasma. MIDD0301S was more protein bound for human plasma than MIDD0301 but significantly less protein binding was observed for mouse plasma. Metabolizing enzymes can only interact with free drug, thus, faster metabolism is expected for MIDD0301S in mouse based on its protein binding. Indeed, we observed a larger AUC for MIDD0301S glucuronide than MIDD0301 glucuronide in blood.

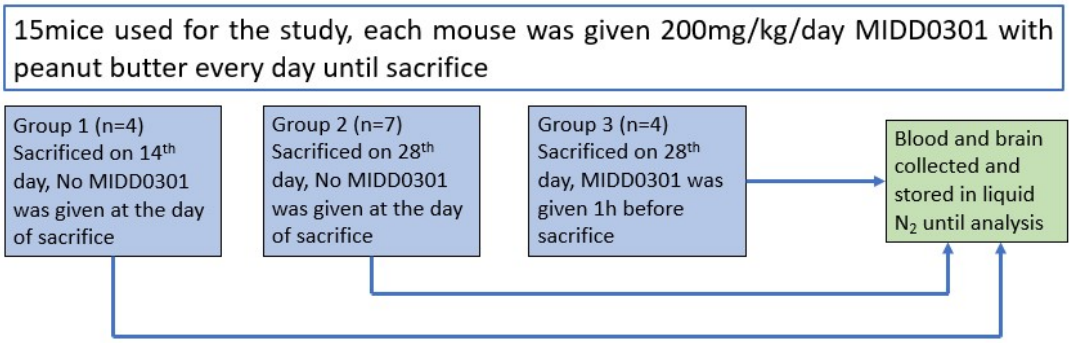

Figure 89. Schematic of the 28 days repeated dose study (200 mg/kg/day).

Finally, we conducted a 28 days repeated high dose study of MIDD0301 to investigate if MIDD0301 or any metabolites accumulate in brain over time. Figure 89 illustrates the study design. The results of the study are summarized in Figure 90. Only about 3% of MIDD0301 and its metabolites were found in brain compared to their blood concentrations demonstrating good tissue selectivity (Figure 90A). Although the selected dose was higher than the therapeutic dose, the majority of MIDD0301 and its metabolites were eliminated after 24 h (Figure 90B). When comparing the brain concentration of MIDD0301 and its metabolites at day 14 vs day 28, we did not observe any signs of accumulation as a result of repeated dose administration of MIDD0301 (Figure 90C). In summary, we found that both compounds have equal affinity for the $GABA_AR$ expressed in the rat brain with an IC_{50} of 25.1 nM for MIDD0301S and 26.3 nM for MIDD0301, respectively. Molecular modeling of these ligands at the benzodiazepine site of a $GABA_AR$

chloride channel resulted in a preference for the high energy conformer of MIDD0301S and a low

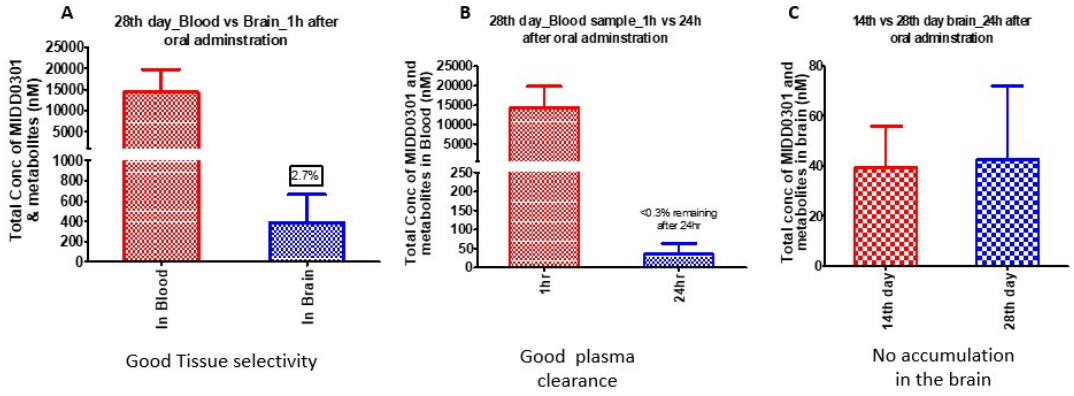

Figure 90. 28 days repeated dose study (200 mg/kg/day). A) Mice were sacrificed on 28th day and received oral MIDD0301 one hour before sacrifice; B) mice sacrificed on 28th day and blood concentrations after 1 h vs 24 h after oral administration are compared; C) comparison of brain concentrations on day 14 day vs day 28. Mice were sacrificed 24 h after oral administration. In all cases concentration presented included MIDD0301 and all its metabolites.

energy conformation for MIDD0301. The positioning of both ligands differs in the orientation of the methyl group, which apparently does not influence the binding affinity. A screen of 48 receptors, did not reveal any affinity for other receptor predominately expressed in the brain. *In vitro*, MIDD0301 and MIDD0301S are stable in present of liver microsomes and therefore do not undergo phase I metabolism. However, hepatic glucuronidation was observed for both compounds and intestinal glucuronidation was especially rapid for MIDD0301 when compared to MIDD0301S. We also found that glucosidation only occurred in mouse kidney. For the pharmacokinetic analysis, we identified the glucuronide as the major metabolites with concentrations of up to 20-fold of the parent compound. The glucuronides were rapidly cleared with half-live between 21-27 min in contrast to the parent compounds with half-lives between 48-50 min. Overall, MIDD0301S was better absorbed, reaching concentration that were three-fold higher than MIDD0301. MIDD0301 brain distribution was very low and no accumulation was observed during a 28 day repeated dose study. The large AUC of MIDD0301 glucuronide prompts

further safety evaluation of that metabolite according to the FDA guidelines, which will be addressed in future studies.

Chapter 6: Development of inhaled $GABA_A$ receptor modulators to improve airway function in bronchoconstrictive disorders

A long-term, affordable oral medication to control asthma symptoms with negligible adverse effects is still unavailable, prompting further research to validate new therapeutic modalities. Among those, we have investigated imidazodiazepines, which relax constricted human airway smooth muscle and reduce airway hyperresponsiveness (AHR) in several murine asthma models.[12-14,22,23,129] The compounds have high affinity for $GABA_A$ receptors ($GABA_AR$), which are expressed on airway smooth muscle and inflammatory cells. To avoid CNS adverse effects, we engineered pharmacokinetic properties of these compounds to prevent blood brain barrier transit. We determined compound efficacy when nebulized and showed reduction of AHR at doses equivalent or lower than albuterol.[11] As a part of our continuous research for nonsteroidal oral asthma medication based on subtype selective modulation on $GABA_A$ receptor, we were working on the development of the lead candidate MIDD0301. Simultaneously, we explored new substitutions of the acid functionality of MIDD0301 with an amine having a long hydrophobic chain with an intention to achieve long-acting property and limit the rate of phase II conjugation that was observed for MIDD0301.

The addition of a hydrophobic group to a catecholamine scaffold resulted in the generation of long-acting β_2-agonists (LABA), such as formoterol and salmeterol.[130,131] Other LABAs such as vilanterol, have been approved in combination with inhaled corticosteroids such as fluticasone.[132] The long acting properties of salbutamol have been credited to microkinetics

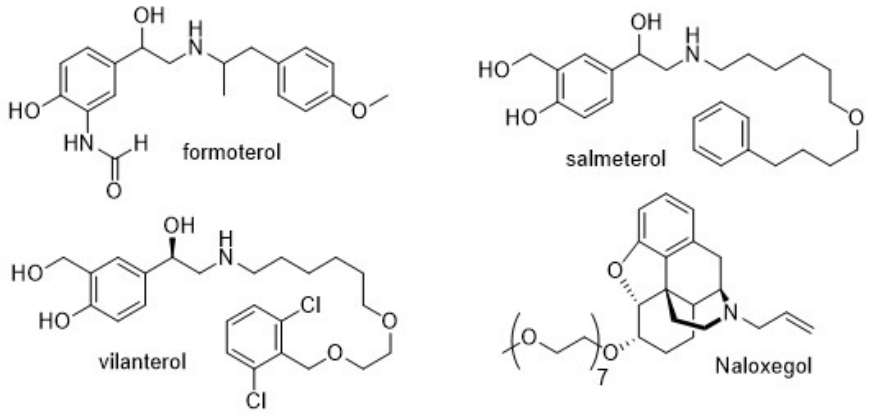

Figure 91. Compound structures of conjugated drugs

related to lipophilicity and exosite binding[133] Procopiou et al. proposed exosite binding for vilanterol, as well.[134]

Pantherics Incorporated synthesized and characterized proprietary new imidazodiazepines that have long alkyl chain substituents like salmeterol and vilanterol for the alleviation of AHR. The first strategy included incorporation of the hydrophobic group found in salmeterol. The second strategy includes the addition of a polyethylene glycol chain. PEGylation has been used extensively for improving the stability and half-life of biologic molecules and has been applied recently for small molecule drugs.[135] Naloxegol, for example, is naloxone with a heptaethylene glycol substitution, which has been approved for opioid-induced constipation.[136] CNS-effects of naloxegol are minimal with a low brain:plasma ratio. PEGylation also increases the water solubility of hydrophobic small molecules, which still retain orally availability dependent on the number of polyethylene glycol units. Distribution and clearance of PEGylated small molecules in the lung have not been described, which prompted investigations of MIDD0301 analogs using constricted tracheal rings *ex vivo* and murine *in vivo* asthma models.

6.1 Experimental

6.1.1 $GABA_A$ receptor binding

Rat brain membranes were prepared from frozen tissue that was thawed on ice and homogenized on ice in 10 volumes of cold lysis buffer (50 mM Tris HCl, pH 7.4, containing protease inhibitor cocktail; Roche) using a Polytron homogenizer (6 pulses and 10 seconds per pulse). The homogenate was centrifuged at 1,000 x g for 10 min at 4°C to obtain the supernatant. The supernatant was then centrifuged at 40,000 x g for 20 min, and the resulting supernatant decanted and replaced with the same ice-cold lysis buffer. Two or three additional rounds of homogenization-centrifugation were performed to ensure thorough homogenization and wash out of endogenous ligands. The final pellet was resuspended in the same buffer and homogenized one last time. The rat brain suspension was diluted in buffer (50 mM Tris HCl, 2.5 mM $CaCl_2$, pH 7.4), followed by the addition of [^{3}H]-flunitrazepam (0.6 - 4.0 nM in DMSO) and PI320 or PI310 (Pantherics Incorporated, La Jolla, CA) in DMSO at different concentrations to reach a final of volume of 125 µl per well. Total binding and nonspecific binding were determined with reference compound clonazepam. In brief, plates are usually incubated at room temperature and in the dark for 90 min. Reactions are stopped by vacuum filtration onto 0.3% polyethyleneimine (PEI) soaked 96-well filter mats using a 96-well Filtermate harvester, followed by three washes with cold PBS buffer. Scintillation cocktail was then melted onto the microwave-dried filters on a hot plate and radioactivity counted in a Microbeta counter. The data (n = 6) were analyzed by nonlinear regression.

6.1.2 Molecular Docking

Molecular docking analysis was performed with MOE 2015.1001 (Molecular Operating Environment, Montreal, Canada). The 6HUO[126] protein database file was downloaded via https://www.ncbi.nlm.nih.gov and prepared for docking studies using the available MOE feature. The pharmacophore query editor was used to determine location and annotations for alprazolam bound to the $\alpha_1\beta_3\gamma_{2L}$ $GABA_AR$. Docking was performed with both thermodynamic rotamers[92] of PI310 and PI320 using the pharmacophore of alprazolam for placement and affinity dG for scoring. Refinement was determined with a rigid receptor structure.

6.1.3 Viability studies (HEK293) PI310 and PI320

Cytotoxicity assay. Human embryonic kidney 293T (HEK293T) cells were purchased (ATCC) and cultured in 75 cm2 flasks (CellStar). Cells were grown in DMEM/High Glucose (Hyclone, #SH3024301) media to which non-essential amino acids (Hyclone, #SH30238.01), 10 mM HEPES (Hyclone, #SH302237.01), 5 x 106 units of penicillin and streptomycin (Hyclone, #SV30010), and 10% of heat inactivated fetal bovine serum (Gibco, #10082147) were added. Cells were harvested using 0.05% Trypsin (Hyclone, #SH3023601), washed with PBS, and dispensed into sterile white, optical bottom 384-well plates (NUNC, #142762). After three hours, small molecule solutions were transferred with a Tecan Freedom EVO liquid handling system equipped with a 100 nL pin tool (V&P Scientific). The controls were 3-dibutylamino-1-(4-hexyl-phenyl)-propan-1-one (25 mM in DMSO, positive control) and DMSO (negative control). The cells were incubated for 48 h followed by the addition of CellTiter-Glo™, a luminescence-based cell viability assay (Promega, Madison, WI). All luminescence readings were performed on a Tecan Infinite M1000 plate reader.

The assay was carried out in quadruplet with three independent runs. The data were normalized to the controls and analyzed by nonlinear regression (GraphPad Prism).

6.1.4 Aqueous solubility assay

About 2 mg of compound was added to 500 µL of PBS buffer at pH 7.4 and agitated with a horizontal shaker in a closed vial for 24 h. The mixtures were transferred to an Eppendorf tube and centrifuged for 5 min at 16000 x g followed by filtration through a 0.22 µm cellulose acetate spin X centrifuge filter (Costar). 200 µL of filtrate was transfer to new Eppendorf tube and 200 µL of methanol was added followed by subsequent dilution using a 50:50 methanol/PBS buffer water if necessary. After mixing, 50 µL were transferred into a 384 well plate (Coring UV star, 781801) for UV detection at 250-600 nm (Tecan M1000). The assay was carried out with four independent samples of each compound. The concentration of each solution was determined with a calibration curve in 50:50 methanol/PBS buffer water. Absorbance of corresponding methanol PBS blank were recorded and subtracted from the absorbance of calibration curve solutions and from the

6.1.5 Parallel Artificial Membrane Permeability Assay (PAMPA)

6.1.5.1 Test Solution

A 10 mM stock solution of each compound was made in DMSO. 50 µL of this stock solution was taken in Eppendorf tube and 950 µL of PBS buffer was added to make a 500 µM compound solution in 5% (v/v) DMSO in PBS. 500 µL of this solution was transferred to another tube and 500 µL of 5% (v/v) DMSO in PBS was added to make 250 µM test solution in 5% (v/v) DMSO in PBS.

6.1.5.2 Equilibrium Solution

150 µL of test solution (250 µM in 5% (v/v) DMSO in PBS) was taken in Eppendorf tube and 300 µL of 5% (v/v) DMSO in PBS was added to make equilibrium solution.

6.1.5.3 Assay protocol

This assay was carried out using Millipore's MultiscreenTM protocol, AN1725EN00. The artificial membrane was prepared by carefully pipetting 15 µl of the 5% (v/v) hexadecane in hexanes solution to each of the wells of the donor plate. The hexane was allowed to evaporate for 30 min in a fume hood forming a clear membrane. 300 µL of PBS with 5% (v/v) DMSO was added to each of the wells of the acceptor plate. The hexadecane treated donor plate was placed on top of the acceptor plate after 150 µl of 250 µM test solution was added to the donor wells in quadruplets. The cover was placed on top of the donor plate and the plate plus lid was wrapped with a wet paper towel and aluminum foil followed by incubation on a reciprocal shaker (100 rpm) for 18 h. The next day, 50 µL of the acceptor plate solutions were transferred to a 384 well UV plate. 50 µL of the equilibrium solution was added to same UV plate. Each plate had standards ranitidine (low permeability) and verapamil (high permeability). Plates were read for absorbance from 250-600 nm with 1 nm steps and a 5 nm bandwidth. All experiments were conducted in quadruplet. The relative permeability (cm/s) of the small molecules was calculated with following Equation:

$$log\ P\text{e}=l\{C \times -\ln(1- [Drug]A/[Drug]E)\}\ ;$$

$$Where\ C= (VA \times VD)/(VD+ VA)A \times t)$$

$[Drug]A$ = Absorbance of the compound from acceptor well

$[Drug]E$ = Absorbance of the compound from the equilibrium solution

VA = Volume in acceptor well, cm3, (in this case: 0.3 cm3)

VD = Volume in donor well, cm3, (in this case: 0.15 cm3)

A = Active surface area of the membrane, cm3, (in this case: 0.283 cm3)

t = Incubation time in second

6.1.5.4 LogP determination

In an Eppendorf tube, 300 µL of water-saturated 1-octanol was added to 200 µL of a 2.5 mM 1-octanol solution of PI310 or PI320 followed by the addition of 500 µL of 1-octanol saturated water. The solution was vortexed and placed on an orbital shaker at 600 rpm overnight and allowed to separate for 1 h. A 10 µL aliquot of the octanol layer were combined with 70 µL of water saturated octanol in 384 well plate (Coring UV star) followed by aspiration dispense 4 times followed by determination of absorbance at 254 nm using a Tecan M1000 microplate reader. Similarly, an aliquot of 40 µL of the water layer was taken in 384 well plate (Coring UV star) and 40 µL of methanol was added to the same well and solution, aspirated and dispensed 4 times followed by absorbance readings at 254 nm. Two calibration curves for each compound were generated, one for water saturated octanol and the other for a 50:50 octanol saturated water:methanol. The assay was carried out in quadruplets for each compound.

6.1.6 Purity of PI310 and PI320

1000 ppm solutions of PI310 and PI320 in ethanol were generated. After dilution to 100 ppm for PI320 and 250 ppm for PI310, the solutions were analyzed by LCMS which was comprised of two

Shimadzu Nexera X2 LC30AD series pumps, autosampler SIL30ACMP, column oven CTO 20A, PDA detector SPD-M30A (Shimadzu, Kyoto, Japan). The PDA range was set to 190-700 nm. The stationary phase used for this method was a Restek Ultra BiPhenyl column (2.1 mm x 100 mm, 3 µm particle size) with gradient elution at a flow rate of 0.5 mL/min. The mobile phase was methanol and water (both containing 0.1% formic acid). Time program: 50% B (0 min) → 100% B (20 min) hold at 100% B (5 min), return to 50% B (2 min), hold at 50% B (3 min); column temperature: ambient. Injection volume of was 1 µL. The purity was calculated for absorbance at 254 nm using area normalization method.

6.1.7 Pharmacokinetic studies compound PI320 and PI310 in mice

Six weeks old female Swiss Webster mice received nebulized PI320 at a dose of 7.2 mg/kg. At 10, 30, 60 and 120 min, mice were sacrificed, and lungs were harvested and stored in liquid nitrogen until analysis (n = 4). Lung tissue samples were thawed, weighed, and homogenized directly into 400 µL methanol containing 0.1 ppm MYM-II-68 (IS) using a Cole Palmer LabGen 7B Homogenizer. Samples were centrifuged for 10 min at 16,000 x g at 4 °C. The supernatant was then spin-filtered through 0.22 µm nylon centrifugal filter units (Costar) and evaporated using a Speedvac concentrator. The residue was reconstituted in 400 µL methanol, sonicated for 1 min, vortexed and filtered through 0.22 um nylon spin X centrifuge. 100 µL of the filtrate was then transferred to a HPLC vial insert and 10 µL of 0.5 ppm MYM-III-22 in methanol was added. The injection volume was 5 µL (LC–MS/MS, Shimadzu 8040). High performance liquid chromatography (HPLC) was performed with Shimadzu Nexera X2 LC30AD series pumps (Shimadzu, Kyoto, Japan). Analytes were separated by with a Restek Ultra BiPhenyl column (2.1 mm x 100 mm, 3 µm particle size) with gradient elution at a flow rate of 0.5 mL/min. The mobile phase was methanol and

water (both containing 0.1% formic acid). Time program: 50% B (0 min) → 99% B (2 min) hold at 99% B (2 min), return to 50% B (0.2 min), hold at 50% B (2.3 min); column temperature: ambient. Analytes were monitored under positive mode using a Shimadzu 8040 triple quadrupole mass analyzer (Shimadzu, Kyoto, Japan) with electrospray and atmospheric pressure ionization run in dual (DUIS) mode. The following transitions were monitored in multiple reaction monitoring (MRM) mode. Ion pairs for PI320 were m/z 647.20 > 439.00 m/z 647.20 > 422.00, m/z 647.20 > 396.00, m/z 649.20 > 441.00 m/z 649.20 > 424.00, m/z 649.20 > 398.00, for MYM-II-68 were m/z 441.90 > 396.00, m/z 441.90 > 326.90 m/z 443.90 > 398.00 m/z 443.90 > 328.90 and transition pairs for MYM-III-22 were m/z 389.00 > 358.00, m/z 389.00 > 330.00, m/z 389.00 > 289.00.

The same protocol was followed for PI310. The only difference were the MRM transitions for PI310: m/z 645.00 > 396.00, m/z 645.00 > 381.00, m/z 647.00 > 398.00, m/z 647.00 > 383.00.

6. 2 Results and discussion

PI310 and PI320 were synthesized using parent compound MIDD0301 and corresponding amines as illustrated in Scheme 11.

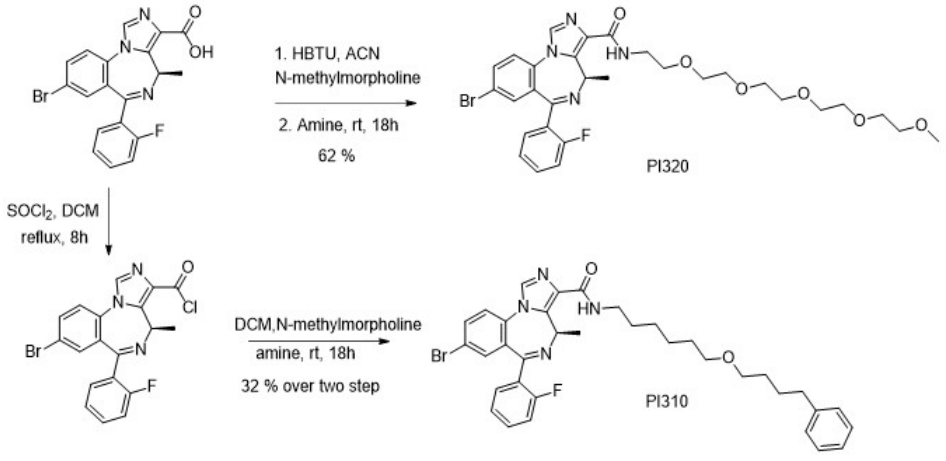

Scheme 12 Synthesis of PI310 and PI320.

MIDD0301 was coupled with 2,5,8,11,14-pentaoxahexadecan-16-amine in the presence of HBTU and N-methylmorpholine resulting in PI320 at 62% yield as a viscous oil. For the synthesis of PI310, 6-(4-phenylbutoxy)hexan-1-amine was used, which has been described as an unstable amine.[18] Therefore, 6-(4-phenylbutoxy)hexan-1-amine was generated from *tert*-butyl (6-(4-phenylbutoxy) hexyl)carbamate with trifluoroacetic acid and used as crude product for the next reaction after neutralization and extraction. The coupling was achieved with the acid chloride of MIDD0301 in the presence of N-methylmorpholine, resulting in PI310 at a 32% overall yield. Like all chiral imidazodiazepines in this class, PI310 and PI320 have two stable configurations that can be distinguished by nuclear magnetic resonance.[92] The purity of the compounds was determined with a LC-PDA system and % purity was calculated at 254 nm with respect to area normalization

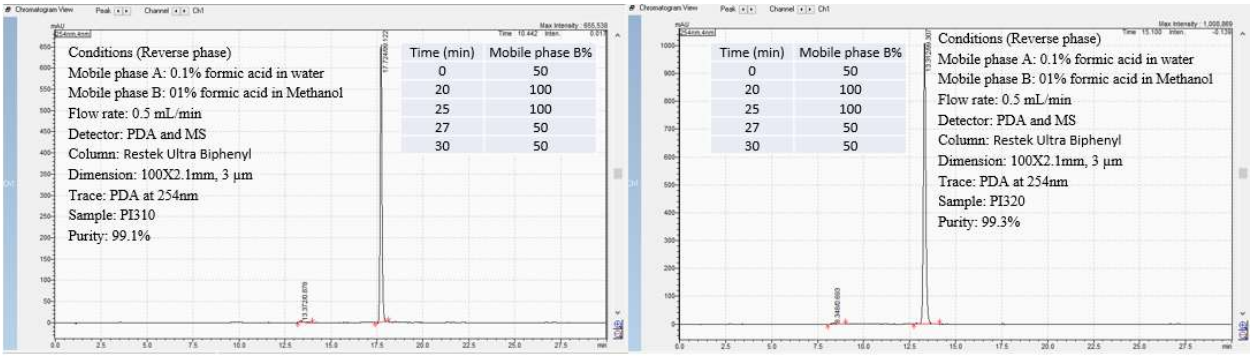

Figure 92. PDA Chromatogram of PI310 (left) and PI320 for purity determination

(Figure 92). The purity of PI310 and PI320 was 99.1% and 99.3% respectively.

Next, we investigated the affinity of these compounds at the $GABA_AR$s. Here, rat brain homogenate was used in combination with ^{3}H-flunitrazepam. $GABA_AR$ subtypes that bind flunitrazepam consist of $\alpha_{1\text{-}3,5,6}\ \beta_{1\text{-}3}\ \gamma_{1\text{-}3}/\delta$ $GABA_AR$s.[121-124]

An IC_{50} of 576 nM was observed for PI310, which is significantly higher than the reported IC_{50} of 72 nM for MIDD0301.[24] Thus the conjugation to 6-(4-phenylbutoxy)hexan-1-amine reduced

binding eight fold. PI320 shows better binding at the $GABA_AR$s with an IC_{50} of 242 nM. Overall,

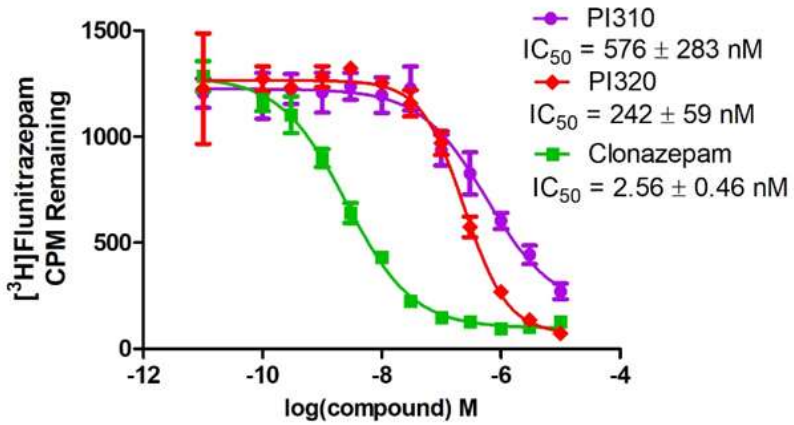

Figure 93. Competition assay of $GABA_AR$ ligand ^3H-flunitrazepam with PI310 and PI320 using rat brain extract.

these data confirm that even large substituents are tolerated at the carboxyl position for imidazobenzodiazepines, however, the hydrophobic nature of the substituents has an influence on binding affinity.

To investigate possible binding modes of these ligands, we used the reported crystal structure of the $\alpha_1\beta_3\gamma_2$ $GABA_AR$ to dock both ligands (Figure 94). The ligands were docked at the alprazolam binding site, which is located at the $\alpha1^+/\gamma2^-$ interface. The bromine atom is near Asn60 and His102. Experiments with isocyanate substituted diazepam have resulted in alkylation of these residues.[137] Halogen bonding with Phe100 located on α1 subunit is possible. Hydrogen bond interactions have been reported for other imidazodiazepines such as Hz166 with Ser205.[138] Amides PI310 and PI320 can additionally interact with Glu189 located on γ2 subunit. The alkyl chain of both compounds is located on the periphery of the protein complex and mostly exposed to water and hydrophilic amino acid residues. In contrast to the 6-(4-phenylbutoxy)hexyl side

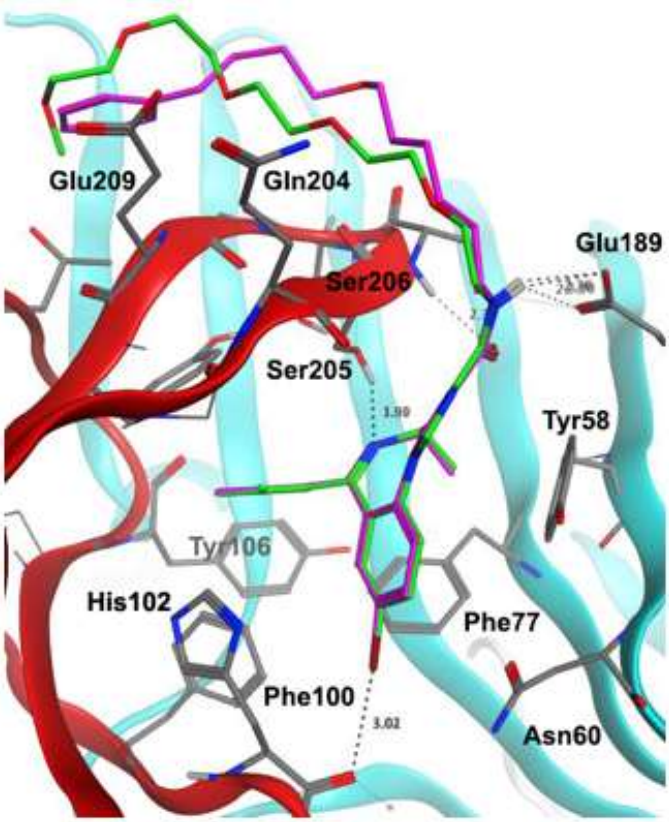

Figure 94. Docking study with PI310 and PI320. Overlay of docked conformations of PI310 (magenta) and PI320 (green) in the complex with the $\alpha_1\beta_3\gamma_{2L}$ $GABA_AA$ receptor using the structure 6HUO.[126] The $\alpha1^+/\gamma2^-$ interface is indicated as α_1 (red) and γ_2 (cyan). Hydrogen and halogen bonds are indicated as dashed lines

chain, the 2,5,8,11,14-pentaoxahexadecanyl side chain has multiple hydrogen accepting groups that can interact via hydrogen bond interactions with charged residues on the protein surface resulting in a higher affinity for $GABA_ARs$.

Our collaborator Prof. Emala from Columbia University investigated *ex vivo* smooth muscle relaxing properties of PI310 and PI320. The results were compared with our current lead compound MIDD0301. It was found PI320 relaxes airway smooth muscle at a lower concentration than MIDD0301 (data is not shown here).

To further characterize the physicochemical properties of PI320 and PI310, solubility, permeability and toxicity assays were conducted (Table 12).

Table 12 Physicochemical data for MIDD0301, PI310 and PI320.

Compound	Solubility (mg/L)[a]	logPe (cm/s)[b]	logD[c]	Viability HEK293 LD_{50} (μM)[d]
PI310	3.9 ± 0.3	insoluble	5.95 ± 0.08	> 300
PI320	1542 ± 55	-5.90 ± 0.01	5.12 ± 0.02	> 300
MIDD0301	3220 ± 102 (pH = 6.75)[7]	-7.12 ± 0.13 (pH = 7.2)	0.33 ± 0.05 (pH = 7)[7]	> 400[24]

[a]Shake flask assay; [b]PAMPA assay (Pion); [c]Octanol:water coefficient; [d]Cell-based viability assay (18h).

Due to the limited aqueous solubility of PI310 of 3.9 mg/L, we were not able to achieve a sufficient high concentration to carry out the corresponding permeability assay. In contrast, the aqueous solubility of PI320 was excellent at 1,542 mg/L. Importantly, the permeability of PI320 (-5.90) was similar to control compound verapamil (-5.76). Verapamil is considered to be a very permeable drug. The parent compound MIDD0301 is negatively charged under neutral pH, which results in high solubility (3.2 g/L) but also lower permeability (-7.1 cm/s). The partition coefficient between water and n-octanol is very high for PI310, which might negatively influence passive diffusion. PI320 has a lower logD than PI310 and is more water solubility. MIDD0301 has a low logD at neutral pH, which increased to 2.0 at pH 4.[92] Finally, all test compounds have very low toxicity, with LD_{50} values in excess of 300 μM using embryonic kidney cell line HEK293.

My coworker Nicolas Zahn tested the *in vivo* efficacy of nebulized PI320 with two murine asthma models and found its efficacy is equivalent or better than albuterol (data is not shown here).

Finally, we quantified the time dependent lung concentration of PI310 and PI320 after a single

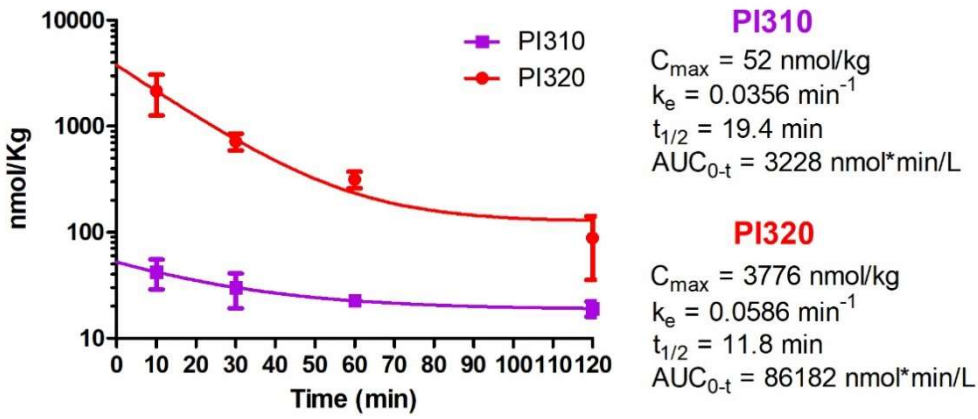

Figure 95. Pharmacokinetics of nebulized PI310 and PI320 in Swiss Webster mice. Groups of four mice were dosed with 7.2 mg/kg of nebulized compound (20 µL). Lungs were harvested at indicated time points and PI310 and PI320 quantified by LCMS/MS. Data are

nebulized dose (Figure 95). The lung concentrations of PI310 and PI320 were very different after 10 min, showing 42 nmol/kg and 2,160 nmol/kg, respectively. Both compounds were soluble in water at 3.2 mg/ml with the addition of 0.17% Tween-20, although only 3.9 mg/L of PI310 was soluble in water. It can be hypothesized that the nebulizing PI310 solution was not homogenous and that nonspecific binding to the nebulizer itself could have reduced the administered dose. Another possibility for the different lung concentrations could involve binding to tissue of the nasal cavity and trachea. Therefore, compounds like PI310 with long alkyl chain substituents, such as salmeterol, are administered by dry powder inhaler, overcoming their challenging physicochemical properties. However, once administered both compounds showed good half-life of 11.8 min and 19.4 min, respectively. This is an improvement compared to parent compound MIDD0301, which exhibited a half-life of 5.2 min.[11] PI320 has also a larger AUC, which was almost ten times as high as MIDD0301.

We can conclude that conjugation of MIDD0301 at the carboxyl group can generate amides that retain $GABA_AR$ affinity. Other examples of MIDD0301 derived amides have been reported.[139,140] Furthermore, compounds like PI320 have excellent physicochemical properties, quick onset of smooth muscle relaxation, and potently alleviate AHR. PI320 can be nebulized as an aqueous solution achieving high lung concentrations and a good half-life. To our knowledge, PI320 is the first example of a PEGylated benzodiazepine. We are currently investigating if compounds like PI320 are available orally and if brain exposure is limited due to the polyethylene glycol chain.

References

1. Centers for Disease Control and Prevention, https://www.cdc.gov/asthma/most_recent_national_asthma_data.htm
2. Pascual, R. M.; Peters, S. P. Airway remodeling contributes to the progressive loss of lung function in asthma: An overview. J Allergy Clin Immunol 2005, 116, (3), 477-86; quiz 487.
3. National Asthma Education and Prevention Program. Expert Panel Report 3: Guidelines for the Diagnosis and Management of Asthma. National Heart, Lung and Blood Institute, National Institutes of Health: U.S. Department of Health and Human Services; 2007 Aug 28. Report No.: NIH Publication No.07-4051.
4. Myers, T. R. Guidelines for asthma management: A review and comparison of 5 current guidelines. Respir Care 2008, 53, (6), 751-67; discussion 767-9.
5. Moorman, J. E.; Rudd, R. A.; Johnson, C. A.; King, M.; Minor, P.; Bailey, C.; Scalia, M. R.; Akinbami, L. J. Centers for Disease Control and Prevention. National surveillance for asthma--united states, 1980-2004. MMWR Surveill Summ 2007, 56, (8), 1-54.
6. Lima, J. J.; Zhang, S.; Grant, A.; Shao, L.; Tantisira, K. G.; Allayee, H.; Wang, J.; Sylvester, J.; Holbrook, J.; Wise, R.; Weiss, S. T.; Barnes, K. Influence of leukotriene pathway polymorphisms on response to montelukast in asthma. Am J Respir Crit Care Med 2006, 173, (4), 379-85. (PMC2662939).
7. Malmstrom, K.; Rodriguez-Gomez, G.; Guerra, J.; Villaran, C.; Pineiro, A.; Wei, L. X.; Seidenberg, B. C.; Reiss, T. F. Oral montelukast, inhaled beclomethasone, and placebo for chronic asthma. A randomized, controlled trial. Montelukast/beclomethasone study group. Ann Intern Med 1999, 130, (6), 487-95.

8. Israel, E.; Chervinsky, P. S.; Friedman, B.; Van Bavel, J.; Skalky, C. S.; Ghannam, A. F.; Bird, S. R.; Edelman, J. M. Effects of montelukast and beclomethasone on airway function and asthma control. J Allergy Clin Immunol 2002, 110, (6), 847-54.

9. Schumann, C.; Kropf, C.; Wibmer, T.; Rudiger, S.; Stoiber, K. M.; Thielen, A.; Rottbauer, W.; Kroegel, C. Omalizumab in patients with severe asthma: The xclusive study. Clin Respir J 2012, 6, (4), 215-27.

10. Abonia, J. P.; Putnam, P. E. Mepolizumab in eosinophilic disorders. Expert Rev Clin Immunol 2011, 7, (4), 411-7. (PMC3201786).

11. Nicolas M Zahn, Brandon N Mikulsky, MS Rashid Roni, Gene T Yocum, Md Yeunus Mian, Daniel E Knutson, James M Cook, Charles W Emala, Douglas C Stafford, Leggy A Arnold, (2020) Nebulized MIDD0301 Reduces Airway Hyperresponsiveness in Moderate and Severe Murine Asthma Models, ACS Pharmacology & Translational Science 3 (6), 1381-1390

12. Forkuo, G. S.; Guthrie, M. L.; Yuan, N. Y.; Nieman, A. N.; Kodali, R.; Jahan, R.; Stephen, M. R.; Yocum, G. T.; Treven, M.; Poe, M. M.; Li, G.; Yu, O. B.; Hartzler, B. D.; Zahn, N. M.; Ernst, M.; Emala, C. W.; Stafford, D. C.; Cook, J. M.; Arnold, L. A. Development of GABAA Receptor Subtype-Selective Imidazobenzodiazepines as Novel Asthma Treatments. Mol. Pharmaceutics 2016, 13 (6), 2026−38.

13. Forkuo, G. S.; Nieman, A. N.; Yuan, N. Y.; Kodali, R.; Yu, O. B.; Zahn, N. M.; Jahan, R.; Li, G.; Stephen, M. R.; Guthrie, M. L.; Poe, M. M.; Hartzler, B. D.; Harris, T. W.; Yocum, G. T.; Emala, C. W.; Steeber, D. A.; Stafford, D. C.; Cook, J. M.; Arnold, L. A. Alleviation of Multiple

Asthmatic Pathologic Features with Orally Available and Subtype Selective GABAA Receptor Modulators. Mol. Pharmaceutics 2017, 14 (6), 2088−2098.

14. Jahan, R.; Stephen, M. R.; Forkuo, G. S.; Kodali, R.; Guthrie, M. L.; Nieman, A. N.; Yuan, N. Y.; Zahn, N. M.; Poe, M. M.; Li, G.; Yu, O. B.; Yocum, G. T.; Emala, C. W.; Stafford, D. C.; Cook, J. M.; Arnold, L. A. Optimization of substituted imidazobenzodiazepines as novel asthma treatments. Eur. J. Med. Chem. 2017, 126, 550−560.

15. Olsen, R. W.; Sieghart, W. International Union of Pharmacology. LXX. Subtypes of gamma-aminobutyric acid(A) receptors: classification on the basis of subunit composition, pharmacology, and function. Update. Pharmacol Rev. 2008, 60 (3), 243−60.

16. Mortensen, M.; Patel, B.; Smart, T. G. GABA Potency at GABA(A) Receptors Found in Synaptic and Extrasynaptic Zones. Front. Cell. Neurosci. 2012, 6, 1−10.

17. Clayton, T.; Poe, M. M.; Rallapalli, S.; Biawat, P.; Savic, M. M.; Rowlett, J. K.; Gallos, G.; Emala, C. W.; Kaczorowski, C. C.; Stafford, D. C.; Arnold, L. A.; Cook, J. M. A Review of the Updated Pharmacophore for the Alpha 5 GABA(A) Benzodiazepine Receptor Model. Int. J. Med. Chem. 2015, 2015, 430248.

18. Gallos, G.; Yim, P.; Chang, S.; Zhang, Y.; Xu, D.; Cook, J. M.; Gerthoffer, W. T.; Emala, C. W., Sr. Targeting the restricted alphasubunit repertoire of airway smooth muscle GABAA receptors augments airway smooth muscle relaxation. Am. J. Physiol.: Lung Cell. Mol. Physiol. 2012, 302 (2), 248−56.

19. Gallos, G.; Yocum, G. T.; Siviski, M. E.; Yim, P. D.; Fu, X. W.; Poe, M. M.; Cook, J. M.; Harrison, N.; Perez-Zoghbi, J.; Emala, C. W., Sr. Selective targeting of the alpha5-subunit

of GABAA receptors relaxes airway smooth muscle and inhibits cellular calcium handling. Am. J. Physiol.: Lung Cell. Mol. Physiol. 2015, 308 (9), L931−L942.

20. Mizuta, K.; Xu, D.; Pan, Y.; Comas, G.; Sonett, J. R.; Zhang, Y.; Panettieri, R. A., Jr.; Yang, J.; Emala, C. W., Sr. GABAA receptors are expressed and facilitate relaxation in airway smooth muscle. Am. J. Physiol.: Lung Cell. Mol. Physiol. 2008, 294 (6), L1206−L1216.

21. Xiang, Y. Y.; Wang, S.; Liu, M.; Hirota, J. A.; Li, J.; Ju, W.; Fan, Y.; Kelly, M. M.; Ye, B.; Orser, B.; O'Byrne, P. M.; Inman, M. D.; Yang, X.; Lu, W. Y. A GABAergic system in airway epithelium is essential for mucus overproduction in asthma. Nat. Med. 2007, 13 (7), 862−7.

22. Forkuo, G. S.; Nieman, A. N.; Kodali, R.; Zahn, N. M.; Li, G.; Rashid Roni, M. S.; Stephen, M. R.; Harris, T. W.; Jahan, R.; Guthrie, M. L.; Yu, O. B.; Fisher, J. L.; Yocum, G. T.; Emala, C. W.; Steeber, D. A.; Stafford, D. C.; Cook, J. M.; Arnold, L. A. A Novel Orally Available Asthma Drug Candidate That Reduces Smooth Muscle Constriction and Inflammation by Targeting GABAA Receptors in the Lung. Mol. Pharmaceutics 2018, 15, 1766−1777.

23. Yocum, G. T.; Perez-Zoghbi, J. F.; Danielsson, J.; Kuforiji, A. S.; Zhang, Y.; Li, G.; Rashid Roni, M. S.; Kodali, R.; Stafford, D. C.; Arnold, L. A.; Cook, J. M.; Emala, C. W., Sr. A novel GABAA receptor ligand MIDD0301 with limited blood-brain barrier penetration relaxes airway smooth muscle ex vivo and in vivo. Am. J. Physiol.: Lung Cell. Mol. Physiol. 2019, 316, L385−L390.

24. Zahn, N. M.; Huber, A. T.; Mikulsky, B. N.; Stepanski, M. E.; Kehoe, A. S.; Li, G.; Schussman, M.; Rashid Roni, M. S.; Kodali, R.; Cook, J. M.; Stafford, D. C.; Steeber, D. A.; Arnold, L. A. MIDD0301 - A first-in-class anti-inflammatory asthma drug targets GABAA receptors

without causing systemic immune suppression. Basic Clin. Pharmacol. Toxicol. 2019, 125, 75−84.

25. Dias R, Sheppard WF, Fradley RL, Garrett EM, Stanley JL, Tye SJ, Goodacre S, Lincoln RJ, Cook SM, Conley R, Hallett D, Humphries AC, Thompson SA, Wafford KA, Street LJ, Castro JL, Whiting PJ, Rosahl TW, Atack JR, McKernan RM, Dawson GR, Reynolds DS. Evidence for a significant role of alpha 3-containing GABAA receptors in mediating the anxiolytic effects of benzodiazepines. J Neurosci. 2005; 25(46):10682–8. [PubMed: 16291941]

26. Jacob TC, Moss SJ, Jurd R. GABA(A) receptor trafficking and its role in the dynamic modulation of neuronal inhibition. Nat Rev Neurosci. 2008; 9(5):331–43. [PubMed: 18382465]

27. Rudolph U, Crestani F, Benke D, Brunig I, Benson JA, Fritschy JM, Martin JR, Bluethmann H, Mohler H. Benzodiazepine actions mediated by specific gamma-aminobutyric acid(A) receptor subtypes. Nature. 1999; 401(6755):796–800. [PubMed: 10548105]

28. Mizuta K, Xu D, Pan Y, Comas G, Sonett JR, Zhang Y, Panettieri RA Jr, Yang J, Emala CW Sr. GABAA receptors are expressed and facilitate relaxation in airway smooth muscle. Am J Physiol Lung Cell Mol Physiol. 2008; 294(6):L1206–16. [PubMed: 18408071]

29. Yocum GT, Gallos G, Zhang Y, Jahan R, Stephen MR, Varagic Z, Puthenkalam R, Ernst M, Cook JM, Emala CW. Targeting the gamma-Aminobutyric Acid A Receptor alpha4 Subunit in Airway Smooth Muscle to Alleviate Bronchoconstriction. Am J Respir Cell Mol Biol. 2016; 54(4):546– 53. [PubMed: 26405827]

30. Gallos G, Yocum GT, Siviski ME, Yim PD, Fu XW, Poe MM, Cook JM, Harrison N, Perez-Zoghbi J, Emala CW Sr. Selective targeting of the alpha5-subunit of GABAA receptors relaxes airway smooth muscle and inhibits cellular calcium handling. Am J Physiol Lung Cell Mol Physiol. 2015; 308(9):L931–42. [PubMed: 25659897]

31. Alam S, Laughton DL, Walding A, Wolstenholme AJ. Human peripheral blood mononuclear cells express GABAA receptor subunits. Molecular immunology. 2006; 43(9):1432–42. [PubMed: 16213022]

32. Bjurstrom H, Wang J, Ericsson I, Bengtsson M, Liu Y, Kurnar-Mendu S, Issazadeh-Navikas S, Birnir B. GABA, a natural immunomodulator of T lymphocytes. J Neuroimmunol. 2008; 205(1-2): 44–50. [PubMed: 18954912]

33. Wheeler DW, Thompson AJ, Corletto F, Reckless J, Loke JCT, Lapaque N, Grant AJ, Mastroeni P, Grainger DJ, Padgett CL, O'Brien JA, Miller NGA, Trowsdale J, Lummis SCR, Menon DK, Beech JS. Anaesthetic Impairment of Immune Function Is Mediated via GABA(A) Receptors. PloS one. 2011; 6(2)

34. Christopher A. Lipinski", Franco Lombardo, Beryl W. Dominy, Paul J. Feeney, Experimental and computational approaches to estimate solubility and permeability in drug discovery and development settings, Advanced Drug Delivery Reviews 23 (1997) 3-25

35. Attila A. Seyhan, Lost in translation: the valley of death across preclinical and clinical divide – identification of problems and overcoming obstacles, Translational Medicine Communications (2019) 4:18

36. Lap Hing Chi, Allan D. Burrows, Robin L. Anderson, Can preclinical drug development help to predict adverse events in clinical trials? Drug Discovery Today 2021, ISSN 1359-6446

37. Hanan Awad, Mona M. Khamis, Anas El-Aneed, Mass Spectrometry, Review of the Basics: Ionization. Applied Spectroscopy Reviews Volume 50, 2015 - Issue 2

38. Dass, Chhabil (2007). *Fundamentals of Contemporary Mass Spectrometry || Modes of Ionization*

39. Alec Saitman, *Critical Issues in Alcohol and Drugs of Abuse Testing (second edition),* 2019, Chapter 13 Pages 157-171

40. Jennifer Griffiths, A Brief History of Mass Spectrometry, Anal. Chem. 2008, 80, 15, 5678–5683

41. Y. Wang; S. Liu; Y. Hu; P. Li; J. Wan. Current state-of-the-art of mass spectrometry-based metabolomics studies-A review focusing on wide coverage, high throughput and easy identification. RSCAdv.,2015,5,78728

42. Shibdas Banerjee , Shyamalava Mazumdar, Electrospray ionization mass spectrometry: a technique to access the information beyond the molecular weight of the analyte. Int J Anal Chem. 2012; 2012:282574

43. Korfmacher, Walter A. Using Mass Spectrometry for Drug Metabolism Studies. CRC Press. 2009. p. 342. ISBN 978142009221944. Edmond de Hoffmann and Vincent Stroobant, Mass Spectrometry Principles and Applications, Third Edition

45. Sharad Medhe, Mass Spectrometry: Detectors Review, Chemical and Biomolecular Engineering 2018; 3(4): 51-58

46. Bioanalytical Method Validation Guidance for Industry, May 2018, Biopharmaceutics

47. N J Clarke 1, D Rindgen, W A Korfmacher, K A Cox, Systematic LC/MS metabolite identification in drug discovery. Anal Chem. 2001 Aug 1;73(15):430A-439A.

48. https://www.creative-proteomics.com/technology/maldi-tof-mass-spectrometry.htm

49. Simon Maher, Fred P. M. Jjunju, and Stephen Taylor, Colloquium : 100 years of mass spectrometry: Perspectives and future trends, January 2015, Review of Modern Physics 87(1):113-135

50. https://www.asthmafriendly.ca/home/about-asthma

51. Y. Wang; S. Liu; Y. Hu; P. Li; J. Wan, Current state-of-the-art of mass spectrometry-based metabolomics studies-A review focusing on wide coverage, high throughput and easy identification. RSCAdv.,2015,5,78728

52. https://www.shimadzu.com/an/service-support/technical-support/analysis-basics/fundamental/mass_analyzers.html

53. Neelja Singhal, Manish Kumar, Pawan K. Kanaujia and Jugsharan S. Virdi, MALDI-TOF mass spectrometry: an emerging technology for microbial identification and diagnosis, Frontiers in Microbiology, august 2015, volume 6, article 791

54. Stefani N. Thomas, Chapter 10 - Mass spectrometry, Contemporary Practice in Clinical Chemistry (Fourth Edition), Academic Press, 2019, Pages 171-185

55. M.L. Howard, J. J. Hill, G.R. Galluppi and M.A. McLean. Plasma Protein Binding in Drug Discovery and Development, Combinatorial Chemistry & High Throughput Screening, 2010, Vol. 13, No. 2

56. Henrik Silléna, Melanie Cook, Patty Davis. Determination of unbound ticagrelor and its active metabolite (AR-C124910XX) in human plasma by equilibrium dialysis and LC–MS/MS , Journal of Chromatography B, 879 (2011) 2315–2322

57. Angelica M. Merlot, Danuta S. Kalinowski, Des R. Richardson. Unraveling the mysteries of serum albumin—more than just a serum protein, Front. Physiol., 12 August 2014

58. Roopenian, D. C.; Low, B. E.; Christianson, G. J.; Proetzel, G.; Sproule, T. J.; Wiles, M. V.. Albumin-deficient Mouse Models for Studying Metabolism of Human Albumin and Pharmacokinetics of Albumin-based Drugs. mAbs 2015, 7 (2), 344–351.

59. Y. Gao, C. Gesenberg, W. Zheng. Developing Solid Oral Dosage Forms (Second Edition), Chapter 17 - Oral Formulations for Preclinical Studies: Principle, Design, and Development Considerations. Academic press 2017, Pages 455-495.

60. Kuwayama, T.; Yashiro, T. The behavior of 1,4-benzodiazepine drugs in acidic media. IV. Proton and carbon-13 nuclear magnetic resonance spectra of diazepam and fludiazepam in acidic aqueous solution. Chem. Pharm. Bull. 1985, 33, 5503−5510.

61. Kuwayama, T.; Kato, S.; Yashiro, T. The behavior of 1,4- benzodiazepine drugs in acidic media. VII. Carbon-13 nuclear magnetic resonance spectra of flurazepam in acidic aqueous solution. Yakugaku Zasshi 1987, 107, 318−322.

62. Han, W. W.; Yakatan, G. J.; Maness, D. D. Kinetics and mechanisms of hydrolysis of 1,4-benzodiazepines II: oxazepam and diazepam. J. Pharm. Sci. 1977, 66, 573−577.

63. Kuwayama, T.; Yashiro, T.; Kurono, Y.; Ikeda, K. The behavior of 1,4-benzodiazepine drugs in acidic media. VI. Hydrogen exchange reaction and proton and carbon-13 nuclear magnetic resonance spectra of estazolam. Chem. Pharm. Bull. 1986, 34, 2994−2998.

64. Andersin, R. Solubility and acid-base behaviour of midazolam in media of different pH, studied by ultraviolet spectrophotometry with multicomponent software. J. Pharm. Biomed. Anal. 1991, 9, 451− 455.

65. Sternbach, L. H.; Fryer, R. I.; Metlesics, W.; Reeder, E.; Sach, G.; Saucy, G.; Stempel, A. Quinazolines and 1,4-Benzodiazepines. VI.1a Halo-, Methyl-, and Methoxy-substituted 1,3-Dihydro-5-phenyl 2H-1,4-Benzodiazepin-2-ones1b,c. J. Org. Chem. 1962, 27, 3788−3796.

66. Walser, A.; Benjamin, L. E.; Flynn, T.; Mason, C.; Schwartz, R.; Fryer, R. I. Quinazolines and 1,4-benzodiazepines. 84. Synthesis and reactions of imidazo[1,5-a][1,4]benzodiazepines. J. Org. Chem. 1978, 43, 936−944.

67. Exploratory IND Studies, Guidance for Industry, Investigators, and Reviewers, January 2006, Food and drug administration.

68. Cook, J. M.; Zhou, H.; Huang, S.; Sarma, P. V.; Zhang, C. Stereospecific anxiolytic and anticonvulsant agents with reducedmuscle relaxant, sedative-hypnotic and ataxic effects. US Patent US76189582006

69. Knutson, D. E., Roni, M. S. Rashid, Mian, Y., Cook, J. M., Stafford, D. C., and Arnold, L. A. (2020) Improved scale-up synthesis and purification of clinical asthma candidate MIDD0301. Org. Process Res. Dev. 24, 1467−1476

70. Cook, J.; Li, G.; Golani, L.; Jahan, R.; Rashid, F. Improved Synthesis of Anxiolytic, Anticonvulsant, and Antinociceptive α2/α3-GABA(A)-ergic Receptor Subtype Selective Ligands as Promising Agents to Treat Anxiety, Epilepsy, and Neuropathic Pain. Synthesis 2018, 50, 4124−4132.

71. Carpino, L. A.; Cohen, B. J.; Stephens, K. E.; Sadat-Aalaee, S. Y.; Tien, J. H.; Langridge, D. C. (Fluoren-9-ylmethoxy)carbonyl (Fmoc) amino acid chlorides. Synthesis, characterization, and application to the rapid synthesis of short peptide segments. J. Org. Chem. 1986, 51, 3732−3734.

72. Prabhu, G.; Basavaprabhu; Narendra, N.; Vishwanatha, T. M.; Sureshbabu, V. V. Amino acid chlorides: a journey from instability and racemization toward broader utility in organic synthesis including peptides and their mimetics. Tetrahedron 2015, 71, 2785−2832.

73. Fier, P. S.; Whittaker, A. M. An Atom-Economical Method To Prepare Enantiopure Benzodiazepines with N-Carboxyanhydrides. Org. Lett. 2017, 19, 1454−1457.

74. Wilder, R.; Mobashery, S. The use of triphosgene in preparation of N-carboxy.alpha.-amino acid anhydrides. J. Org. Chem. 1992, 57, 2755−2756.

75. Safety Testing of Drug Metabolites Guidance for Industry. U.S. Department of Health and Human Services Food and Drug Administration Center for Drug Evaluation and Research (CDER) 2016.

76. Meunier, B.; de Visser, S. P.; Shaik, S., Mechanism of oxidation reactions catalyzed by cytochrome p450 enzymes. Chem Rev 2004, 104 (9), 3947-80.

77. Basaran, R.; Can Eke, B., Flavin Containing Monooxygenases and Metabolism of Xenobiotics. Turk J Pharm Sci 2017, 14 (1), 90-94.

78. Vasiliou, V.; Pappa, A.; Estey, T., Role of human aldehyde dehydrogenases in endobiotic and xenobiotic metabolism. Drug Metab Rev 2004, 36 (2), 279-99.

79. Tafazoli, S.; O'Brien, P. J., Peroxidases: a role in the metabolism and side effects of drugs. Drug Discov Today 2005, 10 (9), 617-25.

80. Oppermann, U., Carbonyl reductases: the complex relationships of mammalian carbonyl- and quinone-reducing enzymes and their role in physiology. Annu Rev Pharmacol Toxicol 2007, 47, 293-322.

81. Laizure, S. C.; Herring, V.; Hu, Z.; Witbrodt, K.; Parker, R. B., The role of human carboxylesterases in drug metabolism: have we overlooked their importance? Pharmacotherapy 2013, 33 (2), 210-22.

82. Hazai, E.; Rona, K.; Vereczkey, L., [Human drug metabolizing enzymes III. Epoxide hydrolases, esterases, and amidases]. Acta Pharm Hung 1999, 69 (4), 208-12.

83. Meech, R.; Hu, D. G.; McKinnon, R. A.; Mubarokah, S. N.; Haines, A. Z.; Nair, P. C.; Rowland, A.; Mackenzie, P. I., The UDP-Glycosyltransferase (UGT) Superfamily: New Members, New Functions, and Novel Paradigms. Physiol Rev 2019, 99 (2), 1153-1222.

84. Tsirka, T.; Konstantopoulou, M.; Sabbagh, A.; Crouau-Roy, B.; Ryan, A.; Sim, E.; Boukouvala, S.; Fakis, G., Comparative analysis of xenobiotic metabolising N-acetyltransferases from ten non-human primates as in vitro models of human homologues. Sci Rep 2018, 8 (1), 9759.

85. Zhu, B. T., Catechol-O-Methyltransferase (COMT)-mediated methylation metabolism of endogenous bioactive catechols and modulation by endobiotics and xenobiotics: importance in pathophysiology and pathogenesis. Curr Drug Metab 2002, 3 (3), 321-49.

86. Morgenstern, R.; Zhang, J.; Johansson, K., Microsomal glutathione transferase 1: mechanism and functional roles. Drug Metab Rev 2011, 43 (2), 300-6.

87. Gamage, N.; Barnett, A.; Hempel, N.; Duggleby, R. G.; Windmill, K. F.; Martin, J. L.; McManus, M. E., Human sulfotransferases and their role in chemical metabolism. Toxicol Sci 2006, 90 (1), 5-22.

88. Mihalik, S. J.; Steinberg, S. J.; Pei, Z.; Park, J.; Kim, D. G.; Heinzer, A. K.; Dacremont, G.; Wanders, R. J.; Cuebas, D. A.; Smith, K. D.; Watkins, P. A., Participation of two members of the very long-chain acyl-CoA synthetase family in bile acid synthesis and recycling. J Biol Chem 2002, 277 (27), 24771-9.

89. Falany, C. N.; Johnson, M. R.; Barnes, S.; Diasio, R. B., Glycine and taurine conjugation of bile acids by a single enzyme. Molecular cloning and expression of human liver bile acid CoA:amino acid N-acyltransferase. J Biol Chem 1994, 269 (30), 19375-9.

90. Sieghart, W.; Savic, M. M., International Union of Basic and Clinical Pharmacology. CVI: GABAA Receptor Subtype- and Function-selective Ligands: Key Issues in Translation to Humans. Pharmacol Rev 2018, 70 (4), 836-878.

91. Prud'homme, G. J.; Glinka, Y.; Wang, Q., Immunological GABAergic interactions and therapeutic applications in autoimmune diseases. Autoimmun Rev 2015, 14 (11), 1048-56.

92. Roni, M. S. R.; Li, G.; Mikulsky, B. N.; Knutson, D. E.; Mian, M. Y.; Zahn, N. M.; Cook, J. M.; Stafford, D. C.; Arnold, L. A., The Effects of pH on the Structure and Bioavailability of Imidazobenzodiazepine-3-Carboxylate MIDD0301. Mol Pharm 2020, 17 (4), 1182-1192.

93. Hooper, W. D.; Watt, J. A.; McKinnon, G. E.; Reilly, P. E., Metabolism of diazepam and related benzodiazepines by human liver microsomes. Eur J Drug Metab Pharmacokinet 1992, 17 (1), 51-9.

94. Yasumori, T.; Nagata, K.; Yang, S. K.; Chen, L. S.; Murayama, N.; Yamazoe, Y.; Kato, R., Cytochrome P450 mediated metabolism of diazepam in human and rat: involvement of human CYP2C in N-demethylation in the substrate concentration-dependent manner. Pharmacogenetics 1993, 3 (6), 291-301.

95. Wandel, C.; Bocker, R.; Bohrer, H.; Browne, A.; Rugheimer, E.; Martin, E., Midazolam is metabolized by at least three different cytochrome P450 enzymes. Br J Anaesth 1994, 73 (5), 658-61.

96. Stamenic, T. T.; Poe, M. M.; Rehman, S.; Santrac, A.; Divovic, B.; Scholze, P.; Ernst, M.; Cook, J. M.; Savic, M. M., Ester to amide substitution improves selectivity, efficacy and kinetic behavior of a benzodiazepine positive modulator of GABAA receptors containing the alpha5 subunit. European journal of pharmacology 2016, 791, 433-443.

97. Perrie, J. A.; Harding, J. R.; Holt, D. W.; Johnston, A.; Meath, P.; Stachulski, A. V., Effective synthesis of 1beta-acyl glucuronides by selective acylation. Org Lett 2005, 7 (13), 2591-4.

98. Vollmer, M.; Klingebiel, M.; Rohn, S.; Maul, R., Alamethicin for using in bioavailability studies? - Re-evaluation of its effect. Toxicol In Vitro 2017, 39, 111-118.

99. Oleson, L.; Court, M. H., Effect of the beta-glucuronidase inhibitor saccharolactone on glucuronidation by human tissue microsomes and recombinant UDP-glucuronosyltransferases. J Pharm Pharmacol 2008, 60 (9), 1175-82.

100. Regan, S. L.; Maggs, J. L.; Hammond, T. G.; Lambert, C.; Williams, D. P.; Park, B. K., Acyl glucuronides: the good, the bad and the ugly. Biopharm Drug Dispos 2010, 31 (7), 367-95.

101. Patel, S. R., Bioanalytical challenges and strategies for accurately measuring acyl glucuronide metabolites in biological fluids. Biomed Chromatogr 2020, 34 (1), e4640.

102. Behrens, C.; Bu, H.-Z.; Cheng, J.-F.; Dong, H.; Gu, X.-H.; Guo, X.; Hu, E.; Li, H.-Y.; Li, Z.; Lin, G.-Q.; Liu, D.; Liu, Y.; Liu, R.; Lu, W.; Ni, C.-Y.; Qing, F.-L.; Qiu, X.-L.; Sun, J.; Sun, X.-W.; Wang, D. H.; Wang, J.; Wang, Z.; Yang, G.; You, Q.-D.; Yue, X.; Zhang, J.-G., Chiral Drugs. John Wiley & Sons: Hoboken, New Jersey, US, 2011.

103. U.S. Food and Drug Administration "Development of New Stereoisomeric Drugs" https://www.fda.gov/regulatory-information/search-fda-guidance-documents/development-new-stereoisomeric-drugs. May 1992.

104. Ranade, V. V.; Somberg, J. C., Chiral cardiovascular drugs: an overview. Am J Ther 2005, 12 (5), 439-59.

105. Chirumamilla, R. R.; Marchant, R.; Nigam, P., Captopril and its synthesis from chiral intermediates. J. Chem. Technol. Biotechnol. 2001, 76, 123-127.

106. Tynes, C. R.; Livingston, B.; Patel, H.; Arnold, J. J., Chiral stability of an extemporaneously prepared clopidogrel bisulfate oral suspension. J Pediatr Pharmacol Ther 2014, 19 (1), 25-9.

107. Caner, H.; Groner, E.; Levy, L.; Agranat, I., Trends in the development of chiral drugs. Drug Discov Today 2004, 9 (3), 105-10.

108. Banitt, E. H.; Schmid, J. R.; Newmark, R. A., Resolution of flecainide acetate, N-(2-piperidylmethyl)-2,5-bis(2,2,2-trifluoroethoxy)benzam ide acetate, and antiarrhythmic properties of the enantiomers. J Med Chem 1986, 29 (2), 299-302.

109. Wong, D. T.; Fuller, R. W.; Robertson, D. W., Fluoxetine and its two enantiomers as selective serotonin uptake inhibitors. Acta Pharm Nord 1990, 2 (3), 171-80.

110. Itoh, T.; Ono, K.; Koido, K. I.; Li, Y. H.; Yamada, H., Stereoselectivity of the folate transporter in rabbit small intestine: studies with amethopterin enantiomers. Chirality 2001, 13 (3), 164-9.

111. Hamunen, K.; Maunuksela, E. L.; Sarvela, J.; Bullingham, R. E.; Olkkola, K. T., Stereoselective pharmacokinetics of ketorolac in children, adolescents and adults. Acta Anaesthesiol Scand 1999, 43 (10), 1041-6.

112. Kristensen, K.; Blemmer, T.; Angelo, H. R.; Christrup, L. L.; Drenck, N. E.; Rasmussen, S. N.; Sjogren, P., Stereoselective pharmacokinetics of methadone in chronic pain patients. Ther Drug Monit 1996, 18 (3), 221-7.

113. Lu, H., Stereoselectivity in drug metabolism. Expert Opin Drug Metab Toxicol 2007, 3 (2), 149-58.

114. Thijssen, H. H.; Flinois, J. P.; Beaune, P. H., Cytochrome P4502C9 is the principal catalyst of racemic acenocoumarol hydroxylation reactions in human liver microsomes. Drug Metab Dispos 2000, 28 (11), 1284-90.

115. Sten, T.; Qvisen, S.; Uutela, P.; Luukkanen, L.; Kostiainen, R.; Finel, M., Prominent but reverse stereoselectivity in propranolol glucuronidation by human UDP-glucuronosyltransferases 1A9 and 1A10. Drug Metab Dispos 2006, 34 (9), 1488-94.

116. Fujimaki, M.; Shintani, S.; Hakusui, H., Stereoselective metabolism of carvedilol in the rat. Use of enantiomerically radiolabeled pseudoracemates. Drug Metab Dispos 1991, 19 (4), 749-53.

117. Savic, M. M.; Huang, S.; Furtmuller, R.; Clayton, T.; Huck, S.; Obradovic, D. I.; Ugresic, N. D.; Sieghart, W.; Bokonjic, D. R.; Cook, J. M., Are GABAA receptors containing alpha5

subunits contributing to the sedative properties of benzodiazepine site agonists? Neuropsychopharmacology 2008, 33 (2), 332-9.

118. Li, G.; Nieman, A. N.; Mian, M. Y.; Zahn, N. M.; Mikulsky, B. N.; Poe, M. M.; Methuku, K. R.; Liu, Y.; Cook, J. M.; Stafford, D. C.; Arnold, L. A., A Structure-Activity Relationship Comparison of Imidazodiazepines Binding at Kappa, Mu, and Delta Opioid Receptors and the GABAA Receptor. Molecules 2020, 25 (17).

19. Li, G.; Stephen, M. R.; Kodali, R.; Zahn, N. M.; Poe, M. M.; Tiruveedhula, V.; Huber, A. T.; Schussman, M. K.; Qualmann, K.; Panhans, C. M.; Raddatz, N. J.; Baker, D. A.; Prevot, T. D.; Banasr, M.; Sibille, E.; Arnold, L. A.; Cook, J. M., Synthesis of chiral GABAA receptor subtype selective ligands as potential agents to treat schizophrenia as well as depression. ARKIVOC 2018, 2018 (4), 158-182.

120. Arnold, A. E.; Stafford, D. C.; Cook, J. M.; Emala, C. W.; Forkuo, G. S.; Jahan, R.; Kodali, R.; Li, G.; Stephen, M. R. Gaba(A) receptor modulator and methods to control airway hyperresponsiveness and inflammation in asthma. 2018.

121. Liu, J.; Chen, T.; Norris, T.; Knappenberger, K.; Huston, J.; Wood, M.; Bostwick, R., A high-throughput functional assay for characterization of gamma-aminobutyric acid(A) channel modulators using cryopreserved transiently transfected cells. Assay Drug Dev Technol 2008, 6 (6), 781-6.

122. Im, W. B.; Pregenzer, J. F.; Thomsen, D. R., Effects of GABA and various allosteric ligands on TBPS binding to cloned rat GABA(A) receptor subtypes. Br J Pharmacol 1994, 112 (4), 1025-30.

123. Sur, C.; Quirk, K.; Dewar, D.; Atack, J.; McKernan, R., Rat and human hippocampal alpha5 subunit-containing gamma-aminobutyric AcidA receptors have alpha5 beta3 gamma2 pharmacological characteristics. Mol Pharmacol 1998, 54 (5), 928-33.

124. Hauser, C. A.; Wetzel, C. H.; Berning, B.; Gerner, F. M.; Rupprecht, R., Flunitrazepam has an inverse agonistic effect on recombinant alpha6beta2gamma2-GABAA receptors via a flunitrazepam-binding site. J Biol Chem 1997, 272 (18), 11723-7.

125. Chuang, S. H.; Reddy, D. S., Genetic and Molecular Regulation of Extrasynaptic GABA-A Receptors in the Brain: Therapeutic Insights for Epilepsy. The Journal of pharmacology and experimental therapeutics 2018, 364 (2), 180-197.

126. Masiulis, S.; Desai, R.; Uchanski, T.; Serna Martin, I.; Laverty, D.; Karia, D.; Malinauskas, T.; Zivanov, J.; Pardon, E.; Kotecha, A.; Steyaert, J.; Miller, K. W.; Aricescu, A. R., GABAA receptor signalling mechanisms revealed by structural pharmacology. Nature 2019, 565 (7740), 454-459.

127. Nguyen, L. A.; He, H.; Pham-Huy, C., Chiral drugs: an overview. Int J Biomed Sci 2006, 2 (2), 85-100.

128. Meech, R., Miners, J. O., Lewis, B. C., & Mackenzie, P. I. (2012). The glycosidation of xenobiotics and endogenous compounds: versatility and redundancy in the UDP glycosyltransferase superfamily. Pharmacology & therapeutics, 134(2), 200-218.

129. Yocum, G. T., Turner, D. L., Danielsson, J., Barajas, M. B., Zhang, Y., Xu, D., Harrison, N. L., Homanics, G. E., Farber, D. L., and Emala, C. W. (2017) GABAA receptor alpha4-subunit knockout enhances lung inflammation and airway reactivity in a murine asthma model, Am J Physiol Lung Cell Mol Physiol 313, L406-L415.

130. Cheer, S. M., and Scott, L. J. (2002) Formoterol: a review of its use in chronic obstructive pulmonary disease, Am J Respir Med 1, 285-300.

131. Johnson, M., Butchers, P. R., Coleman, R. A., Nials, A. T., Strong, P., Sumner, M. J., Vardey, C. J., and Whelan, C. J. (1993) The pharmacology of salmeterol, Life Sci 52, 2131-2143.

132. O'Byrne, P. M., Bleecker, E. R., Bateman, E. D., Busse, W. W., Woodcock, A., Forth, R., Toler, W. T., Jacques, L., and Lotvall, J. (2014) Once-daily fluticasone furoate alone or combined with vilanterol in persistent asthma, Eur Respir J 43, 773-782.

133. Coleman, R. A. (2009) On the mechanism of the persistent action of salmeterol: what is the current position?, Br J Pharmacol 158, 180-182.

134. Procopiou, P. A., Barrett, V. J., Bevan, N. J., Biggadike, K., Butchers, P. R., Coe, D. M., Conroy, R., Edney, D. D., Field, R. N., Ford, A. J., Guntrip, S. B., Looker, B. E., McLay, I. M., Monteith, M. J., Morrison, V. S., Mutch, P. J., Richards, S. A., Sasse, R., and Smith, C. E. (2009) Synthesis and structure-activity relationships of long-acting beta2 adrenergic receptor agonists incorporating arylsulfonamide groups, J Med Chem 52, 2280-2288.

135. Park, E. J., Choi, J., Lee, K. C., and Na, D. H. (2019) Emerging PEGylated non-biologic drugs, Expert Opin Emerg Drugs 24, 107-119.

136. Floettmann, E., Bui, K., Sostek, M., Payza, K., and Eldon, M. (2017) Pharmacologic Profile of Naloxegol, a Peripherally Acting micro-Opioid Receptor Antagonist, for the Treatment of Opioid-Induced Constipation, J Pharmacol Exp Ther 361, 280-291.

137. Middendorp, S. J., Hurni, E., Schonberger, M., Stein, M., Pangerl, M., Trauner, D., and Sigel, E. (2014) Relative positioning of classical benzodiazepines to the gamma2-subunit of GABAA receptors, ACS Chem Biol 9, 1846-1853.

138. Pandey, K. P., Khan, Z. A., Golani, L. K., Mondal, P., Mian, Y., Rashid, F., Tiruveedhula, V., Knutson, D. E., Sharmin, D., Ahmed, T., Rezvanian, S., Zahn, N. M., Arnold, L. A., Witkin, J. M., and Cook, J. M. (2020) Design, synthesis and characterization of novel gammaaminobutyric acid type A receptor ligands, ARKIVOC 2020, 242-256.

139. Li, G., Nieman, A. N., Mian, M. Y., Zahn, N. M., Mikulsky, B. N., Poe, M. M., Methuku, K. R., Liu, Y., Cook, J. M., Stafford, D. C., and Arnold, L. A. (2020) A Structure-Activity Relationship Comparison of Imidazodiazepines Binding at Kappa, Mu, and Delta Opioid Receptors and the GABAA Receptor, Molecules 25.

140. Li, G., Stephen, M. R., Kodali, R., Zahn, N. M., Poe, M. M., Tiruveedhula, V., Huber, A. T., Schussman, M. K., Qualmann, K., Panhans, C. M., Raddatz, N. J., Baker, D. A., Prevot, T. D., Banasr, M., Sibille, E., Arnold, L. A., and Cook, J. M. (2018) Synthesis of chiral GABAA receptor subtype selective ligands as potential agents to treat schizophrenia as well as depression, ARKIVOC 2018, 158-182.

141. Nshanian M, Lakshmanan R, Chen H, Ogorzalek Loo RR, Loo JA. (2018) Enhancing Sensitivity of Liquid Chromatography-Mass Spectrometry of Peptides and Proteins Using Supercharging Agents. Int J Mass Spectrom. 2018;427:157-164.

CURRICULUM VITAE

Md Shadiqur Rashid Roni

Place of Birth: Faridpur, Bangladesh

Education

BS in Chemistry, University of Dhaka, Bangladesh, 2000-2005

MS in Analytical Chemistry, University of Dhaka, Bangladesh, 2006-2007

PhD in Chemistry, University of Wisconsin-Milwaukee, 2016-2021

Expected Graduation, December 2021

Research Advisor: Dr. Alexander (Leggy) Arnold

Dissertation: Mass spectrometry directed pre-clinical studies of asthma candidate MIDD0301 and its analogs

Positions Held

2008-2016	Product in charge/Sr Application Chemist, AQC Science & Synergy Pvt Ltd, Bangladesh
2016-Present	Graduate Research and Teaching Assistant,
	University of Wisconsin-Milwaukee, Milwaukee, WI.

Awards

Eurofins Analytical Chemistry Award	Fall 2019
Graduate student excellence fellowship award	2020-21
Sosnovsky award for excellence in graduate research	2020-21

Publications

1. **MS Rashid Roni**, Nicolas M. Zahn, Brandon N. Mikulsky, Daniel Webb, Md Yeunus Mian, Daniel E. Knutson, Margaret Guthrie, James M. Cook, Douglas C. Stafford and Leggy A. Arnold, **(2021)** Identification and quantification of MIDD0301 metabolites. (Got Provisional acceptance letter from current drug metabolism)
2. **MS Rashid Roni**, Guanguan Li, Brandon N Mikulsky, Daniel E Knutson, Md Yeunus Mian, Nicolas M Zahn, James M Cook, Douglas C Stafford, Leggy A Arnold, **(2020)** The Effects of pH on the Structure and Bioavailability of Imidazobenzodiazepine-3-Carboxylate MIDD0301, *Molecular Pharmaceutics* 17, 4, 1182-1192

3. Daniel E Knutson, **MS Rashid Roni**, Md Yeunus Mian, James M Cook, Douglas C Stafford, Leggy A Arnold, **(2020)** Improved Scale-up Synthesis and Purification of Clinical Asthma Candidate MIDD0301, *Organic Process Research & Development* 24 (8), 1467-1476

4. Nicolas M Zahn, Brandon N Mikulsky, **MS Rashid Roni**, Gene T Yocum, Md Yeunus Mian, Daniel E Knutson, James M Cook, Charles W Emala, Douglas C Stafford, Leggy A Arnold, **(2020)** Nebulized MIDD0301 Reduces Airway Hyperresponsiveness in Moderate and Severe Murine Asthma Models, *ACS Pharmacology & Translational Science* 3 (6), 1381-1390

5. Nicolas M Zahn, Alec T Huber, Brandon N Mikulsky, Mae E Stepanski, Alexander S Kehoe, Guanguan Li, Melissa Schussman, **MS Rashid Roni**, Revathi Kodali, James M Cook, Douglas C Stafford, Douglas A Steeber, Leggy A Arnold, **(2019)** MIDD0301 – A first-in-class anti-inflammatory asthma drug targets GABAA receptors without causing systemic immune suppression, *Basic & Clinical Pharmacology & Toxicology* 125, 75-84.

6. Gene T Yocum, Jose F Perez-Zoghbi, Jennifer Danielsson, Aisha S Kuforiji, Yi Zhang, Guanguan Li, **MS Rashid Roni**, Revathi Kodali, Douglas C Stafford, Leggy A Arnold, James M Cook, Charles W Emala Sr, **(2018)** A Novel $GABA_A$ Receptor ligand MIDD0301 with Limited Blood Brain Barrier Penetration Relaxes Airway Smooth Muscle Ex Vivo and In Vivo, *American Journal of Physiology-Lung Cellular and Molecular Physiology* 316 (2), 385-390.

7. Gloria S Forkuo, Amanda N Nieman, Revathi Kodali, Nicolas M Zahn, Guanguan Li, **MS Rashid Roni**, Michael Rajesh Stephen, Ted W Harris, Rajwana Jahan, Margaret L Guthrie, Olivia B Yu, Janet L Fisher, Gene T Yocum, Charles W Emala, Douglas A Steeber, Douglas C Stafford, James M Cook, Leggy A Arnold, **(2018)** A Novel Orally Available Asthma Drug Candidate That Reduces Smooth Muscle Constriction and Inflammation by Targeting $GABA_A$ Receptors in the Lung, *Molecular Pharmaceutics*, 15(5), 1766-1777

Research Profiles

https://www.researchgate.net/profile/Shadiqur-Rashid-Roni

https://scholar.google.com/citations?user=0TsGKfMAAAAJ&hl=en

https://orcid.org/0000-0002-3105-0540